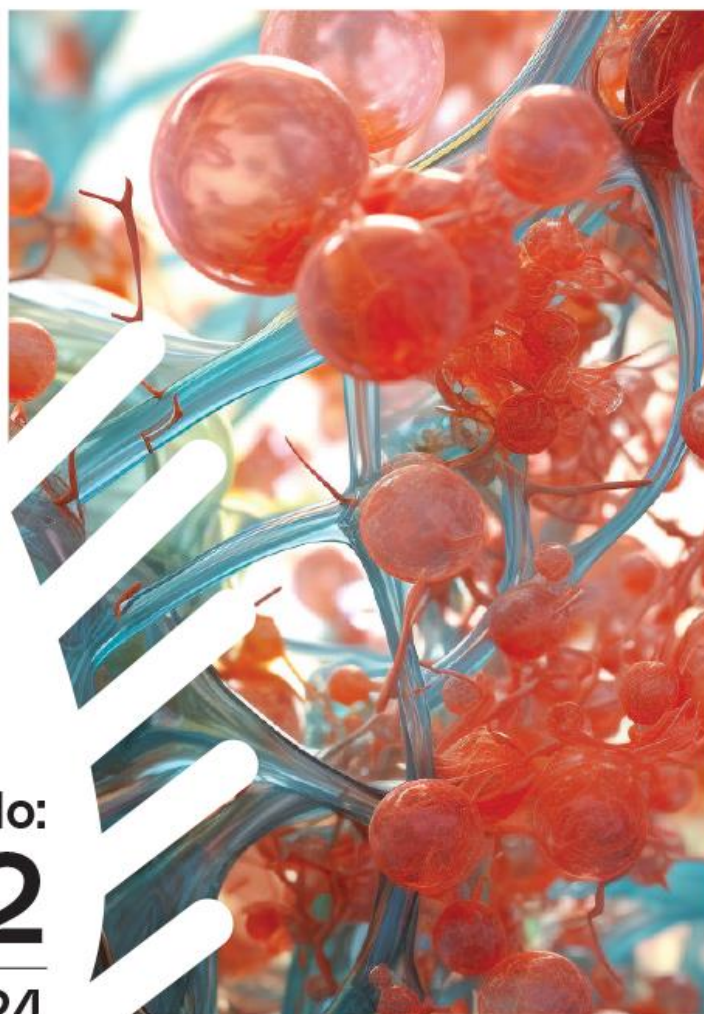


# EUCHEMBIO J

ISSN: 3023-5839

[www.euchembioj.com](http://www.euchembioj.com)

*The European*  
**Chemistry and**  
**Biotechnology**  
*Journal*



No:  
**02**  
2024

# The European Chemistry and Biotechnology Journal

Issue 2 • July 2024

## Editor-in-chief

Tunc Catal, Uskudar University, Türkiye  
E-mail: tunc.catal@uskudar.edu.tr (<https://orcid.org/0000-0003-2990-8680>)

## Editorial board

Abhilasha Singh Mathuriya, Ministry of Environment, Forest and Climate Change, India  
E-mail: imabhilasha@gmail.com  
(<https://orcid.org/0000-0002-6601-8241>)

Ahad Mokhtarzadeh, Tabriz University of Medical Sciences, Iran  
E-mail: ahad.mokhtarzadeh@gmail.com  
(<https://orcid.org/0000-0002-4515-8675>)

Baris Binay, Gebze Technical University, Türkiye  
E-mail: binay@gtu.edu.tr  
(<https://orcid.org/0000-0002-6190-6549>)

Bharat Patel, Queensland University of Technology, Australia  
E-mail: bharat.patel@qut.edu.au  
(<https://orcid.org/0000-0002-5332-1858>)

Chontisa Sukkasem, Thaksin University, Thailand  
E-mail: chontisa.s@gmail.com  
(<https://orcid.org/0000-0001-8043-4981>)

Deniz Yildirim, Cukurova University, Türkiye  
E-mail: dyildirim@cu.edu.tr  
(<https://orcid.org/0000-0002-5041-8160>)

Irina Nakashidze, Batumi Shota Rustaveli State University, Georgia  
E-mail: irinanakashidze@yahoo.com  
(<https://orcid.org/0000-0001-8934-6312>)

Jean-Marie Fontmorin, Chemical Engineering Research Center of Toulouse, France  
E-mail: jeanmarie.fontmorin@toulouse-inp.fr  
(<https://orcid.org/0000-0002-0832-7185>)

Jordi Villà i Freixa, Universitat de Vic - Universitat Central de Catalunya (UVic-UCC), Spain  
E-mail: jordi.villa@uvic.cat  
(<https://orcid.org/0000-0002-6359-3929>)

Lakhveer Singh, Sardar Patel University, Mandi, H.P., India  
E-mail: lakhveer@spumandi.ac.in  
(<https://orcid.org/0000-0002-4926-9778>)

Luguang Wang, Utah State University, USA  
E-mail: luguang.wang@usu.edu  
(<https://orcid.org/0000-0002-4566-6143>)

Muhsin Konuk, Uskudar University, Türkiye  
E-mail: muhsin.konuk@uskudar.edu.tr  
(<https://orcid.org/0000-0002-6651-718X>)

Oliver Feeney, The Eberhard Karls University of Tübingen, Germany  
E-mail: oliver.feeney@uni-tuebingen.de  
(<https://orcid.org/0000-0003-3585-448X>)

Rabah Boukherroub, CNRS & University Lille, France  
E-mail: rabah.boukherroub@univ-lille.fr  
(<https://orcid.org/0000-0002-9795-9888>)

Rahinah Ibrahim, Universiti Putra Malaysia, Malaysia  
E-mail: rahinah.ibrahim@gmail.com  
(<https://orcid.org/0000-0001-6741-6439>)

Raikhan Beisenova, LN Gumilyov Eurasian National University, Kazakhstan  
E-mail: raihan\_b\_r@mail.ru  
(<https://orcid.org/0000-0003-0913-9503>)

Ramazan Solmaz, Bingol University, Türkiye  
E-mail: rsolmaz@bingol.edu.tr  
(<https://orcid.org/0000-0002-9295-1203>)

Sirin Korulu Koc, Tallinn University, Estonia  
E-mail: sirinkorulu@gmail.com  
(<https://orcid.org/0000-0001-6762-0659>)

Suhendan Ekmekcioglu, MD Anderson Cancer Center, USA  
E-mail: sekmekcioglu@mdanderson.org  
(<https://orcid.org/0000-0003-4079-6632>)

Tommaso Beccari, Università degli Studi di Perugia, Italy  
E-mail: tommaso.beccari@unipg.it  
(<https://orcid.org/0000-0001-9637-6579>)

Yolina Hubenova, Institute of Electrochemistry and Energy Systems, Bulgaria  
E-mail: jolinahubenova@yahoo.com  
(<https://orcid.org/0000-0003-1783-758X>)

## Language editor

Cigdem Sezer Zhmurov, Uskudar University, Türkiye  
E-mail: cigdem.sezerzhmurov@uskudar.edu.tr  
(<https://orcid.org/0000-0002-8423-5063>)

## Publicity managers

Dilan Akagunduz, Istanbul Technical University, Türkiye  
E-mail: dilanakagunduz@gmail.com  
(<https://orcid.org/0000-0002-8057-6688>)

Rumeysa Cebecioglu, Koc University, Türkiye  
E-mail: rmyscbeclu@gmail.com  
(<https://orcid.org/0000-0002-5996-5363>)

Sila Arslan, Istanbul University, Türkiye  
E-mail: arslansilaa@gmail.com  
(<http://orcid.org/0000-0001-8757-264X>)

## Editorial assistant

Burak Kilinc, Uskudar University, Türkiye  
E-mail: burakliosman.kilinc@uskudar.edu.tr  
(<https://orcid.org/0009-0005-0533-8064>)

**Publisher:** Tunc Catal

**Publishing manager:** Prof. Dr. Tunc Catal

**Editorial office:** Uskudar University, Universite Sok. No:14 34662 Altunizade Uskudar, Istanbul-Türkiye

**Email:** editor@euchembioj.com; **Phone:** +90 216 400 2222 (ext. 2417)

**WEB:** <https://euchembioj.com/index.php/pub> **DOI:** <https://doi.org/10.62063/ecb-no2.2024>

**ISSN:** 3023-5839

# The European Chemistry and Biotechnology Journal

Issue 2 • July 2024

## CONTENTS

---

### RESEARCH ARTICLES

---

- Detecting viable but non-culturable lactic acid bacteria following spray-drying and during storage  
Meriam Bouri, Sibel Simsek Yazici, Fikrettin Sahin..... 1-16  
*Editor: Prof. Dr. Tunc Catal*
- 
- Assessing the impact of oleuropein on dyslipidemia in male rats subjected to D-galactose-induced aging: A preliminary study  
Shirin Tarbiat, Beyrivan Aydın, Kübra Ergün, Ali Reza Mohseni..... 17-26  
*Editor: Prof. Dr. Muhsin Konuk*
- 
- A comparative study of glutathione-coated iron oxide and glutathione-coated core-shell magnetic nanoparticles for their antiviral activities  
Pinar Sen, Sevda Demir, Bekir Can Altindisogullari, Fikrettin Sahin..... 27-38  
*Editor: Prof. Dr. Baris Binay*
- 
- Exploring biofilm-forming bacteria for integration into BioCircuit wastewater treatment  
Chontisa Sukkasem..... 39-52  
*Editor: Prof. Dr. Yolina Hubenova*
- 
- Investigation of antiproliferative and antimicrobial activities of carbon nanofiber based aerogels loaded with rutin and krill oil  
Berkan Aktas, Merve Gurboga, Sinem Angin, Pervin Rayaman, Elif Caliskan Salihi, Ozlem Bingol Ozakpinar..... 53-66  
*Editor: Assoc. Prof. Dr. Irina Nakashidze*
-

## RESEARCH ARTICLE

# Detecting viable but non-culturable lactic acid bacteria following spray-drying and during storage

Meriam Bouri <sup>1\*</sup>  | Sibel Simsek Yazici <sup>1,2</sup>  | Fikrettin Sahin <sup>1</sup> <sup>1</sup> Department of Genetics and Bioengineering, Faculty of Engineering, Yeditepe University, İstanbul, Türkiye<sup>2</sup> Yeditepe University R&D and Analysis Central Laboratories, İstanbul, Türkiye\*Corresponding author: E-mail: [mariem\\_bouri@hotmail.fr](mailto:mariem_bouri@hotmail.fr); Ph.: +90-216-578-0619.

**Citation:** Bouri, M., Simsek Yazıcı, S., & Sahin, F. (2024). Detecting viable but non-culturable lactic acid bacteria following spray-drying and during storage. The European chemistry and biotechnology journal, 2, 1-16.  
<https://doi.org/10.62063/ecb-20>

**License:** This article is licensed under a Creative Commons Attribution-NonCommercial 4.0 International License (CC BY-NC 4.0).

**Peer review:** Externally peer reviewed.

**Received:** 27.02.2024

**Accepted:** 23.04.2024

**Published:** 25.07.2024



## Abstract

Microencapsulation with various materials has been used as an efficient method to improve the viability of probiotic bacteria in multiple food products and the human gastrointestinal tract. Although plate count agar is the most commonly used method for evaluating the viability of encapsulated bacteria, it is still far from providing reliable information about the intermediate state between viable and dead bacteria. This study optimized a tetrazolium salt-based colorimetric method for the detection of viable but non-culturable state within encapsulated *Lactobacillus rhamnosus* and *Lactobacillus plantarum* probiotic strains. The viability of encapsulated bacteria was assessed after different spray-drying conditions and also during two months of storage at room temperature. The ability to reduce tetrazolium salts of two lactic acid bacteria was verified and calibrated according to the experimental conditions (strains, incubation time, and microencapsulation material). The loss of bacterial cultivability was species-specific and more problematic throughout the processing than during the storage period. An outlet temperature of 73-75°C yielded a higher viable but non-culturable state level than at 68-69°C, especially in maltodextrin and trehalose powders. Whey protein was statistically the best carrier in preserving viable and culturable encapsulated bacteria after spray-drying and during storage, as compared to sugar-based carriers. The tetrazolium-optimized method was more sensitive and accurate for the evaluation of viable bacteria in microcapsules as compared to the conventional plate count methods available. It showed the high variability of CFU counts on Man-Rogosa-Sharpe (MRS) agar. This colorimetric technique could be considered a real-time, simple, cost-effective, and reliable alternative to culture-based methods in evaluating probiotic microencapsulation efficiency.

**Keywords:** microencapsulation, maltodextrin, plate count agar, probiotic bacteria, tetrazolium salt, trehalose, whey protein.

## Introduction

Many microencapsulation technologies have been developed to accommodate the increasing use of probiotics in functional foods. In the food industry, spray-drying is the most common method to encapsulate probiotic bacteria. This technique presents the advantages of low cost, reproducibility, and rapidity in incorporating probiotics into dairy products (Gardiner et al., 2002; Sharma et al., 2022). On the other hand, the major disadvantage of this technology is the use of high air temperatures that can cause a decrease in bacterial survival after incorporating the bacteria into the encapsulating material through the spray drying process (Tripathi and Giri, 2014; Bommasamudram et al., 2022). In this regard, many encapsulating materials have been tested to produce innovative matrices maintaining the viability of probiotic bacteria at a functional rate during the spray-drying process (Tirta et al., 2023), the subsequent storage (Gullifa et al., 2023), and finally, their passage through the human gastrointestinal tract. In these instances, the viability of the bacteria is evaluated by the direct culturing on agar, also known as colony plate count method (Guerin et al., 2017). Although culture-dependent methods are always used, they do not always provide reliable information about the viability of cells since they cannot detect viable but non-cultivable (VBNC) bacteria. The VBNC state is induced naturally in cells by environmental stresses such as high temperature and drying (Zhao et al., 2017), as exemplified by the case of spray drying. Bacterial cells in this state may not grow on the standard bacteriological media on which they previously developed colonies. However, they are still alive and can show metabolic activity (Oliver, 2005). Bacterial physiological indicators should be more sensitive to estimate bacterial survival. Among various methods using the level of enzymatic activity to monitor microbial population density, assays based on biotransformations of tetrazolium salts (TS) have gained much popularity. This test principle is based on the enzymatic reduction of lightly colored TS into an intense purple-blue colored formazan, which can be quantified spectrophotometrically. For a long time, the use of TS reduction has been limited to eukaryotic cell research. In contrast, the application of this procedure for viability estimation of microbial cells following TS reduction by bacteria is still poorly understood (Tachon et al., 2009). One of the most common examples of TS used in bioassays is 3-(4,5-dimethylthiazol-2-yl)-2,5-diphenyl tetrazolium bromide (MTT). MTT has been applied in cell proliferation assays (Tsukatani et al., 2008), multidrug-resistant bacteria detection (Montoro et al., 2005), biofilm formation evaluation (Brambilla et al., 2014) and indirect quantification of antibacterial compounds (Wang et al., 2007). MTT produces less background absorbance than WST-5, WST-8, and XTT, making it a more reliable choice (Wang et al., 2010). MTS (3-(4,5-dimethylthiazol-2-yl)-5-(3-carboxy-methoxyphenyl)-2-(4-sulfophenyl)-2H tetrazolium) assay is often described as a 'one-step' MTT assay, since it allows a researcher to add the reagent directly to the cell culture without the addition of DMSO or isopropanol, as needed in the MTT assay. The MTS compound produces a formazan product, which in the presence of phenazine methosulfate (PMS), has a maximal absorbance at 490-500 nm in phosphate-buffered saline. The ability of bacteria to reduce tetrazolium salts depends on the salt type and the bacterial species. For example, (Tsukatani et al., 2008) showed that Gram-positive bacteria generally reduced TS that form water-soluble formazan better than Gram-negative bacteria. Thus, the TS assays must be conducted under correctly optimized conditions for a reliable absorbance value proportional to the number of viable cells (Berridge et al., 2005).

The present work investigated the potential of the MTS-based method for monitoring the viability of encapsulated lactic acid bacteria (*Lactobacillus rhamnosus* GG and *Lactobacillus plantarum* 299v) in different matrices after spray-drying. The VBNC state of encapsulated bacteria was estimated through the difference in bacteria enumeration results between the colony plate counting method and the newly optimized MTS assay. The sensitivity of both approaches in assessing bacteria losses and, therefore, the microencapsulation efficiency under different conditions was also evaluated.

## Materials and methods

### **Culture media and growth conditions**

The encapsulation by spray-drying was performed on mesophilic lactic acid bacteria (LAB) reference strains *L. rhamnosus* GG (ATCC 53103) and *L. plantarum* 299v. *L. rhamnosus* GG were purchased from the American Type Culture Collection (Lot: 70006824), while *L. plantarum* 299v was recovered from a commercial probiotic supplement. The identity and the purity of the strain have been confirmed by MALDI TOF (Bruker Daltonics, Bremen, Germany). Man–Rogosa–Sharpe (MRS) agar medium (Acumedia, USA) propagated the bacteria. MRS broth (Acumedia, USA) was used as a pre-culture medium for the inoculum preparation. *L. rhamnosus* GG and *L. plantarum* 299v were cultured at 37 °C and 5% CO<sub>2</sub> for 48 hours on MRS agar and then overnight in MRS broth under shaking.

### **Preparation of microencapsulation materials and feeding solution**

Whey protein isolate (WP) (Davisco, USA), maltodextrin (MD) (Sigma Aldrich, Germany), and trehalose (Tr) (Cargill, Germany) were used as materials for LAB microencapsulation. WP solution was prepared by rehydration of whey protein isolate at 15% (m/v) in 100 mL of sterile distilled water (SDW). Rehydration was carried out as described by Guerin et al. (2017). The solution was stirred briefly for 2 hours at room temperature (25 °C). After rehydration, WP solutions were denatured by heating at 78 °C for 10 minutes and cooled at 4 °C. MD and Tr solutions were prepared by rehydration of the powder at 15% (m/v) in 100 mL of SDW before being autoclaved at 121 °C for 15 minutes. The feeding solution was prepared by mixing the encapsulation material solution (100 mL) with an overnight culture (taken at the beginning of the stationary phase) of the LAB strains to a final concentration of 10<sup>11</sup> cfu/mL.

### **Spray-drying conditions**

LAB strains were encapsulated in different encapsulation materials using a spray-dryer (Bakon B15, Turkey) equipped with a 0.7 mm nozzle under the following conditions: pump 3 mL/min, aspirator 80% and compressor 11 L/min. Different inlet temperatures (InletT) were applied: 105 °C and 115 °C. The outlet temperatures (OutletT) obtained were 68–69 °C and 73–75 °C, respectively (Guerin et al., 2017).

### **Bacterial cultivability**

Conventional colony plate counting was used to study the effect of the spray-drying process and storage conditions on the cultivability of the LAB cells. One gram of dry samples was rehydrated in 10 mL of PBS solution for 5 minutes at room temperature under stirring. The homogenized solution was serially diluted with PBS (1X) (Sigma, Germany) and plated on MRS agar. The colony-forming units were determined after 48 hours of incubation at 37 °C and 5% CO<sub>2</sub>.

### **MTS assay optimization**

The correlation between the MTS absorbance at OD<sub>490</sub> and the number of living cells from fresh cultures of LAB were established in initial experiments to be used for bacterial VBNC state assessment after spray drying and during storage. For this purpose, CellTiter 96® Aqueous MTS Reagent Powder (Promega, USA) was applied according to the manufacturer's instructions. Briefly, ten milliliters of an overnight bacterial culture of *L. rhamnosus* GG or *L. plantarum* 299v were aliquoted into ten Eppendorf tubes and centrifuged at 11,000 g (Sigma 3-18KS, Germany) for 15 min at 4 °C to discard the supernatant. Ten-fold and two-fold serial dilutions of the bacterial pellet were suspended in the MTS master mix containing PBS (1X) + glucose (4.5 g/L) and MTS 10 % (v/v). It is important to note that three passages of the bacterial suspension through an aseptic syringe needle are needed. One milliliter of each bacterial suspension was used to determine colony-forming units (CFU) after plating on MRS agar and incubation at 37 °C and 5% CO<sub>2</sub> for 48 hours. The remaining suspension was incubated under the same conditions for 5 hours. After every 20 minutes, 1 mL of the MTS bacterial solution was centrifuged, the pellet was discarded, and the supernatant was added to a 96-well plate (100 µL/well) for optical density analysis. The optical density was recorded by a microplate scanning spectrophotometer (Bio-Rad xMark, USA). The correlation of the MTS optical density units at OD<sub>490</sub> (ODU490) to colony-forming units of fresh cultures enumerated on MRS agar was established by a regression analysis using Microsoft Excel (2013). Killed bacteria, generated by incubation in 70% isopropyl alcohol for 30 min., were used as a negative control.

### **VBNC state assessment**

The entrapped bacteria were released from microcapsules according to the method of Semyonov et al. (2011) with some modifications. One gram of spray-dried powders was rehydrated in 10 mL of PBS (1X) (Sigma-Adrich, UK) for 5 minutes under stirring at room temperature. As described above, the bacterial pellet obtained by centrifugation was washed twice and re-suspended in the MTS master mix. After 3.5 hours of incubation in the dark at 37 °C and 5% CO<sub>2</sub>, bacterial solutions were centrifuged at 11,000 g for 15 minutes at 4 °C. The optical density of the supernatant was then measured at 490 nm. Killed bacteria obtained from encapsulated LAB dissolved into 70% isopropyl alcohol for 30 minutes (mixed every 15 minutes) were washed with PBS (1X) and recovered for use as a negative control specific for each encapsulation material. A bacteria-free master mix was used as a general negative control.

The amount of viable entrapped LAB is determined according to the previously established correlation between ODU490 and the fresh cultivable inoculum (C) of LAB (cfu/g). The VBNC state is expressed in cfu/g, and the percentage of VBNC level (%) was calculated as follows:

$$\text{VBNC} = V - C \quad [1]$$

$$\text{VBNC (\%)} = \log_{10}(\text{VBNC}) \times [100 / (\log_{10} I)] \quad [2]$$

Where "V" is the viable encapsulated LAB (cfu/g) obtained by MTS assay, "C" is the culturable encapsulated LAB (cfu/g) enumerated on MRS agar by the conventional spread plate technique, and "I" is the initial LAB inoculum (cfu/g) before the spray drying process.

### **Evaluation of the microencapsulation**

The microencapsulation process was evaluated according to the bacterial losses after microencapsulation by the two methods: i/ the conventional colony plate counting technique (MEC)

and ii/ the MTS assay optimized in this study (MER). MEC and MER were calculated as follows:

$$\text{MEC (\%)} = 100 - [100 \times (C/I)], \quad [3]$$

$$\text{MER (\%)} = 100 - [100 \times (V/I)], \quad [4]$$

Where “C” is the culturable microencapsulated LAB (log<sub>10</sub>cfu/g) on MRS agar, “I” is the initial LAB inoculum (log<sub>10</sub>cfu/g) before the spray-drying process, and “V” is the viable microencapsulated LAB (log<sub>10</sub>cfu/g) determined by the MTS assay.

### **Statistical analysis**

All the experiments were conducted in triplicate (n = 3). Data were subjected to analysis of variance (ANOVA) using SPSS software (version 20). The significance of mean differences was determined using Duncan's test, and responses were judged significant at the 5% level ( $P \leq 0.05$ ).

## **Results and discussion**

Measuring the survival of probiotic organisms under harsh conditions encountered during food processing or through the gastrointestinal system is a significant challenge for researchers and producers. The viability of the starter cultures is traditionally quantified by the colony plate counting method, which evaluates the ability of cells to grow in an appropriate medium. Hence, the population of cultivable bacteria is determined. However, under stress conditions and different industrial processes used to produce dried biomass, many bacterial species enter a physiologically VBNC state (Guerin et al., 2017; Semyonov et al., 2011). In the VBNC state, although they are alive, bacteria cannot develop colonies on standard bacteriological media on which they used to grow (Oliver, 2005). Therefore, cell viability evaluation based on the ability to form colonies may lead to an underestimation of viable cells, as in the case of microencapsulation. Additionally, culture-dependent methods lack the resolving power to provide real-time results, and bacteria may occur in chains and/or clumps, resulting in an underestimation of true bacterial counts (Doherty et al., 2010; Guerin et al., 2017). Thus, more sensitive and rapid methods have been developed to monitor probiotic survival, such as quantitative real-time PCR (Gueimonde et al. 2004), fluorescent in situ hybridization (FISH), and flow cytometry (Breeuwer and Abee, 2005; Lahtinen et al., 2006). However, the industrial adoption failure of these methods results from their lack of cost-efficiency and scope for the extension of product applications (Lahtinen et al., 2006). In this context, a simple colorimetric method, based on the bacterial ability to reduce MTS, was optimized to assess the level of the VBNC state within encapsulated LAB under different conditions and evaluate the efficiency of the microencapsulation process.

### **Optimization of the MTS assay**

**Incubation time:** The kinetics of MTS reduction by *L. rhamnosus* GG and *L. plantarum* 299v cells were determined with different inoculum concentrations (obtained from two-fold serial dilutions), as shown in Figure 1. There was a gradual increase in the absorbance at OD<sub>490</sub> and a plateau after almost 3-4 hours for the two LAB strains.



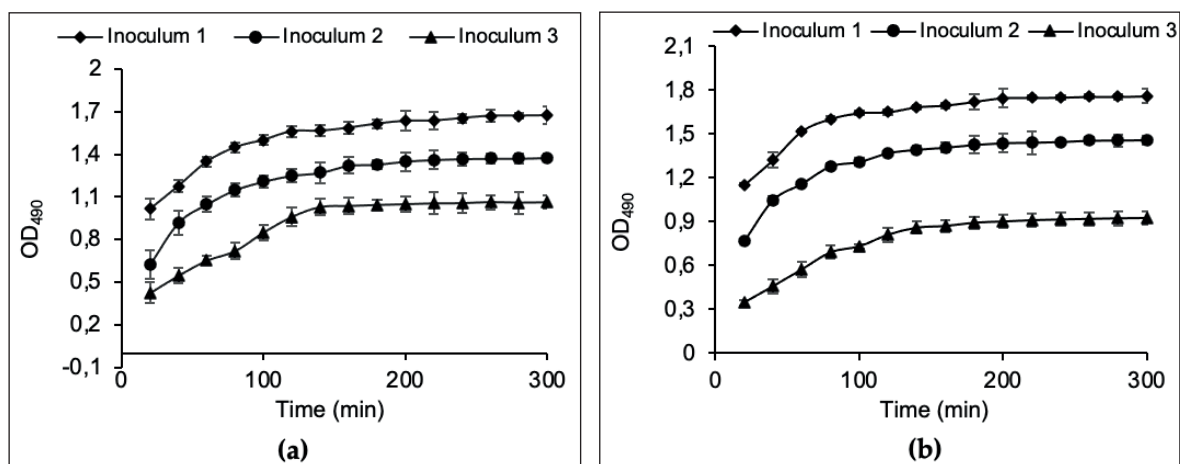


**Figure 1.** Kinetics of MTS reduction by overnight fresh cultures of (a) *L. rhamnosus* GG; and (b) *L. plantarum* 299v, at different cells concentrations: inoculum 1 (▲), inoculum 2 (●), and inoculum 3 (■). Bacterial cells were incubated with MTS and absorbance was read at OD<sub>490</sub> each 20 min. Each point is the mean of three replicates.

Only a few uses of tetrazolium salts have been reported for lactic acid bacteria (LAB), probably because the acid produced by LAB inhibits tetrazolium salt reduction (Tachon et al., 2009). In this respect, the ability of *L. rhamnosus* G.G. and *L. plantarum* 299v to reduce MTS was first verified. We chose 3.5 hours for the standard procedure. Our results agree with the observations of previous works reporting that 3 to 4 hours of incubation with tri-phenyl tetrazolium chloride (TTC) is adequate for developing a measurable color intensity in a log-phase bacterial culture (Tengerdy et al., 1967; Oh and Hong, 2022).

**Correlation between ODU<sub>490</sub> and CFU:** As reported previously, the color intensity of the reduced tetrazolium salt, formed by the reducing activity of bacteria, was proportional to the number of actively growing bacteria in the culture (Tengerdy et al., 1967). Therefore, the correlation between MTS absorbance units at OD<sub>490</sub> to logarithmic colony-forming units on MRS agar media was performed in the initial experiments. No coloration was observed with dead bacteria in negative controls, which means that MTS reduction is related to viable bacteria only. Linear relationships between the absorbance obtained by the present method and the colony-forming units were obtained with good correlation coefficients:  $R_{2r} = 0.9833 (\pm 0.0041)$  and  $R_{2p} = 0.9892 (\pm 0.0036)$  for *L. rhamnosus* GG and *L. plantarum* 299v, respectively. The CFUs obtained at various MTS reduction absorbance levels were regressed to linear functions and yield using the following equations:

$$Y_r = (2.108 \times X_r) - 395648 \quad [5]$$

$$Y_p = (3.109 \times X_p) - 2.108 \quad [6]$$

$Y_r$  and  $Y_p$  represent the CFUMTS (cfu/100  $\mu$ L) of *L. rhamnosus* GG and *L. plantarum* 299v, respectively, and  $X_r$  and  $X_p$  represent the MTS absorbance at OD<sub>490</sub> units (ODU<sub>490</sub>) for *L. rhamnosus* GG and *L. plantarum* 299v, respectively.

MTS reduction was related to viable bacteria only. No coloration was observed with dead bacteria. Differences in linear relationships between MTS absorbance and viable cell density (Equations 5 and 6) regressed from the two LAB strains show that this correlation is species-specific, as reported previously for many bacterial species (Tachon et al., 2009; Tsukatani et al., 2008). Therefore, the

number of actively growing bacteria of a given species should be calculated from its calibration curves. Nevertheless, there was no reliable absorbance for bacterial densities higher than  $5 \times 10^{11}$  cfu/mL and less than  $10^4$  cfu/mL. With high bacterial densities, a discoloration of MTS was observed. This could be because high bacterial densities can transform formazan into colorless derivatives, as observed previously with prolonged bacterial incubation in tetrazolium salt (Stowe et al., 1995; Xu et al., 2023). The MTS assay was not sufficiently sensitive for very low bacterial densities, as reported previously, with several bacterial species and different tetrazolium salts (Tsukatani et al., 2008; Wang et al., 2007). A concentration of  $10^6$  cfu/mL in the product at consumption or a daily intake of  $10^8$ - $10^9$  probiotics is often recommended (Tripathi and Giri, 2014). Considering these reference values, our study's limits of MTS sensitivity levels are not part of evaluating probiotic encapsulation efficiency. Nevertheless, materials used for encapsulation (WP, MD, and Tr) interfered with the MTS and generated a brownish coloration. Several chemicals were reported to cause abiotic TS reduction in cell-free medium (Grela et al., 2018), such as luteolin, quercetin, plant extracts (Peng et al., 2005), enzyme inhibitors (Weyermann et al., 2005), cysteine, and thioglycolate-containing medium (Oren et al., 1987), salts and complexes containing copper (II) (Perez et al., 2017). In this respect, we removed the MRS medium and encapsulation materials before the MTS application. Many colorimetric methods based on the capacity of bacteria to reduce tetrazolium salts have been used as a rapid and indirect alternative for cell growth evaluations (Mshana et al., 1998; Foongladda et al., 2002; Montoro et al., 2005; Wang et al., 2007; Tsukatani et al., 2008; Brambilla et al., 2014). The VBNC state has been recently reported in several LAB strains (Liu et al., 2017; Wang et al., 2020). However, to our knowledge, this is the first optimization of the tetrazolium salt-based method for the survivability assessment of microencapsulated lactic acid bacteria in complex matrices.

### Cultivability of LAB throughout spray drying

The percentage of cultivable and VBNC state of *L. rhamnosus* GG and *L. plantarum* 299v just after the spray drying process were compared under different OutletT(s) and encapsulation materials (Figure 2).

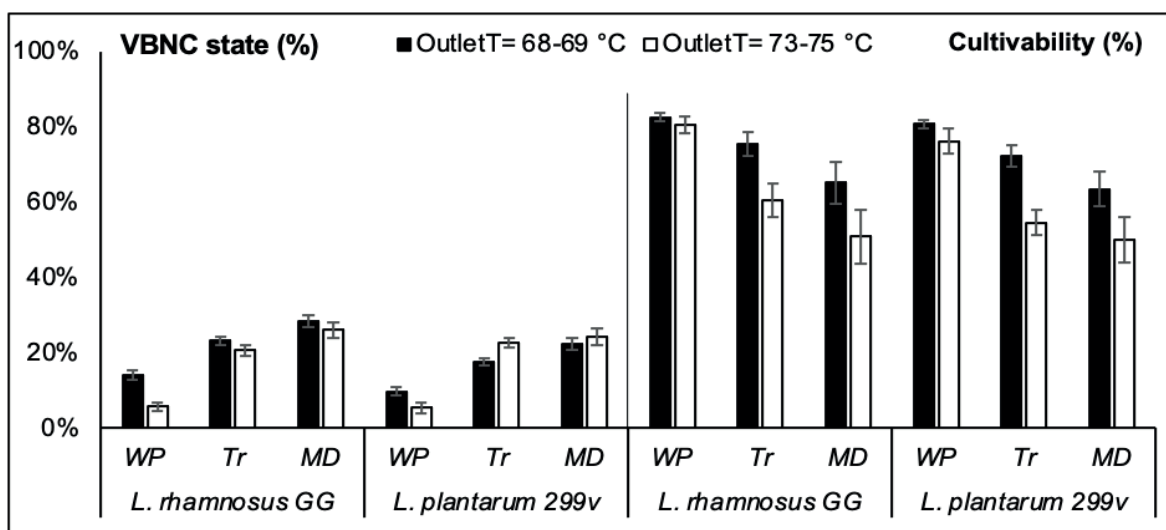


**Figure 2.** The effect of spray drying conditions on the cultivability of LAB strains after microencapsulation with different matrix at different outlet temperatures: WP- whey protein, MD- Maltodextrin and Tr- Trehalose. (■) Outlet temperature = 68-69 °C and (□) Outlet temperature = 73-75 °C.

Viabilities of LAB strains, after spray drying under different conditions estimated according to equations 5 and 6, were compared to the colony plate counts on MRS agar. The difference between the two methods revealed the importance of the VBNC state level within the encapsulated LAB. This physiological state was related to different factors related to microencapsulation and storage conditions. *L. rhamnosus* GG and *L. plantarum* 299v showed different responses, in the matter of VBNC state level, toward the OutletT increasing under various encapsulation materials.

Compared to *L. plantarum* 299v, *L. rhamnosus* GG was a relatively better spray-drying survivor. Heat resistance is a strain-specific trait that has already been reported in previous studies (Gardiner et al., 2002; Goderska and Czarnecki, 2008; Pérez-Chabela et al., 2017; Malmo et al., 2021). Although the loss of cultivability was significantly ( $P \leq 0.05$ ) less exhibited by *L. plantarum* 299v than *L. rhamnosus* GG under OutletT = 68-69 °C, this was not available under OutletT = 73-75 °C. This is consistent with the fact that the viability of bacteria during spray drying is not only related to thermal tolerance, but also associated with cell damage due to shear stress, as reported previously (Corcoran et al., 2004; Lievens et al., 1994; Kiekens et al., 2019). The lowest levels of VBNC state were recorded when microencapsulation was carried with WP, independently to the used LAB strain or OutletT. Our results show the importance of WP in reducing bacterial cell damage during spray drying. Physical stresses like low or high temperatures and drying induce sublethal damaged bacteria to enter the VBNC state (Zhao et al., 2017; Silva et al., 2012; Arvaniti et al., 2021). Generally, milk proteins are known to offer several advantages in comparison to other widely used biomaterials in the microencapsulation of probiotics (Abd El-Salam and El-Shibiny, 2012; Heidebach et al., 2012; Tavares et al., 2014). This was also confirmed by the plate count method used in this study, given that the highest cultivable population on MRS agar was recorded with WP regardless of the strain type or the OutletT. Moreover, the effect of the spray drying temperature on the cultivability of LAB strains was significant ( $P \leq 0.05$ ) only when MD or Tr were used as encapsulation material.

### **Cultivability of LAB during storage**

During storage at room temperature, the percentage of cultivable and VBNC state of spray-dried *L. rhamnosus* GG and *L. plantarum* 299v varied differentially according to the used OutletT and encapsulation material (Figure 3).

The VBNC state of encapsulated LAB strains was significantly more stable ( $P \leq 0.05$ ) during the storage under OutletT (68-69 °C) for both strains encapsulated with different materials. Under higher OutletT (73-75 °C), the VBNC state was more stable with bacteria encapsulated with only WP and Tr. The two LAB strains exhibited the lowest VBNC state in WP powders during storage (i.e., less than 10%). The two LAB strains showed different evolution of their VBNC rate during storage. While the VBNC state of encapsulated *L. rhamnosus* GG increased with time, under OutletT (73-75 °C), encapsulated *L. plantarum* 299v showed a decreasing rate of VBNC state. The number of cultivable encapsulated LAB strains significantly decreased after thirty days of storage regardless of the encapsulation material used and the OutletT. The viability of bacteria encapsulated with MD and Tr decreased drastically after thirty days of storage.

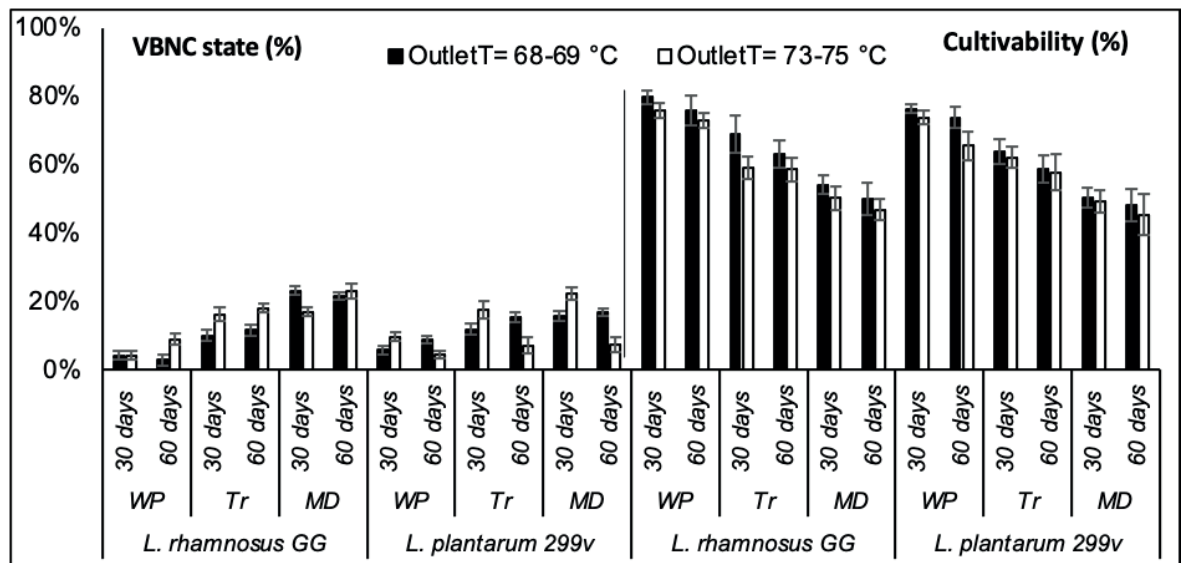


**Figure 3.** The evolution of VBNC state and cultivability percentages of encapsulated LAB strains according to spray drying conditions during storage (30 days and 60 days) at room temperatures: WP- whey protein, MD- Maltodextrin and Tr- Trehalose. (■) Outlet temperature = 68-69 °C and (□) Outlet temperature = 73-75 °C.

Although optimal conditions required to protect probiotics during spray drying and storage are well documented, it is still uncertain that cell damage can effectively predict survival during storage (Chávez and Ledebøer, 2007; Teixeira et al., 1995). In whey powders, LAB strains showed the highest cultivable percentage. Sugar and protein-containing formulations were reported to improve storage stability. Tr was better than MD in maintaining bacterial viability during storage among the two sugar powders used. Silljé et al. (1999) reported that Tr was a storage factor during carbon starvation in *Saccharomyces cerevisiae*. The changes in cultivability of encapsulated LAB strains were not significant between thirty days and sixteen days of storage except for the *L. plantarum* strain in WP powders produced at OutletT=73-75 °C. The difference between the amounts of cultivable bacteria of the two LAB species during storage in different powders shows that this response is species-specific, as reported in previous studies (Pérez-Chabela et al., 2017; Corcoran et al., 2004). The impact of higher OutletT on the change of bacterial cultivability during storage was not always significant. This could be explained by the fact that the physicochemical properties of powders obtained under different drying temperatures in this study are not sufficiently distinct to affect the storage stability differentially. It was reported that at inlet and outlet temperatures above 100 °C and 60 °C, respectively, the moisture content of the dry powder is below 4%, which is required for safe storage (Chávez and Ledebøer, 2007).

#### Microencapsulation evaluation

Microencapsulation efficiency was evaluated based on the percentage of dead bacteria after spray drying and storage, according to the two methods as presented in Figure 4. The difference between bacterial losses observed in the two methods was significant, especially after the spray drying process ( $P < 0.05$ ); the MTS assay showed fewer LAB losses than the direct culture method. Nevertheless, during storage, the effect of the technique used on the recorded bacterial losses was less significant,

especially for bacteria encapsulated in WP.

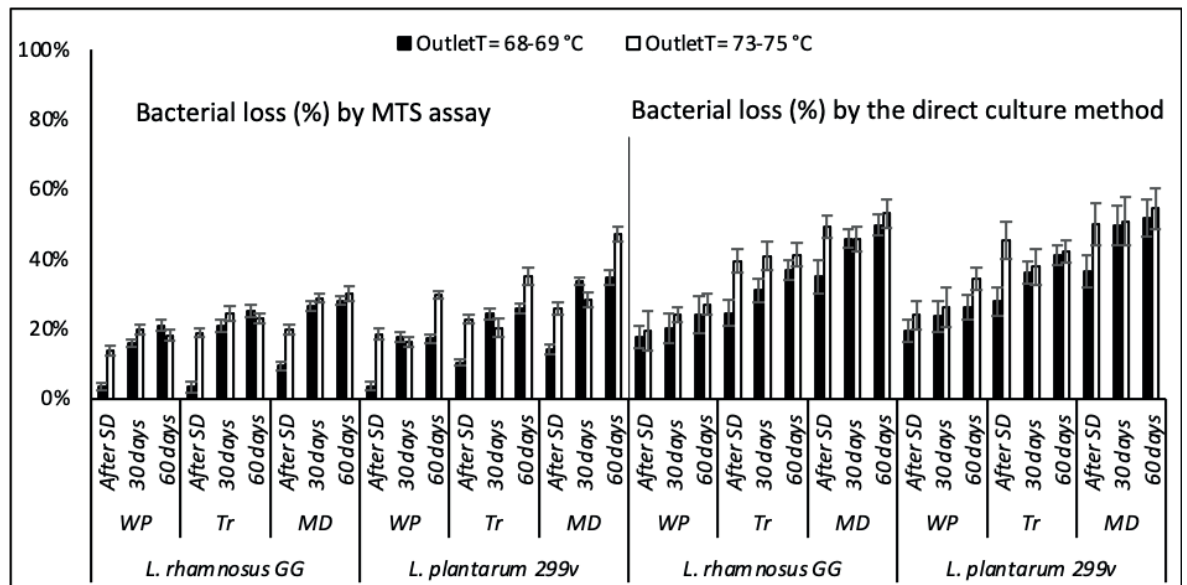


**Figure 4.** Bacteria losses after microencapsulation according to the MTS assay and the direct culture method, after the spray drying process (After S.P.) and during the storage (after 30 days and 60 days) at room temperature: WP- whey protein, MD- Maltodextrin and Tr- Trehalose. (■) Outlet temperature = 68-69 °C and (□) Outlet temperature = 73-75 °C.

The significance of the OutletT effect on LAB viability was consistently observed with the MTS assay, unlike the direct culture method, which rarely could reveal the impact of higher OutletT on bacterial survivability during storage. The microencapsulation process seems more responsible for the VBNC state induction in LAB strains than starvation during storage.

The high standard deviation values of LAB losses recorded by the direct culture method masked the effect of some factors on the efficiency of the microencapsulation process (especially LAB species, OutletTs, and storage time). In contrast, the MTS assay revealed the differences between the effects of the used OutletTs on the bacterial mortality during the first 30 days of storage and the pronounced sensitivity of strain *L. plantarum* 299v toward higher Outlet T during the second month of storage. However, the differences between the effects of encapsulation materials on the LAB losses were significant according to both methods. WP exhibited the lowest LAB losses after spray-drying and during storage at room temperature, according to the MTS assay and the direct culture method.

Based on the above observations, the MTS assay optimized in this study allowed the assessment of the VBNC state within encapsulated LAB strains throughout spray drying and storage. It was more accurate in evaluating the encapsulation efficiency than the direct culture method. Besides the high variability of CFU counts on MRS agar within the same treatment, the direct culture method lacks the resolving power to provide real-time results (Lahtinen et al., 2006). Given the bacterial chain fragmentation outcome (Guerin et al., 2017; Doherty et al., 2010) or/and the VBNC state induced after the spray drying process, the use of a culture-based method may result in underestimation of true bacterial accounts as well as the encapsulation efficiency. Moreover, detecting VBNC and injury states within bacteria is relevant in the food industry. Depreciating the product's safety status may result in a potential risk of foodborne pathogens or reduced shelf life (Silva et al., 2012; Wesche

et al., 2009). Sublethal damaged bacterial cells usually can repair their damages under suitable conditions so they can grow again (Espina et al., 2016). Favorable growth conditions with a source of energy and an ideal stoichiometric ratio of carbon to inorganic elements were reported to be capable of reversing the VBNC state (Ayrapetyan and Oliver, 2016; Ramamurthy et al., 2014). Hence, if recovery phenomena occur, the intermediate state between viable and dead cells should be considered when evaluating the probiotic shelf life, particularly in the case of drying technologies. Nevertheless, VBNC bacteria's fate once they reach their host cells is still unknown.

## Conclusions

This study evaluated the efficacy of MTS utilization to assess the VBNC state and the survivability of LAB strains after spray drying and storage. Once optimized, the MTS assay could be a simple, low-cost, real-time, and reliable alternative for the direct culture method to monitor microencapsulated bacterial survival in complex matrices. The VBNC state was detected within bacteria throughout spray drying and during storage by the difference between the expected colony-forming counts estimated by the MTS assay and the enumerated colonies on MRS agar. The accuracy and reliability of the calorimetric method used in our study should be confirmed with an enzymatic or molecular secondary method. The level of the VBNC state within encapsulated bacteria was related to different conditions of the spray drying process. It is still necessary to know the impact of the loss of cultivability on the product's shelf life and the strain's efficacy in fulfilling probiotic functions in the gastrointestinal tract.

## Acknowledgements

The authors are also grateful to Bernard R. Glick and R. Z. Sayyed, respectively from the University of Waterloo Canada, Department of Biology, and the PSGVP Mandal's Arts, Science and Commerce College Department of Microbiology, Shahada-India, for their critical manuscript reading. The authors would also like to thank Neşe Güldür and Eylem Çalışkan from (YU-AGAM, Istanbul) for their technical support.

## Funding

This research received no external funding.

## Conflict of interest

The authors declare no conflict of interest.

## Data availability statement

All data are available here.

## Ethics committee approval

Ethics committee approval is not required for this study.

## Authors' contribution statement

The authors acknowledge their contributions to this paper as follows: **Study conception and design:** (MB); **Data collection:** (MB); **Analysis and interpretation of results:** (MB and SŞY); **Manuscript draft preparation:** (MB, SŞY and FŞ). All authors reviewed the results and approved the final version of the manuscript.

### ORCID*s* and emails of the authors

Meriam Bouri | <https://orcid.org/0000-0002-2391-8768> | [mariam\\_bouri@hotmail.fr](mailto:mariam_bouri@hotmail.fr)

Sibel Simsek Yazici | <https://orcid.org/0009-0008-8647-5061> | [sibel.simsek@yeditepe.edu.tr](mailto:sibel.simsek@yeditepe.edu.tr)

Fikrettin Sahin | <https://orcid.org/0000-0003-1503-5567> | [fikrettinsahin@gmail.com](mailto:fikrettinsahin@gmail.com)

## References

- Abd El-Salam, M.H., & El-Shibiny, S. (2012). Formation and potential uses of milk proteins as nanodelivery vehicles for nutraceuticals: a review. *Int. J. Dairy. Tech.*, 65, 13-21. <https://doi.org/10.1111/j.1471-0307.2011.00737.x>
- Arvaniti, M., Tsakanikas, P., Papadopoulou, V., Giannakopoulou, A., & Skandamis, P. (2021). Listeria mono-cytogenes Sublethal Injury and Viable-but-Nonculturable State Induced by Acidic Conditions and Disinfectants. *Microbiol Spectr.* 9(3), e0137721. <https://doi.org/10.1128/Spectrum.01377-21>
- Ayrapetyan, M., & Oliver, J.D. (2016). The viable but non-culturable state and its relevance in food safety. *Curr. Op. Food. Sci.*, 8, 127-133. <https://doi.org/10.1016/j.cofs.2016.04.010>
- Berridge, M.V., Herst, M.P., & Tan, A.S. (2005). Tetrazolium dyes as tools in cell biology: new insights into their cellular reduction. *Biotech. Annu. Rev.*, 11, 127–152. [https://doi.org/10.1016/S1387-2656\(05\)11004-7](https://doi.org/10.1016/S1387-2656(05)11004-7)
- Bommasamudram J., Muthu A., & Devappa S. (2022). Effect of sub-lethal heat stress on viability of Lacticaseibacillus casei N in spray-dried powders, *LWT*, 155, 112904. <https://doi.org/10.1016/j.lwt.2021.112904>
- Brambilla, E., Ionescu, A., Cazzaniga, G., Edefonti, V., & Gagliani, M. (2014). The influence of antibacterial toothpastes on in vitro Streptococcus mutans biofilm formation: a continuous culture study. *Am. J. Dent.*, 27(3), 160–166.
- Breeuwer, P., & Abee, T. (2005). Assessment of viability of microorganisms employing fluorescence techniques. *Int. J. Food. Microbiol.*, 5(1-3), 193-200. [https://doi.org/10.1016/S0168-1605\(00\)00163-X](https://doi.org/10.1016/S0168-1605(00)00163-X)
- Chávez, B.E., & Ledebøer, A.M. (2007). Drying of Probiotics: Optimization of Formulation and Process to Enhance Storage Survival. *Drying Technol.*, 25, 1193-1201. <https://doi.org/10.1080/07373930701438576>
- Corcoran, B.M., Ross, R.P., Fitzgerald, G.F., & Stanton, C. (2004). Comparative survival of probiotic lactobacilli spray-dried in the presence of prebiotic substances. *J. App. Microbiol.*, 96(5), 1024-1039. <https://doi.org/10.1111/j.1365-2672.2004.02219.x>
- Doherty, S.B., Wang, L., Ross, R.P., Stanton, C., Fitzgerald, G.F., & Brodkorb, A. (2010). Use of viability staining in combination with flow cytometry for rapid viability assessment of Lactobacillus rhamnosus G.G. in complex protein matrices. *J. Microbiol. Methods.*, 82(3), 301-310. <https://doi.org/10.1016/j.mimet.2010.07.003>
- Espina, L., García-Gonzalo, D., & Pagán, R. (2016). Detection of thermal sublethal injury in Escherichia coli via the selective medium plating technique: mechanisms and improvements.

- Front. Microbiol.*, 7, 1376. <https://doi.org/10.3389/fmicb.2016.01376>
- Foongladda, S., Roengsanthia, D., Arjattanakool, W., Chuchottaworn, C., Chaiprasert, A., & Franzblau, S.G. (2002). Rapid and simple MTT method for rifampicin and isoniazid susceptibility testing of *Mycobacterium tuberculosis*. *Int. J. Tuberc. Lung. Dis.*, 6, 1118–1122.
- Gardiner, G.E., Bouchier, P., O'Sullivan, E., Kelly, J., Collins, J.K., Fitzgerald, G., Ross, R.P., & Catherine, S. (2002). A spray-dried cul-ture for probiotic Cheddar cheese manufacture. *Int. Dairy J.*, 12, 749-756. [https://doi.org/10.1016/S0958-6946\(02\)00072-9](https://doi.org/10.1016/S0958-6946(02)00072-9)
- Goderska, K., & Czarnecki, Z. (2008). Influence of microencapsulation and spray drying on the viability of *Lactobacillus* and *Bifidobacterium* strains. *Pol. J. Microbiol.*, 57(2), 135-40.
- Grela, E., Kozłowska, J., & Grabowiecka, A. (2018). Current methodology of MTT assay in bacteria—a review. *Acta Histochem.*, 120(4), 303-311. <https://doi.org/10.1016/j.acthis.2018.03.007>
- Gueimonde, M., Tölkö, S., Korpimäki, T., & Salminen, S. (2004). New real-time quantitative PCR procedure for quantification of bifidobacteria in human fecal samples. *Appl. Environ. Microbiol.*, 70(7), 4165-4169. <https://doi.org/10.1128/AEM.70.7.4165-4169.2004>
- Guerin, J., Petit, J., Burgain, J., Borges, F., Bhandari, B., Perroud, C., Desorby, S., Scher, J., & Gaiani, C. (2017). *Lactobacillus rhamnosus* G.G. encapsulation by spray-drying: Milk proteins clotting control to produce innovative matrices. *J. Food. Eng.*, 193, 10-19. <https://doi.org/10.1016/j.jfoodeng.2016.08.008>
- Gullifa, G., Risoluti, R., Mazzoni, C., Barone, L., Papa, E., Battistini, A., Martin Fraguas, R., & Materazzi, S. (2023). Microencapsulation by a Spray Drying Approach to Produce Innovative Probiotics-Based Products Extending the Shelf-Life in Non-Refrigerated Conditions. *Molecules*, 28, 860. <https://doi.org/10.3390/molecules28020860>
- Heidebach, T., Först, P., & Kulozik, U. (2012). Microencapsulation of Probiotic Cells for Food Applications. *Crit. Rev. Food Sci. Nutr.*, 52, 291–311. <https://doi.org/10.1080/10408398.2010.499801>
- Kiekens, S., Vandenheuvel, D., Broeckx, G., Claes, I., Allonsius, C., De Boeck, I., Thys, S., Timmermans, J.P., Kiekens, F., Lebeer, S. (2019). Impact of spray-drying on the pili of *Lactobacillus rhamnosus* GG. *Microb Biotechnol.*, 12(5), 849-855. <https://doi.org/10.1111/1751-7915.13426>
- Lahtinen, S.J., Gueimonde, M., Ouwehand, A.C., Reinikainen, J.P., & Salminen, S.J. (2006). Comparison of four methods to enumerate probiotic bifidobacteria in a fermented food product. *Food Microbiol.*, 23, 571-577. <https://doi.org/10.1016/j.fm.2005.09.001>
- Lievense, L.C., Verbreek, M.A., Noomen, A., & Van'tRiet, K. (1994). Mechanism of dehydration inactivation of *Lactobacillus plantarum*. *Appl. Microbiol. Biotechnol.*, 41, 90-94. <https://doi.org/10.1007/BF00166087>
- Liu, J., Li, L., Li, B., Peters, B. M., Deng, Y., Xu, Z., et al. (2017). First study on the formation and resuscitation of viable but nonculturable state and beer spoilage capability of *Lactobacillus lindneri*. *Microb. Pathog.* 107, 219–224. <https://doi.org/10.1016/j.micpath.2017.03.043>
- Malmö, C., Giordano, I., & Mauriello, G. (2021). Effect of Microencapsulation on Survival at Simulated Gastrointestinal Conditions and Heat Treatment of a Non Probiotic Strain, *Lactiplantibacillus plantarum* 48M, and the Probiotic Strain *Limosilactobacillus reuteri* DSM 17938. *Foods*, 10, 217.



<https://doi.org/10.3390/foods10020217>

- Montoro, E., Lemus, D., Echemendia, M., Martin, A., Portaels, F., & Palomino, J.C. (2005). Comparative evaluation of the nitrate re-duction assay, the MTT test, and the resazurin microtitre assay for drug susceptibility testing of clinical isolates of Myco-bacterium tuberculosis. *J. Antimicrob. Chemother.*, 55, 500–505. <https://doi.org/10.1093/jac/dki023>
- Mshana, R.N., Tadesse, G., Abate, G., & Miorner, H. (1998). Use of 3-(4,5-dimethylthiazol-2-yl)-2,5-diphenyl tetrazolium bromide for rapid detection of rifampin-resistant Mycobacterium tuberculosis. *J. Clin. Microbiol.*, 36(5), 1214-1219. <https://doi.org/10.1128/JCM.36.5.1214-1219.1998>
- Oh, Y.J. Hong, J. (2022), Application of the MTT-based colorimetric method for evaluating bacterial growth using different solvent systems. *LWT Food Sci. Technol.*, 153, Article 112565. <https://doi.org/10.1016/j.lwt.2021.112565>
- Oliver, J.D. (2005). The viable but non-culturable state in bacteria. *J. Microbiol.*, 43, 93-100.
- Oren, A. (1987). On the use of tetrazolium salts for the measurement of microbial activity in sediments. *FEMS Microbiol. Ecol.*, 45, 127-133. <https://doi.org/10.1111/j.1574-6968.1987.tb02348.x>
- Peng, L., Wang, B., & Ren, P. (2005). Reduction of MTT by flavonoids in the absence of cells. *Colloids Surf. B.*, 45, 108-111. <https://doi.org/10.1016/j.colsurfb.2005.07.014>
- Perez, M.G., Fourcade, L., Mateescu, M.A., & Paquin, J. (2017). Neutral red versus MTT assay of cell viability in the presence of copper compounds. *Anal. Biochem.*, 535, 43-46. <https://doi.org/10.1016/j.ab.2017.07.027>
- Pérez-Chabela, M.L., Lara-Labastida, R., Rodriguez-Huezo, E., & Totosaus, A. (2017). Effect of spray drying encapsulation of thermo-tolerant lactic acid bacteria on meat batters properties. *Food Bioproc. Tech.*, 6, 1505-1515. <https://doi.org/10.1007/s11947-012-0865-y>
- Ramamurthy, T., Ghosh, A., Pazhani, G.P., & Shinoda, S. (2014). Current perspectives on viable but non-culturable (VBNC) pathogenic bacteria. *Front. Public Health.*, 2(103), 1-9. <https://doi.org/10.3389/fpubh.2014.00103>
- Semyonov, D., Ramon, O., & Shimoni, E. (2011). Using ultrasonic vacuum spray dryer to produce highly viable dry probiotics. *LWT - Food Sci. Technol.*, 44(9), 1844-52. <https://doi.org/10.1016/j.lwt.2011.03.021>
- Sharma, R., Rashidinejad, A. & Jafari, S.M. (2022). Application of Spray Dried Encapsulated Probiotics in Functional Food Formulations. *Food Bioprocess Technol.*, 15, 2135–2154. <https://doi.org/10.1007/s11947-022-02803-6>
- Silljé, H.H., Paalman, J.W., ter Schure, E.G., Olsthoorn, S.Q.B., Verkleij, A.J., Boonstra, J., & Verrips, C.T. (1999). Function of trehalose and glycogen in cell cycle progression and cell viability in *Saccharomyces cerevisiae*. *J. Bacteriol.*, 181(2), 396-400. <https://doi.org/10.1128/JB.181.2.396-400.1999>
- Silva, A., Belda-Galbis, C.M., Zanini, S.F., Rodrigo, D., Martorell, P., & Martínez, A. (2012). Sublethal damage in *Listeria monocytogenes* after non-thermal treatments, and implications for food safety. *Appl. Environ. Microbiol.*, 7570-7577.
- Stowe, R.P., Koenig, D.W., Mishra, S.K., & Pierson, D.L. (1995). Nondestructive and continuous spectrophotometric measurement of cell respiration using a tetrazolium formazan microemulsion.

- J. Microbiol. Methods.*, 22, 283-292. [https://doi.org/10.1016/0167-7012\(95\)00009-A](https://doi.org/10.1016/0167-7012(95)00009-A)
- Tachon, S., Michelon, D., Chambellon, E., Cantonnet, M., Mezange, C., & Henno, L. (2009). Experimental conditions affect the site of tetrazolium violet reduction in the electron transport chain of *Lactococcus lactis*. *Microbiology*, 155, 2941-2948. <https://doi.org/10.1099/mic.0.029678-0>
- Tavares, G.M., Croguennec, T., Carvalho, A.F., & Bouhallab, S. (2014). Milk proteins as encapsulation devices and delivery vehicles: applications and trends. *Trends Food Sci. Technol.*, 37, 5-20. <https://doi.org/10.1016/j.tifs.2014.02.008>
- Teixeira, P., Castro, H., & Kirby, R. (1995). Spray drying as a method for preparing concentrated cultures of *Lactobacillus bulgaricus*. *J. appl. bacteriol.*, 78, 456-460. <https://doi.org/10.1111/j.1365-2672.1995.tb03433.x>
- Tengerdy, R.P., Nagy, J.G., & Martin, B. (1967). Quantitative measurement of bacterial growth by the reduction of tetrazolium salts. *Appl. Microbiol.*, 15(4), 954-955. <https://doi.org/10.1128/am.15.4.954-955.1967>
- Tirta, G.D., Martin, L., Bani, M.D., Kho, K., Pramanda, I.T., Pui, L.P., How, Y.H., Lim, C.S.Y., & Devanathi, P.V.P. (2023). Spray Drying Encapsulation of *Pediococcus acidilactici* at Different Inlet Air Temperatures and Wall Material Ratios. *Foods*, 12, 165. <https://doi.org/10.3390/foods12010165>
- Tripathi, M.K., & Giri, S.K. (2014). Probiotic functional foods: Survival of probiotics during processing and storage. *J. Funct. Foods*, 9(1), 225-241. <https://doi.org/10.1016/j.jff.2014.04.030>
- Tsukatani, T., Suenaga, H., Higuchi, T., Akao, T., Ishiyama, M., Ezoe, K., & Matsumoto, K. (2008). Colorimetric cell proliferation assay for microorganisms in microtiter plate using water-soluble tetrazolium salts. *J. Microbiol. Methods*, 75, 109-116. <https://doi.org/10.1016/j.mimet.2008.05.016>
- Wang, F., Cao, L., & Hu, S. (2007). A rapid and accurate 3-(4,5-dimethyl thiazol-2-yl)-2,5-diphenyl tetrazolium bromide colorimetric assay for quantification of bacteriocins with nisin as an example. *J. Zhejiang Univ. Sci. B.*, 8(8), 549-554. <https://doi.org/10.1631/jzus.2007.B0549>
- Wang, H., Cheng, H., Wang, F., Wei, D., & Wang, X. (2010). An improved 3-(4,5-dimethylthiazol-2-yl)-2,5-diphenyl tetrazolium bromide (MTT) reduction assay for evaluating the viability of *Escherichia coli* cells. *J. Microbiol. Methods.*, 82, 330-333. <https://doi.org/10.1016/j.mimet.2010.06.014>
- Wang, Z., Chao, Y., Deng, Y., Piao, M., Chen, T., Xu, J., Zhang, R., Zhao, J., Deng, Y. (2020). Formation of viable, but putatively non-culturable (VPNC) cells of beer-spoilage lactobacilli growing in biofilms. *LWT*, 133, 109964. <https://doi.org/10.1016/j.lwt.2020.109964>
- Wesche, A.M., Gurtler, J.B., Marks, B.P., & Ryser, E.T. (2009). Stress, sublethal injury, resuscitation, and virulence of bacterial foodborne pathogens. *J. Food Prot.*, 72, 1121-1138. <https://doi.org/10.4315/0362-028X-72.5.1121>
- Weyermann, J., Lochmann, D., & Zimmer, A. (2005). A practical note on the use of cytotoxicity assays. *Int. J. Pharm.*, 288, 369-376. <https://doi.org/10.1016/j.ijpharm.2004.09.018>
- Xu, W., Shi, D., Chen, K., Palmer, J., & Popovich, D. G. (2023). An improved MTT colorimetric method for rapid viable bacteria counting. *J. of Microbiol. Methods*, 214, 106830. <https://doi.org/10.1016/j.mimet.2023.106830>
- Zhao, X., Zhong, J., Wei, C., Lin, C.W., & Ding, T. (2017). Current perspectives on viable but non-

---

culturable state in foodborne path-ogens. *Front Microbiol.*, 8, 580. <https://doi.org/10.3389/fmicb.2017.00580>

## RESEARCH ARTICLE

# Assessing the impact of oleuropein on dyslipidemia in male rats subjected to D-galactose-induced aging: A preliminary study

Shirin Tarbiat <sup>1\*</sup>  | Beyrivan Aydın <sup>2</sup>  | Kübra Ergün <sup>2</sup>  | Ali Reza Mohseni <sup>3</sup> 

<sup>1</sup> Department of Molecular Biology and Genetics (English), Faculty of Engineering and Natural Sciences, Uskudar University, Istanbul, Türkiye

<sup>2</sup> Department of Molecular Biology and Genetics, Graduate School of Science, Uskudar University, Istanbul, Türkiye

<sup>3</sup> Department of Medicine (English), Cerrahpasa Medical Faculty, Istanbul University-Cerrahpasa, Istanbul, Türkiye

\* Corresponding author: E-mail: [shirin.tarbiat@uskudar.edu.tr](mailto:shirin.tarbiat@uskudar.edu.tr); Ph.: +90 543 776 1587.

**Citation:** Tarbiat, S., Aydın B., Ergun K., & Mohseni A.M. (2024). Assessing the impact of oleuropein on dyslipidemia in male rats subjected to D-galactose-induced aging: A Preliminary study. *The European chemistry and biotechnology journal*, 2, 17-26.

<https://doi.org/10.62063/ecb-21>

**License:** This article is licensed under a Creative Commons Attribution-NonCommercial 4.0 International License (CC BY-NC 4.0).

**Peer review:** Externally peer reviewed.

**Received:** 25.03.2024

**Accepted:** 29.04.2024

**Published:** 25.07.2024



## Abstract

Aging unfolds as a complex process marked by numerous physiological and biochemical transformations. These age-related changes intricately influence tissues, cells, and subcellular organelles, thereby impacting metabolic functions. Dyslipidemia, characterized by elevated triglyceride (TAG) and low-density lipoprotein (LDL-C) levels coupled with diminished high-density lipoprotein (HDL-C) levels, stands as a well-recognized risk factor for cardiovascular disease, which increases with age. The regulation of lipoprotein metabolism relies upon various proteins, notably peroxisome proliferator-activated receptor alpha (PPAR- $\alpha$ ). In this study, we sought to elucidate the potential of oleuropein in addressing dyslipidemia associated with aging through a preliminary analysis of liver and plasma samples to assess lipid profiles. Our study included control, D-galactose-treated (aged) (150 mg/kg), and oleuropein (200 mg/kg) pretreated aged groups. The rat plasma levels of TAG, total cholesterol (TC), HDL-C and LDL-C were assessed using their respective kits. Liver tissues were homogenized with PBS at a ratio of 1:9 and PPAR- $\alpha$  levels were assessed using the PPAR- $\alpha$  Elisa kit. D-galactose induced aging resulted in significant increase in plasma TAG, TC, LDL-C ( $p < 0.05$ ) and decrease in plasma HDL-C ( $p < 0.05$ ) and liver PPAR- $\alpha$  ( $p < 0.001$ ) levels. However, oleuropein pretreatment mitigated these affects in the oleuropein+D-galactose group resulting in statistically lower levels of TAG, TC and LDL-C levels ( $p < 0.05$ ) and higher levels of liver PPAR- $\alpha$  ( $p < 0.05$ ) compared to the aged group. Collectively, our study highlights oleuropein's potential as a PPAR agonist in maintaining liver PPAR- $\alpha$  levels, regulating plasma lipid levels, and improving dyslipidemia in aging individuals.

**Keywords:** Aging, dyslipidemia, oleuropein, peroxisome proliferator-activated receptor alpha.

## Introduction

Aging is a multifaceted process characterized by disruptions in the intricate balance of biological systems. This imbalance manifests through alterations in tissue, organ, and intracellular biochemical dynamics. Notably, cellular aging ensues alongside the functional decline of mitochondria, perpetuating a cascade of physiological changes (Palombo et al., 1997; Qadir et al., 2020). Advancing age correlates with a heightened susceptibility to age-related ailments, including type 2 diabetes, hypertension, and dyslipidemia (Giansanti et al., 1996; van den Berg et al., 2009). Dyslipidemia, a condition marked by lipid imbalance, serves as a precursor to various cardiovascular diseases, notably atherosclerosis (Bae & Moon, 2024). Lipids, essential biomolecules, intricately participate in cellular membrane structure, energy reservoirs, signal transduction, and synthesis pathways. Dysregulation in lipid homeostasis can also precipitate neurodegenerative disorders such as Alzheimer's and Parkinson's disease (Schwartz et al., 2013).

Peroxisome proliferator-activated receptors (PPARs), integral members of the nuclear receptor superfamily, exert profound influence on various disease pathologies, including diabetes, cancer, insulin resistance, hyperlipidemia, and inflammation (Balakumar et al., 2009; Chi et al., 2021; Gu et al., 2014). Notably, dysregulation and insufficiency of this receptor activity emerge as pivotal contributors to this pathological state. PPAR- $\alpha$  orchestrates the transcriptional regulation of proteins involved in fatty acid synthesis and modulates lipoprotein metabolism. Pharmacological activation of PPAR- $\alpha$  stimulates fatty acid oxidation and induces alterations in lipoprotein metabolism (Terra et al., 2008). Fibrates, known as PPAR- $\alpha$  agonists, occupy a crucial role in dyslipidemia management. These agents, exemplified by GW590735, effectively modulate plasma triacylglycerol (TAG) and lipoprotein levels by elevating high-density lipoprotein cholesterol (HDL-C) while concurrently reducing low-density lipoprotein (LDL-C), TAG, and very low-density lipoprotein cholesterol levels (Okopien et al., 2017).

Animal models of dyslipidemia, often induced through diverse methodologies, provide invaluable insights into disease pathogenesis. For instance, high fructose intake in animals mirrors dyslipidemia, characterized by diminished HDL-C, elevated LDL-C, TAG, and total cholesterol (TC) levels in serum samples (Jensen et al., 2021). Similarly, in a D-galactose-induced aging model, administration of 100 mg/kg D-galactose demonstrated exacerbation of dyslipidemia and oxidative stress upon silencing Apo lipoprotein E, a key regulator of lipid metabolism and cholesterol homeostasis (Hakimizadeh et al., 2023).

With advancing age, perturbations in intracellular mechanisms become evident, such as compromised fluidity in the lipid-rich cell membrane, impacting permeability. Furthermore, disruption in the antioxidant-oxidative stress equilibrium accompanying aging precipitates heightened lipid peroxidation, culminating in cell membrane integrity compromise via oxygen free radical-mediated attacks on lipids. The resultant formation of peroxide radicals accentuates lipid degradation within the cell membrane, perpetuating cellular dysfunction (Spiteller, 2002). Understanding the intricate interplay between dyslipidemia, aging, and intracellular mechanisms elucidates novel therapeutic avenues and underscores the imperative of targeted interventions in mitigating age-associated dyslipidemia and its attendant complications (Shao et al., 2011).

Oleuropein, a phenolic compound abundant in olive fruits, exhibits diverse therapeutic properties, including anticancer, antioxidant, anti-inflammatory, antimicrobial, and antiviral effects (Campolo et al., 2013). Remarkably, administration of oleuropein mitigated TAG levels in mice through PPAR- $\alpha$  activation and PPAR- $\gamma$  inhibition (Ahamad et al., 2019). To evaluate oleuropein's protective effects against the detrimental manifestations of aging, D-galactose was used to induce the process of aging. Evaluation of oleuropein using this approach is the distinctive feature of our study. D-galactose is a well-known agent used to accelerate and induce the process of aging and its manifestations bringing about decreased antioxidant capability, disturbed lipid parameters and decreased PPAR expression as well as behavioral manifestations (Hakimizadeh et al., 2022; Zhou et al., 2017). Three groups were designed as control (negative control), aged and oleuropein pretreated and aged (Ruan et al., 2013), and the plasma levels of TAG, HDL, LDL, TC, and liver PPAR- $\alpha$  expression were analyzed in all three groups. By scrutinizing dyslipidemia and its associated parameters in light of existing literature, the impact of oleuropein, an antioxidant, on these indices will be assessed. Furthermore, this investigation offers insights into the molecular mechanisms underlying PPAR- $\alpha$  agonists in dyslipidemia, alongside the therapeutic potential of phytochemicals in managing dyslipidemia *in vivo*.

## Materials and methods

### *Chemicals and reagents*

Olive leaves hydro alcoholic extract was collected from Sankara Brain and Biotechnology Research Center (Istanbul, Türkiye) and identified by Professor. Dr. Ihsan Kara. According to the supplier, the extracts were 20% pure oleuropein and the other 80% consisted of various other phytochemicals of olive leaf extracts. D-galactose was acquired from Sigma-Aldrich Co. (Merck KGaA, Darmstadt, Germany) and dissolved in physiological saline at a concentration of 20 mg/mL. All other chemical compounds and kits utilized in this research were also purchased from Sigma-Aldrich Co. (Merck KGaA, Darmstadt, Germany).

### *Preparation of experimental groups*

This study is a continuation of a previously conducted animal experiment with the ethics committee decision taken on 13.08.2020. 24 male Wistar albino rats (220-250g) were provided by the animal lab of Uskudar University, Istanbul, Turkey. The rats were housed in regulated conditions at 22 °C following a 12-hour light and 12-hour dark cycle, within standard cages, ensuring unrestricted availability of both water and food. In this experiment, three groups of 8 were designed. Group 1 was set as the control group and physiological saline (5 ml/Kg) was injected intraperitoneally. Group 2 was given 150 mg/kg/five days a week Dgalactose via subcutaneous injection for 6 weeks (Hakimizadeh et al., 2022; Ruan et al., 2013). In the 3rd group (OLE+D-galactose), oleuropein was administered via intraperitoneal injection at a dose of 200 mg/kg for 30 days. Subsequently, a subcutaneous injection of 150 mg/kg D-galactose was administered for 6 weeks, starting a day or two after the oleuropein treatment.

### *Tissue homogenization*

The liver tissues of the animals were homogenized with cold PBS at a ratio of 1:9. The resulting homogenate was centrifuged at + 4°C, 5000xg for 5 minutes. Following this, the supernatant was taken and stored at -80°C until its utilization for the experiment.

### ***Measurement of plasma TAG, LDL-C, HDL-C levels***

Upon collecting the blood of the test subjects, the plasma was centrifuged at 1000xg for 15 minutes at 2-8 °C. The supernatant of the tubes was collected and stored at -80 °C until the experimental stage. TC, LDL-C, HDL-C and TAG levels were measured using the spectrophotometric method with the help of their respective kits (Albers et al., 1978; Allain et al., 1974; Friedewald et al., 1972; McGowan et al., 1983).

### ***Measurement of PPAR- $\alpha$ levels of liver tissue***

PPAR- $\alpha$  levels of homogenized liver tissues were analyzed with the 'Rat PPAR- $\alpha$  E-EL-R0725' Elisa kit. Analysis of the samples was measured in a spectrophotometer at 450 nm.

### ***Statistical analysis***

Statistical analyses were performed using Graph pad software version 9.5.1. The values were shown as mean  $\pm$  standard deviation. All data were tested for normal distribution using the Kolmogorov Smirnov and Shapiro-Wilk tests and also by graphical quantile-quantile plots. Data conforming to normal distribution were analyzed using one-way ANOVA and post hoc Tukey's test for multiple comparison while for data that was not normally distributed, Kruskal-Wallis and Dunn's test was employed for multiple comparison.  $P < 0.05$  was considered statistically significant.

## **Results and discussion**

Dyslipidemia, characterized by abnormal levels of plasma TAG, LDL-C, and HDL-C, is intricately linked with irregularities and deficiencies in PPAR- $\alpha$  activity (Terra et al., 2008). The experimental design anticipates the manifestation of PPAR- $\alpha$  imbalance and consequent dyslipidemia formation in rats subjected to D-galactose-induced aging. Analysis of the experiment's outcomes reveals elevated plasma TAG and LDL-C levels and decreased HDL-C levels in D-galactose-treated rats compared to the control group. However, administration of 200 mg/kg of our oleuropein sample as pretreatment prior to the aging process of the rats attenuated TAG and LDL-C levels, suggesting a potential therapeutic role for oleuropein in age-related dyslipidemia. Consistent with existing literature, D-galactose-induced aging is associated with diminished PPAR- $\alpha$  expression in the liver, a trend corroborated by our findings (Zhou et al., 2017).

### ***Plasma lipid parameters***

The rat plasma levels of TAG, TC, HDL-C and LDL-C were assessed using their respective kits. Detailed results obtained from the plasma lipid parameter analyses are presented in Table 1. When comparing TAG levels, both D-galactose aged and oleuropein pretreated aged groups exhibited statistically significant increases compared to the control group. However, the increases in the TAG of the OLE+Dgalactose group was significantly lesser than the aged group. In the comparison of TC levels, the pretreated aged group exhibited statistically significant lower levels, whereas the aged group exhibited statistically significant higher levels when compared with the control group. Similar results were also observed in the LDL-C levels. The HDL-C levels were significantly lower in both D-galactose and OLE+D-galactose groups compared to the control group, with no significant difference observed between the two treated groups.

**Table 1.** Lipid parameter levels of control, D-galactose, OLE+D-galactose groups. Pairs with similar superscript alphabets were **not** significantly different at ( $p < 0.05$ ).

Groups	TAG (mg/dL)	TC (mg/dL)	HDL-C (mg/dL)	LDL-C (mg/dL)
Control	52 ± 0.12	65.4 ± 0.1	29.2 ± 0.12	36.2 ± 0.16
D-galactose	60.2 ± 0.19	67.5 ± 0.15	28.61 ± 0.14 <sup>a</sup>	38.8 ± 0.12
OLE+D-galactose	55.92 ± 1.2	63.9 ± 0.12	28.75 ± 0.12 <sup>a</sup>	35.15 ± 0.17

Several natural sources with lipid profile-modulating properties have been identified. These include plants such as *Lippia citriodora*, *Lippia triphylla*, *Grifola frondose*, *Rosmarinus officinalis* Linn and *Curcuma longa* (curcumin), which have demonstrated lipid-lowering abilities through mechanisms such as antioxidant activity and PPAR modulation (Roghani-Shahraki et al., 2021). The list of such natural sources continues to expand with ongoing research. A recent study by Kar et al. (2022), the protective effects of pomegranate juice against aluminum-induced hepato-nephrotoxicity and the subsequent increase in lipid profiles were evaluated. The study found that the pomegranate juice effectively lowered LDL and TC levels.

Oleuropein has been shown to exhibit remarkable protective effects against oxidative damage in tissues, coupled with a significant reduction in serum levels of TC and TAG. This protective mechanism was elucidated in a study by Andreadou et al. (2006), shedding light on OLE's role as a potent antioxidant and lipid-lowering agent. In a separate study conducted by Malliou et al. (2018), the administration of oleuropein at a dosage of 100 mg/kg mixed with the food of mice for a duration of 6 weeks yielded noteworthy reductions in TAG underscoring the therapeutic potential of oleuropein in mitigating dyslipidemia and metabolic disorders. Furthermore, Ahmadvand et al. (2016) evaluated the lipid profile of rats with induced nephrotoxicity treated with oleuropein. Similar to our findings, they also observed protective effects of oleuropein with reduced levels of TAG, TC and LDL. They also witnessed an increase in HDLC which we herein did not observe against d-galactose-induced aging.

#### **Liver PPAR- $\alpha$ levels**

Liver tissues were homogenized together with PBS at a ratio of 1:9 and PPAR- $\alpha$  levels were assessed using the PPAR- $\alpha$  E-EL-R0725' Elisa kit. Samples were run in duplicate. As illustrated in Figure 1, the animal group that underwent the aging process through D-galactose treatment yielded significantly lower liver PPAR- $\alpha$  levels in comparison with the control group. Conversely, OLE+D-galactose group exhibited results akin to those of the control group, significantly surpassing the aged group.



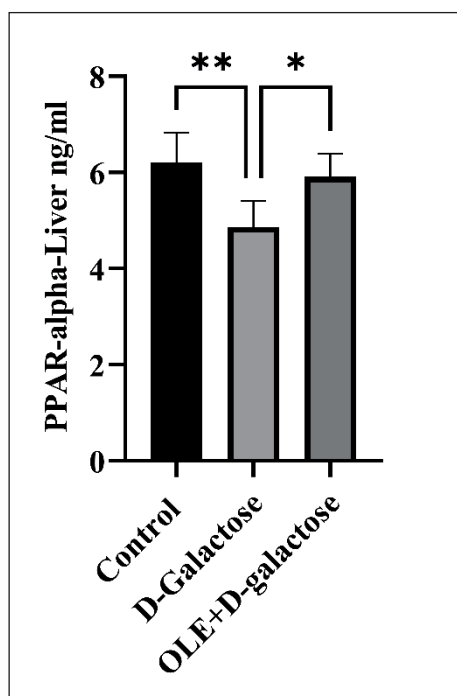


**Figure 1.** PPAR- $\alpha$  measurements of the control, aged (D-galactose) and oleuropein pretreated and aged (OLE+D-galactose) groups. Difference between bar pairs marked with \* ( $p < 0.05$ ) and \*\* ( $p < 0.001$ ) are significant ( $n = 8$ ).

Oleuropein's effect on PPAR- $\alpha$  activation aligns with its ability to reduce TAG levels, as PPAR- $\alpha$  plays a pivotal role in lipid and lipoprotein metabolism. Understanding the molecular mechanisms underlying PPARs and their interplay with lipoprotein metabolism emphasizes the potential of PPAR agonists as pharmacological agents for dyslipidemia management. Synthetic PPAR ligands such as fibrates, statins, and hypolipidemic drugs modulate plasma lipid levels by reducing TAG and LDL-C levels while augmenting HDL-C levels. Notably, oleuropein emerges as a natural PPAR- $\alpha$  ligand, as evidenced by its ability to enhance PPAR- $\alpha$  and retinoid X receptors (RXR) homodimerization. Furthermore, oleuropein upregulates LDL receptor expression in the liver and modulates genes involved in TAG synthesis, uptake, transport, metabolism, and elimination, akin to fibrates, albeit with potentially fewer associated side effects (Malliou et al., 2018). In our study, the observed elevation in PPAR- $\alpha$  levels in the oleuropein treated group further substantiates oleuropein's efficacy in mitigating dyslipidemia. This could indicate that oleuropein acts as both an activating ligand and a facilitator in upregulating PPAR- $\alpha$ , countering the detrimental effects of aging.

In another study regarding oleuropein and PPAR activities, it was determined that oleuropein concentrations between 10-400  $\mu\text{M}$  had an inhibitory effect solely on the transcriptional activity of PPAR $\gamma$ , without impacting other PPARs *in vitro*. The anti-adipogenic effects observed in their study was attributed to this property of oleuropein (Svobodova et al., 2014). In research conducted by Feng et al. (2016), bavachinin, a natural compound extracted from malaytea scurfpea fruit, demonstrated Pan-PPAR agonistic properties and contributed to glucose and lipid reduction in diet-induced obese mice. Combining these findings with our research, it is evident that oleuropein, at high doses, is capable in inhibiting PPAR- $\gamma$  while simultaneously activating PPAR- $\alpha$  yielding anti-adipogenic and

lipid profile lowering effects. This would be more favorable to Pan PPAR agonistic compounds such as bavachinin as continuous activation of PPAR- $\gamma$  has been linked with weight gain, heart failure and bone loss.

The study was limited by the number of animals provided, preventing the designation of negative dyslipidemia controls or positive controls treated with fibrates. Consequently, this limitation positions this study as a preliminary investigation rather than a comprehensive analysis. Nevertheless, these findings highlight the potential of oleuropein as a promising therapeutic agent for managing metabolic disorders as well as a preventive agent against the process of aging, offering valuable insights into its underlying mechanisms of action and paving the way for further exploration in clinical settings.

## Conclusions

In light of our study, we conducted an examination of PPAR- $\alpha$  expression levels, as well as levels of LDL-C, HDL-C, and TAG, pivotal components in the dyslipidemia mechanism within our aging model. By elucidating the effects of our oleuropein sample on liver PPAR- $\alpha$  levels and plasma lipid profiles, we have demonstrated its ability to regulate lipid metabolism and improve dyslipidemia in aging individuals. The profound influence of PPAR agonists on lipid and lipoprotein metabolism underscores their significance as promising targets for drug development. Understanding the intricate molecular mechanisms underlying PPARs and their interplay with lipoprotein metabolism emphasizes the therapeutic potential of PPAR agonists in regulating plasma lipid levels and ameliorating dyslipidemia. To the best of our knowledge, apart from the research by Malliou et al. (2018), no other investigation demonstrated meaningful effects of oleuropein on PPAR- $\alpha$  prior to our study. Further research on the effects of oleuropein on PPAR- $\alpha$  and its subsequent outcomes is warranted. Given the diverse array of natural and synthetic agonists employed in cardiovascular disease management and lipid profile regulation, our study underscores the importance of further investigations into aging, particularly at the genetic level, with emphasis on oleuropein as a natural PPAR- $\alpha$  agonist. Moreover, our study contributes to the growing body of evidence supporting the use of natural compounds as potential interventions for age-related health conditions.

## Acknowledgements

We would like to acknowledge Uskudar University and Ankara University for providing the necessary facilities and study environment that enabled us to conduct this study.

## Funding

This research did not benefit by any funding of any organization.

## Conflict of interest

The authors disclose no conflicts of interest related to the publication of this manuscript.

## Data availability statement

Data can be obtained from the corresponding author upon a reasonable request.

## Ethics committee approval

Animal Research Ethics Board of Uskudar University, Istanbul, Türkiye (UU-HADYEK 2020-06), approved all the experimental procedures.

## Authors' contribution statement

The authors acknowledge their contributions to this paper as follows: **Study conception and design:** S.T.; **Data collection:** B.A., K.E.; **Analysis and interpretation of results:** S.T., A.M.; **Manuscript draft preparation:** S.T., B.A. K.E., A.M. All authors reviewed the results and approved the final version of the manuscript.

### ORCIDs and emails of the authors

Shirin Tarbiat | ORCID 0000-0001-7931-1546 | [shirin.tarbiat@uskudar.edu.tr](mailto:shirin.tarbiat@uskudar.edu.tr)

Beyrivan Aydın | ORCID 0000-0001-8933-4370 | [beyrivanaydn@gmail.com](mailto:beyrivanaydn@gmail.com)

Kübra Ergün | ORCID 0000-0002-8479-8317 | [kubra.ergun@std.yildiz.edu.tr](mailto:kubra.ergun@std.yildiz.edu.tr)

Ali Reza Mohseni | ORCID 0000-0002-8479-8317 | [alirezamohseni12@gmail.com](mailto:alirezamohseni12@gmail.com)

## References

- Ahamad, J., Toufeeq, I., Khan, M. A., Ameen, M. S. M., Anwer, E. T., Uthirapathy, S., Mir, S. R., & Ahmad, J. (2019). Oleuropein: A natural antioxidant molecule in the treatment of metabolic syndrome. *Phytotherapy research*, 33(12), 3112-3128. <https://doi.org/10.1002/ptr.6511>
- Ahmadvand, H., Bagheri, S., Tamjidi-Poor, A., Cheraghi, M., Azadpour, M., Ezatpour, B., Moghadam, S., Shahsavari, G., & Jalalvand, M. (2016). Biochemical effects of oleuropein in gentamicin-induced nephrotoxicity in rats. *ARYA Atheroscler*, 12(2), 87-93.
- Albers, J. J., Warnick, G. R., & Chenng, M. C. (1978). Quantitation of high density lipoproteins. *Lipids*, 13(12), 926-932. <https://doi.org/10.1007/bf02533852>
- Allain, C. C., Poon, L. S., Chan, C. S., Richmond, W., & Fu, P. C. (1974). Enzymatic determination of total serum cholesterol. *Clinical chemistry*, 20(4), 470-475. <https://doi.org/10.1093/clinchem/20.4.470>
- Andreadou, I., Iliodromitis, E. K., Mikros, E., Constantinou, M., Agalias, A., Magiatis, P., Skaltsounis, A. L., Kamber, E., Tsantili-Kakoulidou, A., & Kremastinos, D. T. (2006). The olive constituent oleuropein exhibits anti-ischemic, antioxidative, and hypolipidemic effects in anesthetized rabbits. *Journal of nutrition*, 136(8), 2213-2219. <https://doi.org/10.1093/jn/136.8.2213>
- Bae, S., & Moon, Y. A. (2024). Deletion of *Elovl5* leads to dyslipidemia and atherosclerosis in LDLR-deficient mice. *Biochemical and biophysical research communications*, 690, Article 149292. <https://doi.org/10.1016/j.bbrc.2023.149292>
- Balakumar, P., Arora, M. K., & Singh, M. (2009). Emerging role of PPAR ligands in the management of diabetic nephropathy. *Pharmacological research*, 60(3), 170-173. <https://doi.org/10.1016/j.phrs.2009.01.010>
- Campolo, M., Di Paola, R., Impellizzeri, D., Crupi, R., Morittu, V. M., Procopio, A., Perri, E., Britti, D., Peli, A., Esposito, E., & Cuzzocrea, S. (2013). Effects of a polyphenol present in olive oil, oleuropein aglycone, in a murine model of intestinal ischemia/reperfusion injury. *Journal of leukocyte biology*, 93(2), 277-287. <https://doi.org/10.1189/jlb.0712317>
- Chi, T. G., Wang, M. N., Wang, X., Yang, K., Xie, F. Y., Liao, Z. H., & Wei, P. (2021). PPAR- $\gamma$  Modulators as Current and Potential Cancer Treatments. *Frontiers in oncology*, 11, Article 737776. <https://doi.org/10.3389/fonc.2021.737776>
- Feng, L., Luo, H., Xu, Z., Yang, Z., Du, G., Zhang, Y., Yu, L., Hu, K., Zhu, W., Tong, Q., Chen, K., Guo, F., Huang, C., & Li, Y. (2016). Bavachinin, as a novel natural pan-PPAR agonist, exhibits unique synergistic effects with synthetic PPAR- $\gamma$  and PPAR- $\alpha$  agonists on carbohydrate and lipid

- metabolism in db/db and diet-induced obese mice. *Diabetologia*, 59(6), 1276-1286. <https://doi.org/10.1007/s00125-016-3912-9>
- Friedewald, W. T., Levy, R. I., & Fredrickson, D. S. (1972). Estimation of the concentration of low-density lipoprotein cholesterol in plasma, without use of the preparative ultracentrifuge. *Clinical chemistry*, 18(6), 499-502.
- Giansanti, R., Fumelli, C., Boemi, M., & Fumelli, P. (1996). Age-related macular disease in diabetes mellitus. *Archives of gerontology and geriatrics*, 473-476. [https://doi.org/10.1016/0167-4943\(96\)86985-8](https://doi.org/10.1016/0167-4943(96)86985-8)
- Gu, S. J., Guo, Z. R., Zhou, Z. Y., Hu, X. S., & Wu, M. (2014). PPAR  $\alpha$  and PPAR  $\gamma$  Polymorphisms as risk factors for Dyslipidemia in a Chinese han population. *Lipids in health and disease*, 13, Article 23. <https://doi.org/10.1186/1476-511x-13-23>
- Hakimizadeh, E., Tadayon, S., Zamanian, M. Y., Soltani, A., Giménez-Llort, L., Hassanipour, M., & Fatemi, I. (2023). Gemfibrozil, a lipid-lowering drug, improves hepatorenal damages in a mouse model of aging. *Fundamental & clinical pharmacology*, 37(3), 599-605. <https://doi.org/10.1111/fcp.12865>
- Hakimizadeh, E., Zamanian, M. Y., Borisov, V. V., Giménez-Llort, L., Ehsani, V., Kaeidi, A., Hassanshahi, J., Khajehasani, F., Movahedinia, S., & Fatemi, I. (2022). Gemfibrozil, a lipid-lowering drug, reduces anxiety, enhances memory, and improves brain oxidative stress in d-galactose-induced aging mice. *Fundamental & clinical pharmacology*, 36(3), 501-508. <https://doi.org/10.1111/fcp.12752>
- Jensen, V. S., Fledelius, C., Wulff, E. M., Lykkesfeldt, J., & Hvid, H. (2021). Temporal Development of Dyslipidemia and Nonalcoholic Fatty Liver Disease (NAFLD) in Syrian Hamsters Fed a High-Fat, High-Fructose, High-Cholesterol Diet. *Nutrients*, 13(2), Article 604. <https://doi.org/10.3390/nu13020604>
- Kar, F., Çiftçi, H., Er Çalışkan, Ç., Özkaya, A., & Güçlü, K. (2022). Evaluation of The Effects of Pomegranate Juice on Hepato-Nephrotoxicity in Male Rats Exposed to Aluminum [Alüminyum Maruz Kalmış Erkek Sıçanlarda Nar Suyunun Hepato-Nefrotoksisite Üzerine Etkilerinin Değerlendirilmesi.]. *Kahramanmaraş sütçü imam üniversitesi tarım ve doğa dergisi*, 25(2), 215-222. <https://doi.org/10.18016/ksutarimdogavi.896611>
- Malliou, F., Andreadou, J., Gonzalez, F. J., Lazou, A., Xepapadaki, E., Vallianou, J., Lambrinidis, G., Mikros, E., Marselos, M., Skaltsounis, A. L., & Konstandi, M. (2018). The olive constituent oleuropein, as a PPAR $\alpha$  agonist, markedly reduces serum triglycerides. *Journal of nutritional biochemistry*, 59, 17-28. <https://doi.org/10.1016/j.jnutbio.2018.05.013>
- McGowan, M. W., Artiss, J. D., Strandbergh, D. R., & Zak, B. (1983). A peroxidase-coupled method for the colorimetric determination of serum triglycerides. *Clinical chemistry*, 29(3), 538-542.
- Okopien, B., Buldak, L., & Boldys, A. (2017). Fibrates in the management of atherogenic dyslipidemia. *Expert review of cardiovascular therapy*, 15(12), 913-921. <https://doi.org/10.1080/14779072.2017.1408410>
- Palombo, V., Scurti, R., Muscari, A., Puddu, G. M., Dilorio, A., Zito, M., & Abate, G. (1997). Blood pressure and intellectual function in elderly subjects. *Age and ageing*, 26(2), 91-98. <https://doi.org/10.1093/ageing/26.2.91>
- Qadir, A., Liang, S., Wu, Z., Chen, Z., Hu, L., & Qian, A. (2020). Senile Osteoporosis: The Involvement of Differentiation and Senescence of Bone Marrow Stromal Cells. *International journal of molecular sciences*, 21(1). <https://doi.org/10.3390/ijms21010349>
- Roghani-Shahraki, H., Karimian, M., Valipour, S., Behjati, M., Arefnezhad, R., & Mousavi, A. (2021).

- Herbal therapy as a promising approach for regulation on lipid profiles: A review of molecular aspects. *Journal of cellular physiology*, 236(8), 5533-5546. <https://doi.org/https://doi.org/10.1002/jcp.30282>
- Ruan, Q., Liu, F., Gao, Z., Kong, D., Hu, X., Shi, D., Bao, Z., & Yu, Z. (2013). The anti-inflamm-aging and hepatoprotective effects of huperzine A in d-galactose-treated rats. *Mechanisms of ageing and development*, 134(3), 89-97. <https://doi.org/https://doi.org/10.1016/j.mad.2012.12.005>
- Schwartz, J., Allison, M. A., Ancoli-Israel, S., Hovell, M. F., Patterson, R. E., Natarajan, L., Marshall, S. J., & Grant, I. (2013). Sleep, type 2 diabetes, dyslipidemia, and hypertension in elderly Alzheimer's caregivers. *Archives of gerontology and geriatrics*, 57(1), 70-77. <https://doi.org/10.1016/j.archger.2013.02.008>
- Shao, H., Chen, L. Q., & Xu, J. (2011). Treatment of dyslipidemia in the elderly. *Journal of geriatric cardiology*, 8(1), 55-64. <https://doi.org/10.3724/sp.J.1263.2011.00055>
- Spiteller, G. (2002). Are changes of the cell membrane structure causally involved in the aging process? In D. Harman (Ed.), *Increasing Healthy Life Span: Conventional Measures and Slowing the Innate Aging Process* (Vol. 959, pp. 30-44). <https://doi.org/10.1111/j.1749-6632.2002.tb02080.x>
- Svobodova, M., Andreadou, I., Skaltsounis, A. L., Kopecky, J., & Flachs, P. (2014). Oleuropein as an inhibitor of peroxisome proliferator-activated receptor gamma. *Genes & nutrition*, 9(1), 376. <https://doi.org/10.1007/s12263-013-0376-0>
- Terra, S. G., Francone, O. L., Contant, C. F., Gao, X., Lewin, A. J., & Nguyen, T. T. (2008). Efficacy and safety of a potent and selective peroxisome proliferator activated receptor alpha agonist in subjects with dyslipidemia and type 2 diabetes mellitus. *American journal of cardiology*, 102(4), 434-439. <https://doi.org/10.1016/j.amjcard.2008.03.076>
- van den Berg, E., Kloppenborg, R. P., Kessels, R. P. C., Kappelle, L. J., & Biessels, G. J. (2009). Type 2 diabetes mellitus, hypertension, dyslipidemia and obesity: A systematic comparison of their impact on cognition. *Biochimica et biophysica acta-molecular basis of disease*, 1792(5), 470-481. <https://doi.org/10.1016/j.bbadis.2008.09.004>
- Zhou, Y., Xu, Q., Dong, Y., Zhu, S., Song, S., & Sun, N. (2017). Supplementation of mussel peptides reduces aging phenotype, lipid deposition and oxidative stress in D-galactose-induce aging mice. *Journal of nutrition health & aging*, 21(10), 1314-1320. <https://doi.org/10.1007/s12603-016-0862-3>

## RESEARCH ARTICLE

# A comparative study of glutathione-coated iron oxide and glutathione-coated core-shell magnetic nanoparticles for their antiviral activities

Pinar Sen <sup>1\*</sup>  | Sevda Demir <sup>1</sup>  | Bekir Can Altindisogullari <sup>1</sup>  | Fikrettin Sahin <sup>1</sup> 

<sup>1</sup> Yeditepe University, Department of Genetics and Bioengineering, Faculty of Engineering, Istanbul, 34755, Turkey  
\* Corresponding author: E-mail: [sen\\_pinar@hotmail.com](mailto:sen_pinar@hotmail.com); Ph.: +90 216 578 0619.

**Citation:** Sen, P., Demir, S., Altindisogullari, B.C., & Sahin, F. (2024). Comparative study of glutathione-coated iron oxide and glutathione-coated core-shell magnetic nanoparticles for their antiviral activities. *The European chemistry and biotechnology journal*, 2, 27-38. <https://doi.org/10.62063/ecb-22>

**License:** This article is licensed under a Creative Commons Attribution-NonCommercial 4.0 International License (CC BY-NC 4.0).

**Peer review:** Externally peer reviewed.

**Received:** 11.04.2024

**Accepted:** 28.05.2024

**Published:** 25.07.2024



## Abstract

Iron oxide nanoparticles and its nanocomposites have attracted attention because of their potential applications in biomedicine. Here, firstly the Fe<sub>3</sub>O<sub>4</sub> nanoparticles were prepared and then Ag was deposited by reducing the Ag salt onto the surface of the Fe<sub>3</sub>O<sub>4</sub> nanoparticles. This way, bimetallic nanoparticles were obtained. The synthesized nanoparticles were characterized using ultraviolet-visible absorption spectroscopy, transmission electron microscopy and X-ray diffraction and the size and surface charge of the nanoparticles were determined by the dynamic light scattering (DLS) and zeta potential. The spectrographic data demonstrated the size of the glutathione-coated Fe<sub>3</sub>O<sub>4</sub> nanoparticles to be 4.48 nm and glutathione-coated core-shell magnetic nanoparticles to be 7.98 nm with the spherical morphology and well monodispersed. This study was also designed to investigate the inhibitory effect of Ag@Fe<sub>3</sub>O<sub>4</sub>-GSH, Fe<sub>3</sub>O<sub>4</sub>-GSH and glutathione (GSH) against Human Herpes Simplex Virus Type 1 (HSV-1), Human Adenovirus Type 5, Human Poliovirus Type 1, and Bovine coronavirus. The significant inhibition of Ag@Fe<sub>3</sub>O<sub>4</sub>-GSH was observed against Poliovirus (4 Log), Adenovirus (3 Log), and HSV-1 (2 Log), respectively. GSH showed remarkable antiviral effect against Bovine coronavirus (3 Log) while it exhibited log reduction (1 Log) against HSV-1 and poliovirus. Fe<sub>3</sub>O<sub>4</sub>-GSH showed a reduction of 1 Log only for RNA viruses such as poliovirus and bovine coronavirus. These results demonstrate promising antiviral activity, highlighting the potential of these nanoparticles in combating viral infections.

**Keywords:** Adenovirus, antiviral activity, BCoV, glutathione, HSV-1, iron oxide nanoparticles, magnetic nanoparticles, nanocomposites, poliovirus.

## Introduction

Nanotechnology combines various areas of science. Many nanomaterial types have been introduced up to now, for various applications. Among them, magnetic nanoparticles are of great interest for researchers in biomedical science, catalysis and environmental remediation (Elliott & Zhang, 2001; Govan & Gunko, 2014; Gupta & Gupta, 2005). The iron oxide (II, III) based magnetic nanoparticles are the most promising among the other magnetic nanoparticles (Antone et al., 2019). In particular,  $\text{Fe}_3\text{O}_4$  magnetite nanoparticles have recently attracted great attention due to their different features compared to individual nanoparticles and took place greatly in materials science, biochemistry and diagnostics (Nguyen et al., 2021). Magnetic iron oxide nanoclusters have unique properties, because they combine the properties of individual nanoparticles and exhibit collective behavior through interactions between individual nanoparticles (Kostopoulou & Lappas, 2015). In addition to this, magnetic iron oxide nanoparticles ( $\text{Fe}_3\text{O}_4$  NPs) offer unique properties such as abundance, low toxicity and chemical and photochemical stability, making them an attractive material for usage in certain applications (Naseem & Durrani, 2021). The behaviors of these nanoclusters can be enhanced by the capping molecules leading to novel functional materials. Numerous studies have been conducted on the passivation of iron oxide nanoparticles using capping agents to control the morphology and shape (Mbuyazi & Ajibade, 2023). Besides the synthesis of homogeneous core magnetic  $\text{Fe}_3\text{O}_4$  NPs, advanced nanoarchitectures such as core-shell and composites have been highlighted in biomedical applications (Zhang et al., 2006). For this aim, silver nanoparticles (AgNPs) were used to functionalize the  $\text{Fe}_3\text{O}_4$  NPs as inorganic supports constructing the core-shell structure. Immobilization of Ag NPs on the surface of  $\text{Fe}_3\text{O}_4$  NPs has been shown to limit the aggregation of nanostructure, which renders the applicability of the structures in related applications (Kumari et al., 2019).

Glutathione (GSH) is a water-soluble tripeptide composed of the amino acids and known to function directly or indirectly in many important biological phenomena. GSH plays an important role in plants, mammals, fungi and some prokaryotic organisms as a detoxification agent (Townsend et al., 2003). Several *in vivo* studies have reported the efficiency of this kind of antioxidant substances against viral infections. It was observed that the introduction of GSH reduced some viral infections (Palamara et al., 1996). Although the antiviral activity of antioxidant substances has been demonstrated clearly, the big handicap is that some molecules, such as GSH, are not freely transported into most cells. For this reason, we aimed to combine the target drug with the drug carrier system, allowing easier access to the membranes of many cell types. Magnetic iron oxide and silver nanoparticles as combined or individually have been used in many applications, but GSH coated derivatives of two different nanoparticles will be the first example of *in vivo examination*. Incidences of emerging infections have posed serious public health. Although infectious outbreaks can be controlled within a few years, new dangers of infectious diseases will likely depend on evolving and re-emerging infections. Moreover, viral infections caused by the development of antiviral drug-resistant strains have posed a serious threat globally, resulting in high mortality and economic burden, especially in immunocompromised patients (Parvez & Parveen, 2017). Therefore, it is important to develop new antiviral drugs with a different mode of action than those currently in use.

In our study, glutathione (GSH) functionalized  $\text{Fe}_3\text{O}_4$  NPs ( $\text{Fe}_3\text{O}_4$ -GSH) and glutathione functionalized AgNPs immobilized on  $\text{Fe}_3\text{O}_4$  NPs to obtain  $\text{Ag}@Fe_3O_4$ -GSH as core-shell nanoparticles were obtained. Later, the antiviral activities of the two nanostructures and GSH were examined against different DNA (Human Herpes Simplex Type 1 and Human Adenovirus Type 5) and RNA (Human Poliovirus Type 1, and Bovine Coronavirus) viruses.

## Materials and methods

### Chemicals and instruments

Iron acetylacetonate, benzyl ether, oleic acid, oleylamine, 1,2-Hexadecanediol, ethanol, acetone, chloroform ( $\text{CHCl}_3$ ), methanol, glutathione (GSH),  $\text{Ag}(\text{ac})_3$ , tetramethylammonium hydroxide (TMAOH) were purchased from Sigma–Aldrich. Ultra-pure water was from MilliQ water. Size determination and zeta potential using dynamic light scattering (DLS) was performed using a Nano-ZS instrument (Malvern Instruments Ltd, Malvern, UK). Electronic spectra were recorded on a PerkinElmer LAMBDA 25 Series UV–vis spectrophotometer with a quartz cell of 1 cm. The morphologies of the  $\text{Fe}_3\text{O}_4$ -GSH and  $\text{Ag}@Fe_3\text{O}_4$ -GSH core shell nanoparticles were assessed using transmission electron microscope (TEM) JEOL JEM-2100Plus 200kV. X-ray diffraction (XRD) data were collected over the  $2\theta = 10\text{--}100^\circ$  range using a Bruker D-8 Advance diffractometer, under  $\text{Cu K}\alpha$  radiation ( $\lambda = 1.5405 \text{ \AA}$ , 40kV - 40 mA).

### Synthesis

The  $\text{Fe}_3\text{O}_4$ -GSH was synthesized as outlined in the literature with a slight modification, in two steps (Robinson et al., 2010). In the first step, iron acetylacetonate (0.71 g, 2 mmol) was dissolved in benzyl ether (20 mL) with oleic acid (2 mL, 6 mmol) and oleylamine (2 mL, 4 mmol) under  $\text{N}_2$  with vigorous stirring. 1,2-Hexadecanediol (2.58 g, 10 mmol) was added into the solution and heated under reflux for 2 hours, then cooled to room temperature. The resultant magnetite NPs were separated by precipitation with ethanol (10 mL) and cleaned with acetone. Finally, the product was dried using a vacuum oven at  $50^\circ\text{C}$ . In the second step,  $\text{Fe}_3\text{O}_4$  NPs (0.5 g) suspension in a mixed liquid of  $\text{CHCl}_3$  (15 mL) and methanol (5 mL) was sonicated for 20 minutes. Then, glutathione (0.4 g) dissolved in water (5 mL) was added to the solution, and sonication method was applied to the final colloidal solution for 2 hours. Then, the mixture was precipitated with ethanol and washed few times with ethanol and water, dried in oven at  $50^\circ\text{C}$ , yielding the final magnetic  $\text{Fe}_3\text{O}_4$ -GSH NPs.

The  $\text{Ag}@Fe_3\text{O}_4$ -GSH was synthesized as reported in the literature with slight modification in three steps (Bankole & Nyokong, 2016; Robinson et al., 2010). After applying the same first step for the preparation of  $\text{Fe}_3\text{O}_4$ -GSH, the prepared bare  $\text{Fe}_3\text{O}_4$  NPs (0.5 g),  $\text{Ag}(\text{ac})_3$  (0.83 g, 2.2 mmol), 1,2-hexadecanediol (3.1 g, 12 mmol), oleic acid (0.5 mL, 1.5 mmol) and oleylamine (3 mL, 6 mmol) were added to benzyl ether (30 mL) under  $\text{N}_2$  flow with vigorous stirring. The reaction solution was heated to  $180\text{--}190^\circ\text{C}$  and held at this temperature for 1.5 hours. After cooling to room temperature, ethanol was added into the solution and the magnetic material collected by precipitation. The precipitated product was washed with ethanol and re-dispersed in 15 mL of TMAOH solution. Glutathione (0.125 g) in 2 mL degassed water was added to the NP solution and sonicated for 40 minutes to allow for ligand exchange to take place. Water soluble glutathione functionalized  $\text{Ag}@Fe_3\text{O}_4$  NPs ( $\text{Ag}@Fe_3\text{O}_4$ -GSH) were precipitated and washed with ethanol and water to remove unbound GSH from the surface of the NPs. Finally, the obtained nanoparticles were dried under vacuum at  $50^\circ\text{C}$ .

### Cell culture and viruses

Green monkey kidney cells (Vero-CCL81, ATCC) were used for analyses of human herpes simplex type 1 (MacIntyre, Zeptomatrix), Adenovirus type 5 (Adenoid 75-, ATCC), *Poliovirus type 1*, (*LSc 2ab*, ATCC). Madin Darby Bovine Kidney Cells (MDBK-NBL-1, ATCC) were used for *Bovine coronavirus*



(Mebus, ATCC) analysis. All cell lines and viruses were obtained from the Genetic and Bioengineering Department of Yeditepe University, (Istanbul, Turkey).

### **Cytotoxicity assay and antiviral activity**

Cytotoxicity assay and antiviral activity studies were based on Spearman-Kärber method (Ramakrishnan, 2016) and EN14476 European standard method. Briefly, for cytotoxicity assay, Vero cells were seeded  $4 \times 10^4$  cell/well in 96 well plate with DMEM-H and incubated at 37 °C, 5% CO<sub>2</sub> incubator for 24 hours. Then, cells were treated with *Log10* serial dilution of Ag@Fe<sub>3</sub>O<sub>4</sub>-GSH, Fe<sub>3</sub>O<sub>4</sub>-GSH and GSH and incubated at 37 °C 5% CO<sub>2</sub> incubator for 24 hours to determine maximum nontoxic dose (MNTD). Vero cells were seeded based on the same procedure for monolayer formation in each well to determine antiviral activity. Viruses were diluted based on *Log10* serial dilution with virus medium (1% PSA, MEM, Gibco) and the material MNTD applied on them for 15 minutes. Then, old media was removed from cell monolayer and washed with PBS three times. The mixture of the virus and nanoparticles and GSH were transferred on to cells and incubated for 72 hours. At the end of the incubation period, the cytopathic effect (CPE) due to the viral infection was evaluated under an inverted microscope. Results were calculated with the following formulas; where  $X_k$  refers to highest dilution dose,  $d$ : represents the difference between dilutions,  $n$  represents the number of wells per dilution,  $r$ : (-) is the sum of the answers,  $M_v$  is the value of antiviral activity,  $L_g(V_c)$  refers to the logarithmic average of virus control biological replicates and  $L_g(V_a)$  is the logarithmic average of experimental biological replicates.

$$M = X_k + d \times [0.5 - (1/n) \times (r)] \quad [1]$$

$$M_v = L_g(V_c) - L_g(V_a) \quad [2]$$

## **Results and discussion**

The Fe<sub>3</sub>O<sub>4</sub>-GSH NPs were synthesized in benzyl ether as organic solvent with oleic acid and oleylamine, resulting in surface coated with hydrophobic ligands. This was followed by the ligand exchange procedure to obtain the coated with GSH (Robinson et al., 2010). The Ag@Fe<sub>3</sub>O<sub>4</sub>-GSH NPs were obtained with a two step procedure, including the formation of the Fe<sub>3</sub>O<sub>4</sub> NPs first, followed by the reduction of a silver salt in order to add a layer of Ag on the iron oxide NPs, which was dissolved in benzyl ether. This core-shell nanoparticles were then functionalized with GSH (Bankole & Nyokong, 2016; Robinson et al., 2010). Ultraviolet-visible (UV-vis) absorption spectroscopy and X-ray diffraction (XRD) were used to detect the presence of Ag in the NPs and transmission electron microscopy (TEM) was employed to determine the morphology of the Fe<sub>3</sub>O<sub>4</sub>-GSH NPs and Ag coated Fe<sub>3</sub>O<sub>4</sub> NPs. Dynamic light scattering (DLS) was utilized to demonstrate the size of each nanoparticle and zeta potential measurement was used to see the charge of the each nanoparticle.

### **TEM micrographs**

The transmission electron microscope (TEM) was applied to determine the morphologies and shape of the Fe<sub>3</sub>O<sub>4</sub>-GSH and Ag@Fe<sub>3</sub>O<sub>4</sub>-GSH, as shown in Figure 1. The TEM micrograph for Fe<sub>3</sub>O<sub>4</sub>-GSH showed almost mono dispersed, non-aggregated, quasi-spherical shape particles. Upon capping of Fe<sub>3</sub>O<sub>4</sub> with silver to form Ag@Fe<sub>3</sub>O<sub>4</sub>-GSH NPs, in addition to small, transparent and evenly dispersed Fe<sub>3</sub>O<sub>4</sub> grains, some large, dark-colored Ag NP grains were obtained, and further aggregation was observed as compared to the pure Fe<sub>3</sub>O<sub>4</sub>-GSH NPs.

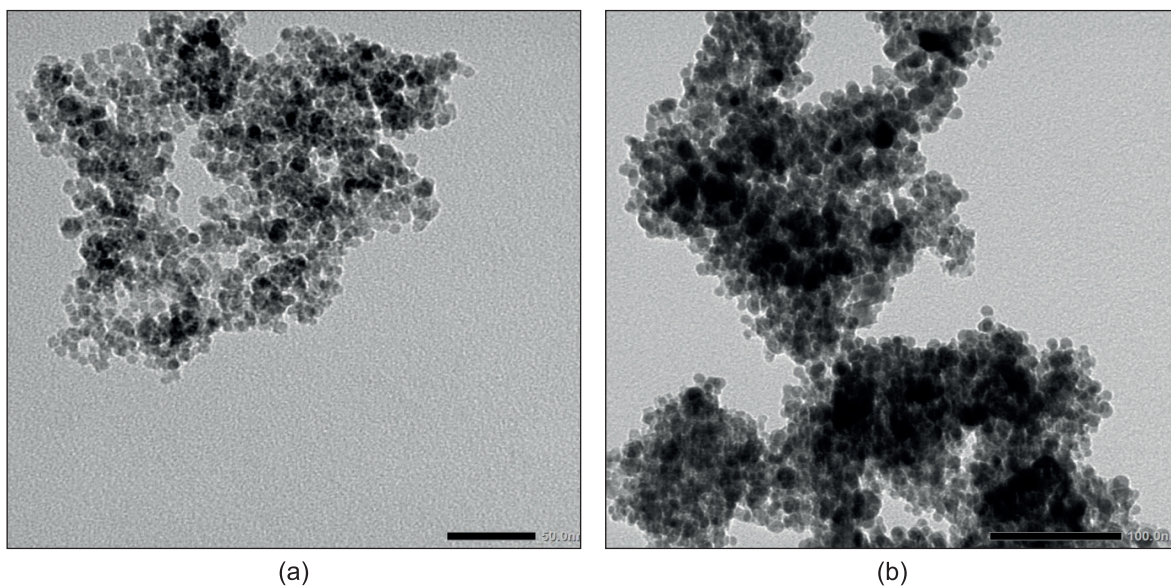


| **Figure 1.** TEM images of a)  $\text{Fe}_3\text{O}_4$ -GSH, b)  $\text{Ag}@\text{Fe}_3\text{O}_4$ -GSH.

#### ***Dynamic light scattering (DLS) spectra and zeta potential***

DLS was used for the determination of particle size for both type of the nanoparticles (Figure 2). The average size determined by DLS was 4.48 nm for  $\text{Fe}_3\text{O}_4$ -GSH. The size increased to 7.98 nm for  $\text{Ag}@\text{Fe}_3\text{O}_4$ -GSH, which indicated the successful surface coating of silver for  $\text{Fe}_3\text{O}_4$  nanoparticles.

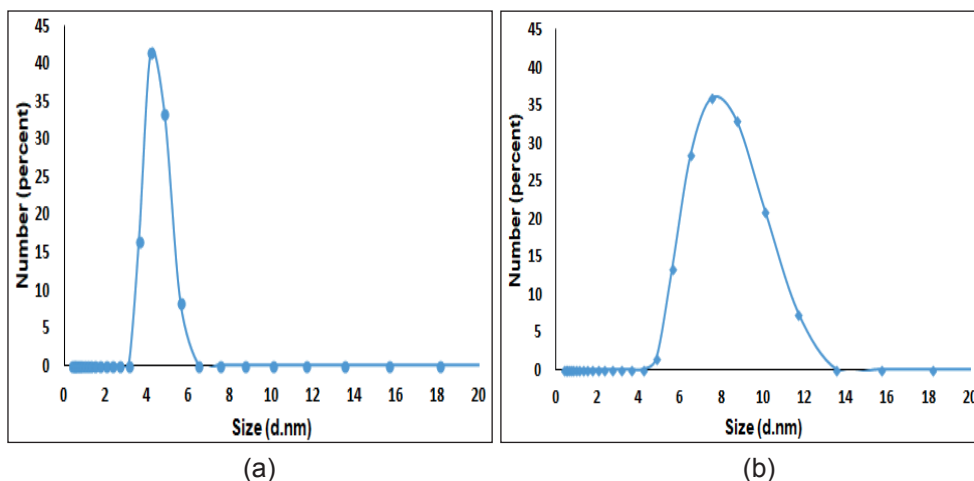


| **Figure 2.** DLS graph showing average particle size of a)  $\text{Fe}_3\text{O}_4$ -GSH, b)  $\text{Ag}@\text{Fe}_3\text{O}_4$ -GSH.

Zeta potential measurements allow us to evaluate the colloidal stability in solution, as well as NPs surface charge. Surface charges of the studied nanoparticles are shown in the zeta potential graphs (Figure 3). The zeta potential value was determined as -19 mV for  $\text{Fe}_3\text{O}_4$ -GSH and -35.7 mV for  $\text{Ag}@\text{Fe}_3\text{O}_4$ -GSH in ethanol suspension. The huge negative surface charge of the  $\text{Ag}@\text{Fe}_3\text{O}_4$ -GSH shows its higher stability due to the repulsive force among particles (Khashan et al., 2017).

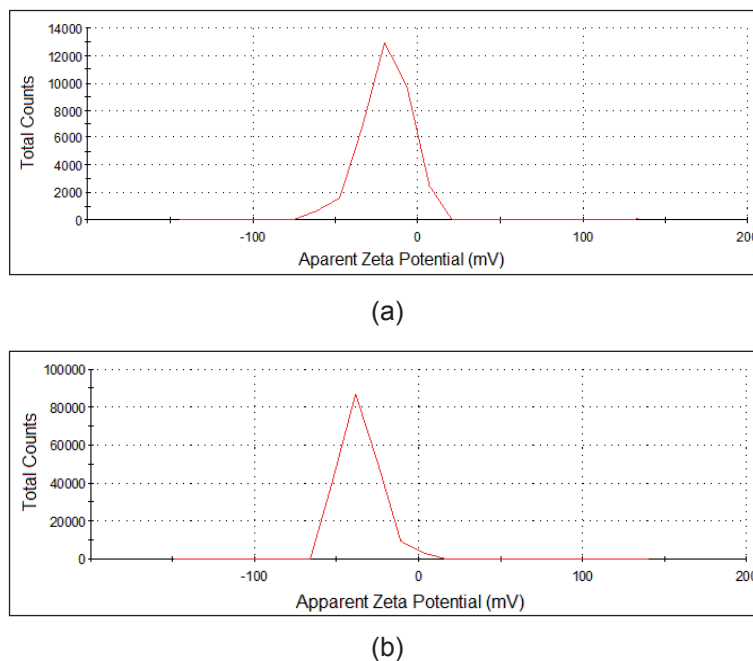


**Figure 3.** Zeta potential of a)  $\text{Fe}_3\text{O}_4$ -GSH, b)  $\text{Ag}@\text{Fe}_3\text{O}_4$ -GSH dispersed in ethanol.

### ***X-ray diffraction (XRD)***

XRD was employed for investigation of crystallinity of the prepared NPs and XRD patterns of  $\text{Fe}_3\text{O}_4$ -GSH nanoparticles and  $\text{Ag}@\text{Fe}_3\text{O}_4$ -GSH core-shell nanoparticles, as shown in Figure 4. The observed characteristic diffraction peaks for  $\text{Fe}_3\text{O}_4$  ( $2\theta = 30.2, 35.5, 43.0, 54.2, 56.7$  and  $62.4^\circ$ ) can be assigned to diffraction of  $\text{Fe}_3\text{O}_4$  crystal with an inverse spinel structure (Malekia et al., 2020). The XRD diffraction patterns of the  $\text{Ag}@\text{Fe}_3\text{O}_4$ -GSH nanoparticles showed well-defined crystalline peaks at  $2\theta = 30.3, 35.7, 38.3, 44.3, 53.8, 57.1, 63.01, 64.5, 77.5$  and  $81.6^\circ$ . The peaks that are characteristic of silver at  $38.3, 44.3, 64.5, 77.5$  and  $81.6^\circ$  corresponding to the face centered-cubic structure of metallic silver were not observed for  $\text{Fe}_3\text{O}_4$ -GSH NPs due to the presence of the Ag shell on the magnetic NPs and the other peaks at  $2\theta = 30.3, 35.7, 53.8, 57.1$  and  $63.01^\circ$  were similar crystalline peaks, which are shifted compared to the  $\text{Fe}_3\text{O}_4$ -GSH NPs crystalline planes.

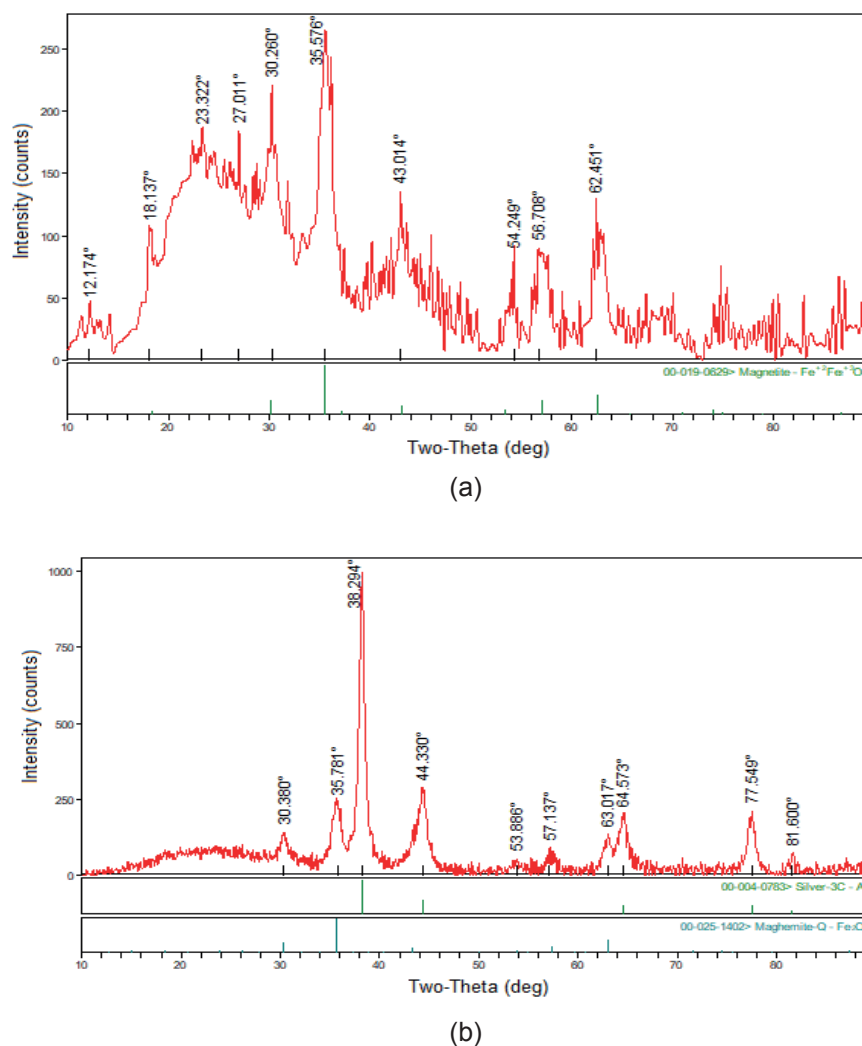


**Figure 4.** X-ray diffraction patterns of a)  $\text{Fe}_3\text{O}_4$ -GSH, b)  $\text{Ag}@\text{Fe}_3\text{O}_4$ -GSH.

### Optical properties

The UV–vis absorption spectrum was applied to characterize the synthesized nanoparticles (Figure 5). The optical absorption spectra of the  $\text{Fe}_3\text{O}_4$ -GSH exhibit absorption peak at around 250 nm. This peak is related to the electrons moving from the oxygen atom to the d-metal orbital (Ramesh et al., 2017). The large bump in absorption spectrum of  $\text{Ag}@\text{Fe}_3\text{O}_4$ -GSH NPs at around 480 nm was due to resonant excitation of surface plasmons (SPR) of the Ag surface (Xu et al., 2006).

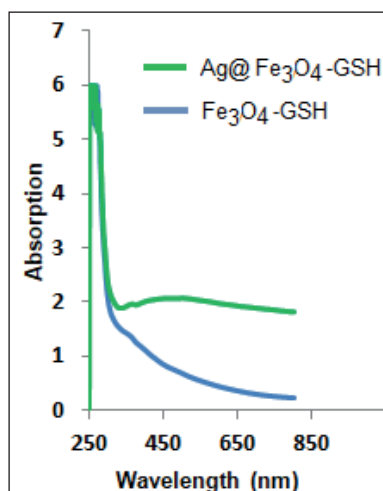


**Figure 5.** UV–Visible absorption spectrum of Fe<sub>3</sub>O<sub>4</sub>-GSH NPs and Ag@Fe<sub>3</sub>O<sub>4</sub>-GSH NPs.

### **Antiviral activity**

Antiviral activity analysis can be performed for screening and evaluating viral entry inhibition, viral genome replication blocking and viral maturation inhibition (Rumlová & Ruml, 2017). In this research, antiviral activities of Ag@Fe<sub>3</sub>O<sub>4</sub>-GSH, Fe<sub>3</sub>O<sub>4</sub>-GSH and GSH were evaluated for viral entry inhibition. Ultimately, significant inhibition was observed with Ag@Fe<sub>3</sub>O<sub>4</sub>-GSH against Poliovirus (4 Log), Adenovirus (3 Log), and HSV-1 (2 Log). GSH exhibited remarkable antiviral effects against Bovine coronavirus (3 Log) and showed a log reduction of 1 Log against HSV-1 and Poliovirus. Fe<sub>3</sub>O<sub>4</sub>-GSH demonstrated a reduction of 1 Log, particularly against RNA viruses, such as Poliovirus and Bovine coronavirus (Table 1). Among these, only Ag@Fe<sub>3</sub>O<sub>4</sub>-GSH nanoparticles have an antiviral effect against all type of viruses at least 99%, while their activity against Bovine coronaviruses was 90%. This situation demonstrates that GSH and Fe<sub>3</sub>O<sub>4</sub> molecules, when combined with silver to form Ag@Fe<sub>3</sub>O<sub>4</sub>-GSH nanoparticles, exhibit a synergistic effect against human DNA and RNA viruses. However, synergistic effect was not observed against bovine coronavirus. This can be attributed to host differences, variations in viral membrane proteins, and diversity in host receptors (Teissier et al., 2011). Studies have shown that a deficiency in glutathione, a potent antioxidant, can lead to the accumulation of reactive oxygen species (ROS) in cells, potentially resulting in immune suppression and faster progression of infections (Khanfari & Al Qaroot, 2020). The obtained results regarding glutathione support this information. This is because glutathione alone demonstrates a reduction of 1 log against HSV-1 and Poliovirus, and a reduction of 3 logs against bovine coronavirus, particularly enhancing its efficacy against human viruses in nanoparticle form. Given that bovine coronavirus belongs to the same family as SARS-CoV-2 and is considered as a model virus for SARS-CoV-2 in the literature (Naqvi et al., 2020), it is believed that glutathione, either alone or in combination with human host cells, may also exhibit antiviral activity against SARS-CoV-2.

Although it has been revealed that GSH depletion plays a role in a wide variety of viral infections (Beck et al., 2000) and nanoparticles made of silver can be effective antiviral agents against varieties such as HIV-1 (Sun et al., 2005), hepatitis B virus (Lu et al., 2008), herpes simplex virus type 1 (Baram-Pinto et al., 2009), influenza virus (Papp et al., 2010), the antiviral activity of GSH coated silver nanoparticles as shell around the magnetic nanoparticle core have not been reported.

| **Table 1.** *In vitro* antiviral activity of the studied samples.

Compounds	Log reduction			
	HSV-1	Adenovirus	Poliovirus	BCoV
Ag@Fe <sub>3</sub> O <sub>4</sub> -GSH	2	3	4	1
Fe <sub>3</sub> O <sub>4</sub> -GSH	-	-	1	1
GSH	1	-	1	3

## Conclusions

The antiviral activity of iron oxide nanoparticles against HSV-1, poliovirus, adenovirus and bovine coronavirus were investigated. In order to see the capping agent (GSH) effect over the studied viruses, GSH was also investigated. Among the prepared magnetic nanoparticles, the nanoparticles containing a magnetic core and a silver shell (Ag@Fe<sub>3</sub>O<sub>4</sub>-GSH) exhibited remarkable activity than the bare magnetic nanoparticles (Fe<sub>3</sub>O<sub>4</sub>-GSH).

## Acknowledgements

We are thankful to the Department of Genetic and Bioengineering, Yeditepe University for providing necessary facilities to carry out the experiment of this work.

## Conflict of interest

The authors declare no conflict of interest.

## Data availability statement

Data can be obtained from the corresponding author upon a reasonable request.

## Ethics committee approval

Ethics committee approval is not required for this study.

## Authors' contribution statement

**Study conception and design:** P.S.; **Data collection:** P.S. S.D., B.C.A., **Analysis and interpretation of results:** P.S., S.D., B.C.A., F.S.; **Manuscript draft preparation:** P.S., S.D., B.C.A., F.S. All authors reviewed the results and approved the final version of the manuscript.

## ORCIDs and emails of the authors

Pinar Sen | ORCID 0000-0002-3181-9890 | [sen\\_pinar@hotmail.com](mailto:sen_pinar@hotmail.com)

Sevda Demir | ORCID 0000-0003-0427-3519 | [sevda.demir@yeditepe.edu.tr](mailto:sevda.demir@yeditepe.edu.tr)

Bekir Can Altindisogullari | ORCID 0000-0002-2753-6046 | [bekir.can@yeditepe.edu.tr](mailto:bekir.can@yeditepe.edu.tr)

Fikrettin Sahin | ORCID 0000-0003-3993-1630 | [fsahin@yeditepe.edu.tr](mailto:fsahin@yeditepe.edu.tr)

## References

- Antone, A.J., Sun, Z., & Bao, Y. (2019). Preparation and Application of Iron Oxide Nanoclusters. *Magnetochemistry*, 5, 45. <https://doi.org/10.3390/magnetochemistry5030045>
- Bankole, O.M., & Nyokong, T. (2016). Comparative studies on photophysical and optical limiting characterizations of low symmetry phthalocyanine linked to Fe<sub>3</sub>O<sub>4</sub>-Ag core-shell or hybrid nanoparticles. *New journal of chemistry*, 40, 10016-10027. <https://doi.org/10.1039/c6nj01511e>
- Baram-Pinto, D., Shukla, S., Perkas, N., Gedanken, A., & Sarid, R. (2009). Inhibition of herpes simplex virus type 1 infection by silver nanoparticles capped with mercaptoethane sulfonate. *Bioconjugate chemistry*, 20, 1497-1502. <https://doi.org/10.1021/bc900215b>
- Beck, M.A., Handy, J., & Levander, O.A. (2000). The role of oxidative stress in viral infections. *Annals of the new york academy of sciences*, 917, 906-912. <https://doi.org/10.1111/j.1749-6632.2000.tb05456.x>
- Govan, J., & Gunko Y.K. (2014). Recent Advances in the Application of Magnetic Nanoparticles as a Support for Homogeneous Catalysts. *Nanomaterials*, 4, 222-241. <https://doi.org/10.3390/nano4020222>
- Gupta, A.K., & Gupta, M. (2005). Synthesis and surface engineering of iron oxide nanoparticles for biomedical applications. *Biomaterials*, 26, 3995-4021. <https://doi.org/10.1016/j.biomaterials.2004.10.012>
- Elliott, D.W., & Zhang, A. (2001). Field Assessment of Nanoscale Bimetallic Particles for Groundwater Treatment. *Environmental science and technology*, 35, 4922-4926. <https://doi.org/10.1021/es0108584>
- Khashan, S., Dagher, S., Tit, N., Alazzam, A., & Obaidat, I. (2017). Novel Method for Synthesis of Fe<sub>3</sub>O<sub>4</sub>@TiO<sub>2</sub> Core/Shell Nanoparticles. *Surface and coating technology*, 322, 92-98. <https://doi.org/10.1016/j.surfcoat.2017.05.045>
- Khanfari, A., & Al Qaroot, B. (2020). Could glutathione depletion be the Trojan horse of COVID-19 mortality?. *European Review for Medical and Pharmacological Sciences*, 24, 12500-12509.
- Kostopoulou, A., & Lappas, A. (2015). Colloidal magnetic nanocrystal clusters: Variable length-scale interaction mechanisms, synergetic functionalities and technological advantages. *Nanotechnology reviews*, 2015, 4, 595-624. <https://doi.org/10.1515/ntrev-2014-0034>
- Kumari, M., Gupta, R., & Jain, Y. (2019). Fe<sub>3</sub>O<sub>4</sub>-Glutathione stabilized Ag nanoparticles: A new magnetically separable robust and facile catalyst for aqueous phase reduction of nitroarenes. *Applied organometallic chemistry*, 33, 5223. <https://doi.org/10.1002/aoc.5223>
- Lu, L., Sun, R.W. Chen, R., Hui, C.K., Ho, C.M., Luk, J.M., Lau, G.K., & Che, C.M. (2008). Silver nanoparticles inhibit hepatitis B virus replication. *Antiviral therapy*, 13, 253-262. <https://doi.org/10.1177/135965350801300210>

- Malekia, B., Esmailnezhad, E., Choi, H.J., Koushkid, E., Aliabad, H.A.R., & Esmaeili, M. (2020). Glutathione-capped core-shell structured magnetite nanoparticles: Fabrication and their nonlinear optical characteristics. *Current applied physics*, 20, 822–827. <https://doi.org/10.1016/j.cap.2020.03.020>
- Mbuyazi, T.B., & Ajibade, P.A. (2023). Influence of Different Capping Agents on the Structural, Optical, and Photocatalytic Degradation Efficiency of Magnetite (Fe<sub>3</sub>O<sub>4</sub>) Nanoparticles. *Nanomaterials*, 13, 2067. <https://doi.org/10.3390/nano13142067>
- Nguyen, M.D., Tran, H., Xu, S., & Lee, T.R. (2021). Fe<sub>3</sub>O<sub>4</sub> Nanoparticles: Structures, Synthesis, Magnetic Properties, Surface Functionalization, and Emerging Applications. *Applied sciences*, 11, 11301. <https://doi.org/10.3390/app112311301>
- Naqvi, A.A.T., Fatima, K., Mohammad, T., Fatima, U., Singh, I.K., Singh, A., Atif, S.M., Hariprasad, G., Hasan, G.M., & Hassan, I. (2020). Insights into SARS-CoV-2 genome, structure, evolution, pathogenesis and therapies: Structural genomics approach. *BBA - Molecular basis of disease*, 1866, 1658. <https://doi.org/10.1016/j.bbadis.2020.165878>
- Naseem, T., & Durrani, T. (2021). The role of some important metal oxide nanoparticles for wastewater and antibacterial applications: A review. *Environmental chemistry and ecotoxicology*, 3, 59–75. <https://doi.org/10.1016/j.enceco.2020.12.001>
- Palamara, AT., Perno, C.F, Aquaro, S., Bue, M.C., Dini, L., & Garaci, E. (1996) Glutathione inhibits HIV replication by acting at late stages of the virus life cycle. *AIDS research & human retroviruses*, 12, 1537–1541. <https://doi.org/10.1089/aid.1996.12.1537>
- Papp, I., Sieben, C., Ludwig, K., Roskamp, M., Böttcher, C., Schlecht, S., Herrmann, A., & Haag, R. (2010). Inhibition of influenza virus infection by multivalent sialic-acid-functionalized gold nanoparticles. *Small*, 6, 2900–2906. <https://doi.org/10.1002/smll.201001349>
- Parvez, M.K., & Parveen, S. (2017). Evolution and Emergence of Pathogenic Viruses: Past, Present, and Future. *Intervirology*, 60, 1–7. <https://doi.org/10.1159/000478729>
- Ramakrishnan, M.A. (2016). Determination of 50% endpoint titer using a simple formula. *World Journal of virology*, 5(2), 85-86. <https://doi.org/10.5501/wjv.v5.i2.85>
- Ramesh, R., Geerthana, M., Prabhu, S., & Sohila, S. (2017). Synthesis and Characterization of the Superparamagnetic Fe<sub>3</sub>O<sub>4</sub>/Ag Nanocomposites. *Journal of cluster science*, 28, 963–969. <https://doi.org/10.1007/s10876-016-1093-9>
- Robinson, L, Tung, L.D., Maenosono, S., Walti, C., & Thanh, N.T.K. (2010). Synthesis of core-shell gold coated magnetic nanoparticles and their interaction with thiolated DNA. *Nanoscale*, 2, 2624–2630. <https://doi.org/10.1039/c0nr00621a>
- Rumlová, M., & Ruml, T. (2017). In vitro methods for testing antiviral drugs. *Biotechnology advances*, 36(3), 557–576. <https://doi.org/10.1016/j.biotechadv.2017.12.016>
- Sun, R.W., Chen, R., Chung, N.P., Ho, C.M., Lin, C.L., & Che, C.M. (2005). Silver nanoparticles



- fabricated in HEPES buffer exhibit cytoprotective activities toward HIV-1 infected cells. *Chemical communications*, 40, 5059–5061. <https://doi.org/10.1039/B510984A>
- Teissier, E., Penin, F., & Pécheur, E. (2011). Targeting Cell Entry of Enveloped Viruses as an Antiviral Strategy. *Molecules*, 16, 221-250. <https://doi.org/10.3390/molecules16010221>
- Townsend, D.M., Tew, K.D., & Tapiero, H. (2003). The importance of glutathione in human disease. *Biomedicine & pharmacotherapy*, 57, 145–155. [https://doi.org/10.1016/S0753-3322\(03\)00043-X](https://doi.org/10.1016/S0753-3322(03)00043-X)
- Xu, G., Chen, Y., Tazawa, M., & Jin, P. (2006). Surface Plasmon Resonance of Silver Nanoparticles on Vanadium Dioxide. *The journal of physical chemistry b*, 110, 2051-2056. <https://doi.org/10.1021/jp055744j>
- Zhang, L., Dou, Y., & Gu, H. (2006). Synthesis of Ag–Fe<sub>3</sub>O<sub>4</sub> heterodimeric nanoparticles. *Journal of colloid and interface science*, 297, 660–664. <https://doi.org/10.1016/j.jcis.2005.11.009>

## RESEARCH ARTICLE

# Exploring biofilm-forming bacteria for integration into BioCircuit wastewater treatment

Chontisa Sukkasem<sup>1,2\*</sup> <sup>1</sup> Department of Food Science and Technology, Faculty of Agro and Bio Industry, Thaksin University, Thailand<sup>2</sup> BioCircuit- Microbial Fuel Cell laboratory, Inno Green Tech company, Thailand\* Corresponding author: E-mail: [chontisa.s@gmail.com](mailto:chontisa.s@gmail.com); Ph.: +66-84-212-1788.

**Citation:** Sukkasem, C. (2024). Exploring biofilm-forming bacteria for integration into BioCircuit wastewater treatment. The European chemistry and biotechnology journal, 2, 39-52.  
<https://doi.org/10.62063/ecb-28>

**License:** This article is licensed under a Creative Commons Attribution-NonCommercial 4.0 International License (CC BY-NC 4.0).

**Peer review:** Externally peer reviewed.

**Received:** 09.05.2024

**Accepted:** 24.06.2024

**Published:** 25.07.2024



## Abstract

This study aimed to investigate the presence of biofilm-forming bacteria within high sulfide sludge obtained from a rubber wastewater treatment plant and assess their suitability for application within a BioCircuit System (BCS) as a symbiotic community for treating nutrient-rich wastewater. The sludge samples were collected and subjected to microbial culture techniques, wherein pure cultures were isolated based on morphological characteristics observed under a light microscope, followed by assessment of motility using swarm agar. Subsequent identification was conducted utilizing the 16S rRNA gene sequencing method, and the isolated bacteria were introduced into the BCS. A 12 mL microbial fuel cell test was conducted to evaluate their power generation capabilities. The wastewater treatment process involved inoculating the BCS with 20% crude rubber wastewater sludge, and the system was initiated at a flow rate of 0.5 L/min for a month. Upon achieving an open-circuit voltage exceeding 50 mV, the BCS was operated at incremental flow rates (0.5-1.0, 1.0-1.5, and 1.5-2.0 mL/min) over a period of 6 months. Real-time monitoring of voltage, flow rate, and energy consumption was facilitated through an internet-of-things online program. Weekly sampling and analysis of influent and effluent, focusing on chemical oxygen demand (COD), sulfate, and sulfide concentrations, were conducted. Additionally, the BioCircuit voltage was recorded every 5 minutes. The results revealed the presence of six group-forming shaped bacteria identified as *Bacillus tequilensis*, *Bacillus sp.*, *Ferribacterium limneticum*, *Bacillus weihenstephanesis*, and *Mycobacterium sp.*, respectively. The optimal flow rate of 1.5 L/min yielded a maximum voltage of 1.2 V and demonstrated high wastewater treatment efficiency. Economically, the BCS operation exhibited a power consumption rate of 0.257 kWh/m<sup>3</sup> of treated wastewater, leading to an 88.90% reduction in carbon footprint

compared to aerated lagoon treatment, equivalent to 50.94 kg CO<sub>2</sub>/m<sup>3</sup> of treated wastewater or 183,384 kg CO<sub>2</sub>/yr for a 10 m<sup>3</sup> plant. These findings underscore the potential of the BCS in conjunction with group-forming shaped bacteria communities for various industrial wastewater treatment applications.

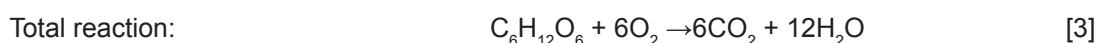
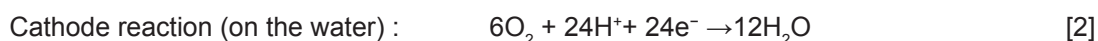
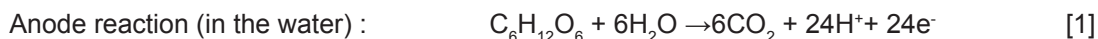
**Keywords:** BioCircuit system, biofilm-forming bacteria, chemical oxygen demand, sulfate, sulfide, wastewater treatment

## Introduction

The formation of biofilms by group-forming bacteria is a significant phenomenon with implications across various fields. Biofilms, which are intricate communities of microorganisms adhering to surfaces, contribute to processes such as nutrient cycling, bioremediation, and pathogenesis (Bridier et al., 2011; Davey & O'toole, 2000; Flemming & Wingender, 2010; Hall-Stoodley et al., 2004; Stewart & Franklin, 2008). Microbial fuel cells (MFCs) are biotechnological devices capable of generating electricity, while treating wastewater. A MFC typically consists of an anode, a cathode, a separator (proton exchange membrane or PEM), and an external circuit for electron flow (Asensio et al., 2016; Kim et al., 2007). In the anode, microorganisms oxidize organic or inorganic substrates, producing electrons. These electrons are transferred to the cathode through an external circuit, where they react with protons and oxygen to generate water, producing electrical power (Fan et al., 2024; Quan et al., 2012; Sonmez et al., 2024; Wang et al., 2011; Zhuo et al., 2011).

The relationship between group-forming bacteria and MFCs is vital, as biofilms formed by these bacteria significantly influence MFC performance and efficiency. Biofilm-forming bacteria, including those from genera such as *Bacillus*, *Pseudomonas*, and *Geobacter*, dominate MFC biofilms, facilitating electron transfer and enhancing substrate utilization (Rabaey et al., 2005; Logan et al., 2006; Huang & Logan, 2008).

The BioCircuit: biocatalyst microbial fuel cell, developed in previous studies (Sukkasem et al., 2008, 2011; Sukkasem & Laehlah, 2013, 2015), aims to treat nutrients like nitrate and sulfate in wastewater. The configuration, adapted from the UBFC single chamber to double chambers, maintains the concept of membrane-less operation and avoids platinum catalysts. Electrons and protons transfer from the anode to the cathode via a circuit and a pipe, facilitating reactions crucial for wastewater treatment (Figure 1).



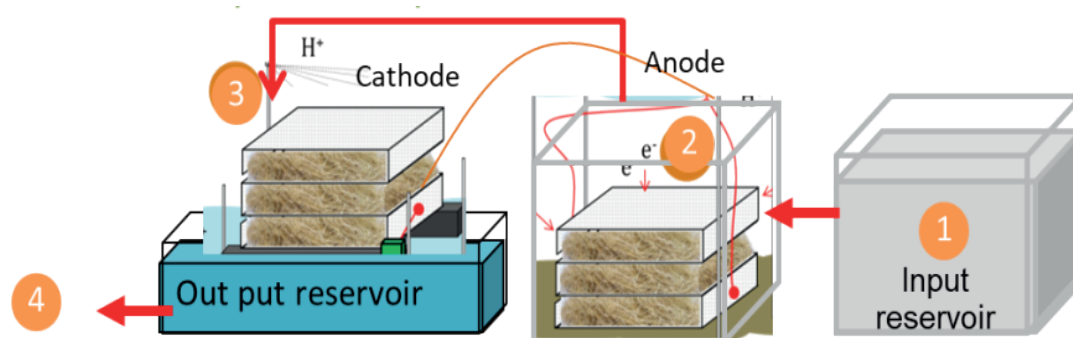
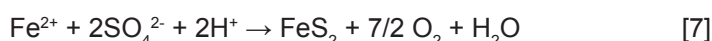
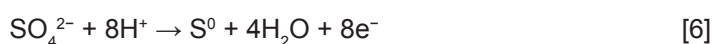
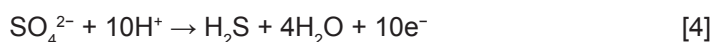


**Figure 1.** Schematic of the BioCircuit system 1) input reservoir 2) the circuit for the electron transfers from anode to cathode 3) the pipe for protons transferring form anode to cathode 4) output reservoir.

Natural rubber is a pivotal material in our economy and daily lives due to its exceptional properties, such as strength, surpassing those of synthetic rubber. However, the production process of natural rubber from raw latex results in substantial wastewater discharge. This rubber processing wastewater is typically contaminated with sulfur compounds stemming from sulfuric acid coagulation, preservatives, and inherent latex constituents. Under anaerobic conditions, sulfate reduction occurs, leading to the release of toxic hydrogen sulfide gas ( $\text{H}_2\text{S}$ ). The emission of  $\text{H}_2\text{S}$  not only poses significant health and environmental hazards, but also incurs economic repercussions due to its corrosive effects on metallic structures. The discharge of such wastewater into groundwater reservoirs has severe consequences, particularly in southern Thailand (Sukkasem & Laehlah, 2015).

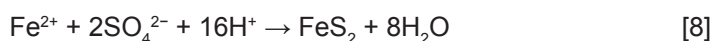
The biocatalyst microbial fuel cell demonstrates remarkable efficacy in treating inorganic substances like sulfate and sulfide, which serve as precursors to malodorous and hazardous hydrogen sulfide gas. It facilitates the conversion of soluble sulfate and sulfide into solid forms, such as elemental sulfur or pyrite (Eq. 4-Eq. 8), which precipitate within the system and can be easily separated from the wastewater stream.

*Anode reaction:*



*The reaction for pyrite formation is shown in eq (7) which occurs both in anode and cathode when the excess sulfate and iron ions present:*

*Cathode reaction:*



The formation of pyrite (iron sulfide,  $\text{FeS}_2$ ) involves a chemical reaction that can occur both at the anode and cathode under specific conditions when there is an excess of sulfate and iron ions present. This reaction is crucial to understanding various contexts, including geochemistry,

environmental science, and electrochemistry. In electrochemistry, the formation of pyrite can occur in electrochemical cells under certain conditions. For example, in microbial fuel cells (MFCs) or other bioelectrochemical systems, sulfate-reducing bacteria can catalyze the reduction of sulfate to sulfide at the cathode, where iron ions may be present. This can lead to the precipitation of pyrite on the cathode surface, affecting the performance and longevity of the electrochemical system. Overall, discussing the reaction for pyrite formation provides insight into a complex interplay of chemical processes that occur in various natural and engineered systems. Understanding these reactions is essential for addressing environmental challenges, optimizing industrial processes, and advancing our knowledge of Earth's geochemical cycles.

Consequently, the rubber process wastewater treatment by the BioCircuit was investigated in this study to determine the performance, efficiency, and feasibility for practical application.

## Materials and methods

### *Sample collection and bacterial cultivation*

Rubber wastewater sludges (10 g) were obtained from two sampling sites within a rubber wastewater treatment plant located in Phatthalung province, Thailand. The sludge samples were inoculated into 100 mL of sterile nutrient broth (1 g/L beef extract, 2 g/L yeast extract, 5 g/L peptone, and 5 g/L sodium chloride), supplemented with 50 mg/L nystatin to eliminate fungal contamination. The nutrient broth was then incubated for 24 hours at room temperature with agitation at 150 rpm.

### *Bacterial isolation*

The incubated broth from the previous step was streaked onto nutrient agar plates (1 g/L beef extract, 2 g/L yeast extract, 5 g/L peptone, 5 g/L sodium chloride, and 15 g/L agar) and incubated for 24 hours at room temperature. The cultures were streaked repeatedly until pure cultures were obtained.

### *Microscopic screening and motility test*

Pure cultures were examined under light microscope to identify group-forming bacterial shapes, and those exhibiting such characteristics were selected. The motility of these cultures was determined using the swarming motility test, which assesses rapid multicellular bacterial surface movement.

### *Identification*

Genomic DNA was extracted from selected bacterial strains using the Bio-Rad DNA Extraction Kit (Biorad, United States). The 16S rRNA gene was amplified using the universal primer pair Bact-0341 (CCTACGGGNGGCWGCAG) and Bact-0785 (GACTACHVGGGTATCTAATC). The PCR products were sequenced, and the obtained sequences were compared to sequences in the GenBank database for identification.

### *Electricity generation property test*

Each group-forming bacterial culture was grown in potato dextrose broth for 3 days. The half-cell potential and electricity generation properties were tested using an Ag/AgCl reference electrode and microbial fuel cell (MFC), respectively. In the MFC test, each bacterial culture was introduced into the anode compartment, and the voltage of each MFC was recorded using a data logger program at intervals of 1000 milliseconds.

### *Wastewater treatment*

A 10 m<sup>3</sup> BioCircuit Reactor was utilized for wastewater treatment. Wastewater from an anaerobic

pond was introduced into the BCS and operated at three different flow rates (1.0, 1.5, and 2.0 L/min) for a duration of 6 months. Weekly sampling of influent and effluent was conducted, and chemical analysis was performed. Additionally, voltage and power consumption were recorded every 5 minutes via an Internet of Things (IoT) program.

### ***Analysis and calculations***

Current (I) and power (P) was calculated as Eq. (9) and (10);

$$I = V/R \quad (9)$$

$$P = V^2/R \quad (10),$$

where V is a cell voltage (V), R is an external resistance ( $\Omega$ ). Volumetric current or power is calculated by dividing the current or power by an anode volume.

The COD, sulfate and sulfide concentrations were analyzed using standard method. A complete block design (CBD) and Duncan test were used for statistical analysis. Denaturing gradient gel electrophoresis (DGGE) genetic analysis was used to identify microbial communities. All analyses were performed in SPSS version 24.0 (IBM, United States). Values mentioned in the tables and text are averages  $\pm$  one sample standard deviation.

## **Results and discussion**

### ***Isolation, microscopic screening, motility, and identification***

A total of 78 bacterial strains were isolated from the rubber wastewater sludge obtained from the first-sampling site. Among these strains, only 8 exhibited the characteristic group-forming shape. These strains, denoted as A7, A13, A16, A21, A26, A36, A40, and A52, are depicted in Figure 2.

This finding highlights the diversity of bacterial species present in the rubber wastewater sludge and underscores the selective nature of the group-forming shape trait. Identification of these strains and further characterization of their properties will provide valuable insights into their potential applications, particularly in the context of wastewater treatment and bioremediation. The motility of these group-forming bacteria is of particular interest, as it can influence their ability to colonize surfaces and participate in biofilm formation, thereby affecting their efficacy in various environmental processes. Future studies will focus on elucidating the metabolic capabilities and ecological roles of these bacterial strains to harness their potential for sustainable biotechnological applications.

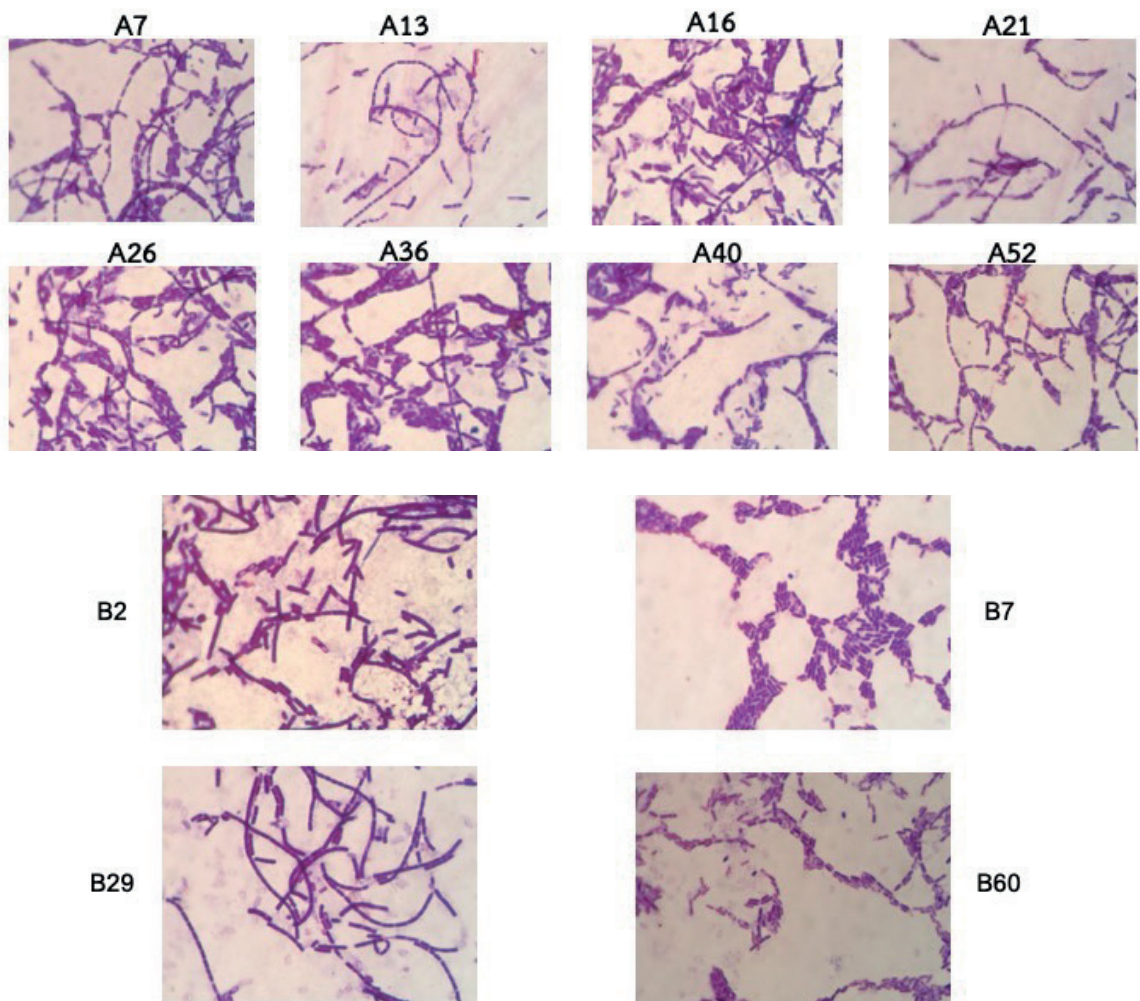


**Figure 2.** The biofilm-forming shape bacterial strains isolated from the rubber wastewater sludge.

Four of bacterial strains showed the motility ability (strains A7, A21, A36 and A40). In PCR reaction, the 16S rRNA products were amplified. The result revealed the 400-500 base-pairs were achieved from the PCR reaction (Figure 3).

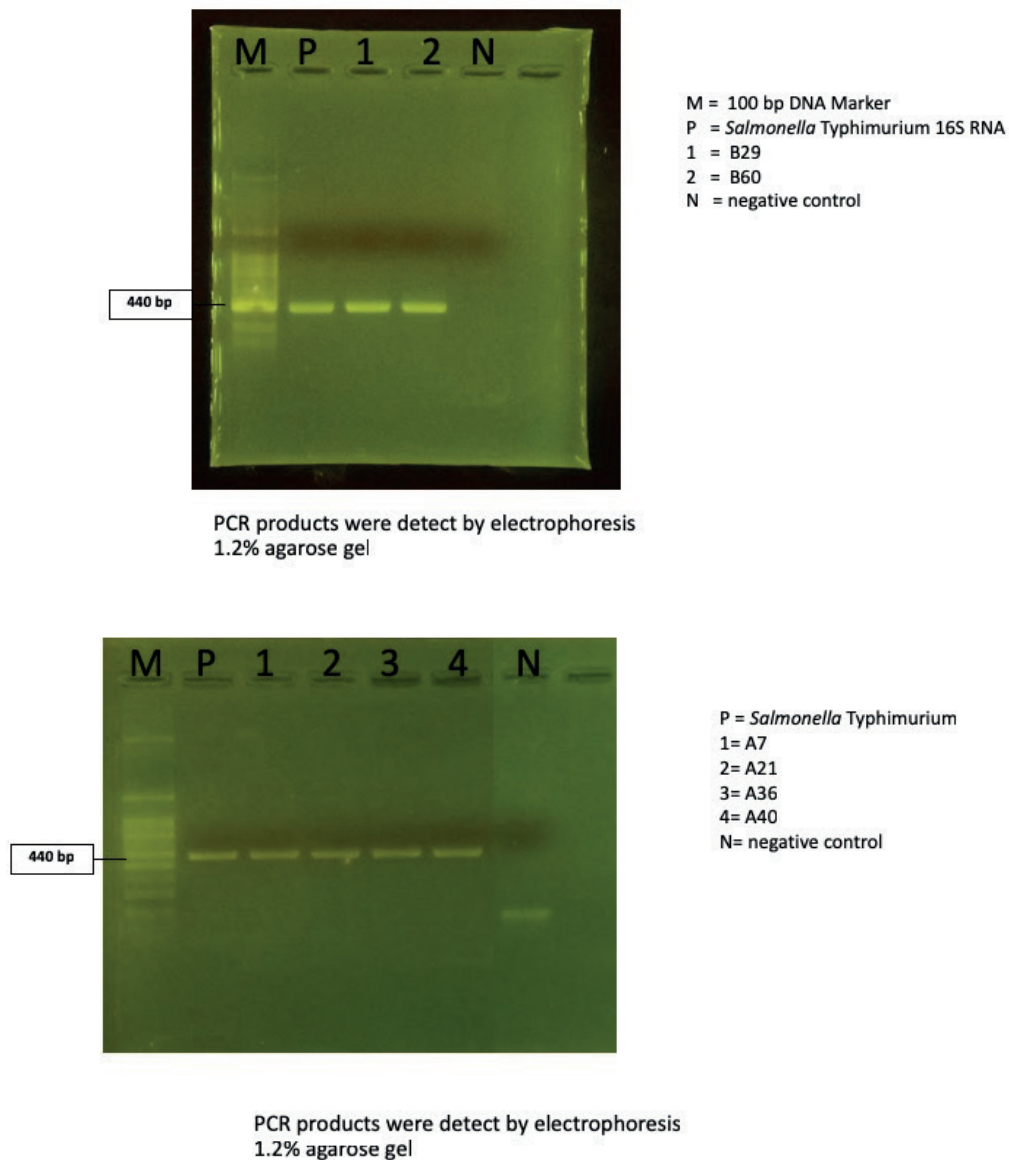


**Figure 3.** The PCR products of 16S rRNA gene of group-forming shape-forming bacterial strains.

The BLAST results revealed that strains A7, A21, A36, and A40 shared similarities with *Bacillus tequilensis*, *Bacillus sp.*, *Ferribacterium limneticum*, and *Bacillus weihenstephanensis*, respectively. The phylogenetic tree illustrating these relationships is shown in Figure 4. From the rubber wastewater sludge of the second-sampling site, a total of 61 strains were isolated, with only 4 strains exhibiting the group-forming shape, namely strains B2, B7, B29, and B60, as depicted in Figure 2. Among these strains, two (B29 and B60) demonstrated motility ability.

In the PCR reaction, amplification of the 16S rRNA gene resulted in products ranging from 400 to



500 base pairs, as depicted in Figure 3. BLAST analysis indicated that strain B29 exhibited 87% identity with *Mycobacterium* sp., while strain B60 showed a distinct sequence compared to those in the GenBank database. The phylogenetic tree representing these findings is displayed in Figure 4.

The electricity generation properties of these strains were also assessed. *Bacillus* sp., as described by N.A. Logan and De Vos (2009), encompasses various species with diverse applications, including enzyme production and bioremediation. Cummings et al. (1999) highlighted the significance of *Ferribacterium limneticum* within the phylum *Bacteroidetes*, particularly in freshwater environments, due to its role in biogeochemical cycles and bioremediation.

Furthermore, Martin and Huq (2007) discussed *Bacillus weihenstephanensis*, emphasizing its applications in antimicrobial compound production and its potential in various industries. Alvarez and Steinbüchel (2002) provided insights into *Mycobacterium* sp., noting its diverse roles in biodegradation and bioremediation, highlighting its importance in environmental cleanup efforts. These references collectively underscore the diverse characteristics and applications of the bacterial strains identified in the study.

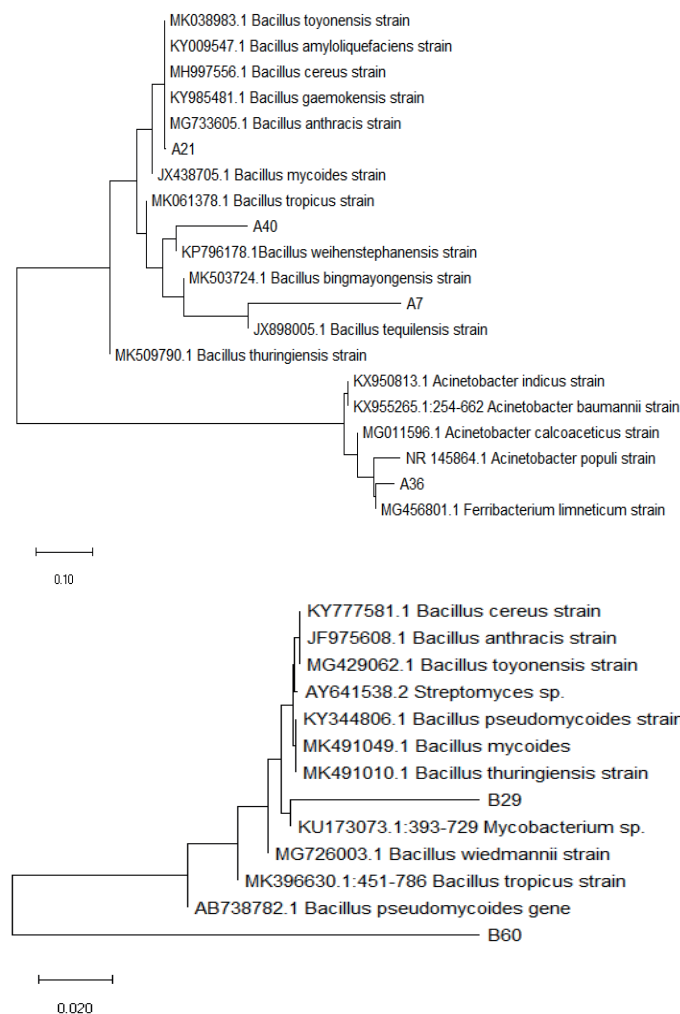


| **Figure 4.** The phylogenetic tree of the group-forming shape bacteria.

Following the cultivation of each group-forming shape in potato dextrose broth for three days, the half-cell potential and electricity generation properties were systematically evaluated using an Ag/AgCl reference electrode and microbial fuel cell (MFC), as outlined by Logan et al. (2004). In the MFC testing procedure, cultures of each group-forming shape were introduced into the anode compartment, and the voltage generated by each culture was meticulously recorded using a data logger program at intervals of 1000 milliseconds (Table 1).

**Table 1.** Electrochemical potential (V) (Ag/AgCl reference electrode) and power potential (MFC test) (V) of each biofilm-forming bacteria.

Code of bacteria	Species	Electrochemical potential (V) (Ag/AgCl reference electrode)	Power potential across 1 k $\Omega$ (MFC test) (V)
A07	<i>Bacillus tequilensis</i>	0.409	0.172
A21	<i>Bacillus anthracis</i> , <i>Bacillus gaemokensis</i> , <i>Bacillus cereus</i> , <i>Bacillus amyloliquefaciens</i> , <i>Bacillus toyonensis</i>	0.468	0.241
A36	<i>Ferribacterium limneticum</i>	0.418	0.128
A40	<i>Bacillus weihenstephanensis</i>	0.425	0.167
B29	<i>Mycobacterium sp.</i>	0.350	0.166
B60	ND	0.392	0.313

The sludge obtained from the two sources was combined and inoculated into a 1 m<sup>3</sup> reactor, constituting 20% of the working volume. This mixture was allowed to settle for a period of 30 days. Subsequently, the system was initiated at a flow rate of 0.5 L/min for an additional 30 days in open circuit mode. Following this initial phase, the system was fully operationalized at three different flow rates (1.0, 1.5, and 2.0 L/min) in closed circuit mode, with connection to a 10k $\Omega$  external resistance.

The results obtained demonstrated that the optimal flow rate of 1.5 L/min yielded a maximum voltage output of 1.2 V, as illustrated in Figure 5. Additionally, this flow rate was associated with high wastewater treatment efficiency, as depicted in Figure 6. This phenomenon may be attributed to the enhanced generation of electrons through biodegradation and bioelectrochemical reactions, which were maximized at this specific flow rate.

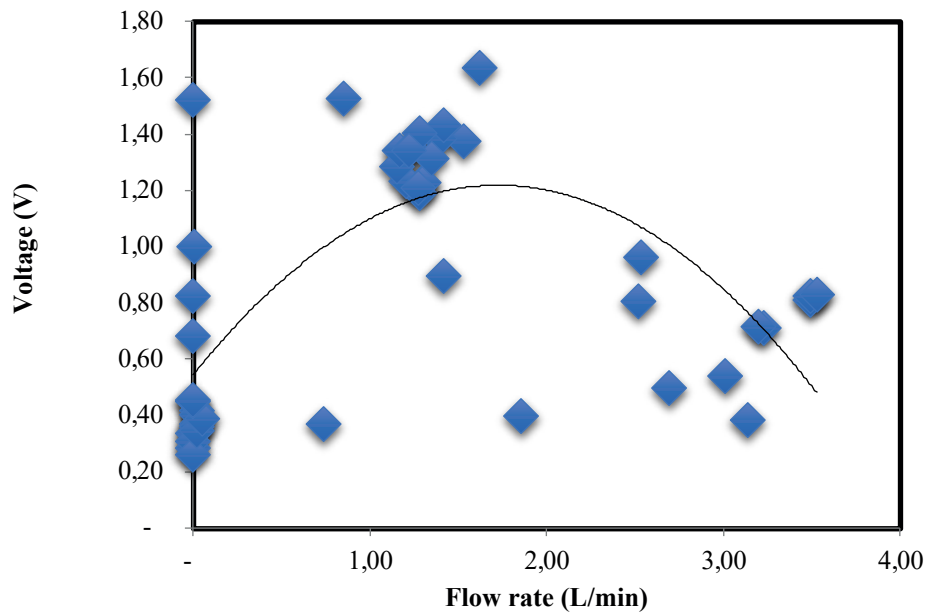


Figure 5. Power potential across 10kΩ external resistance of the BioCircuit at various flow rates.

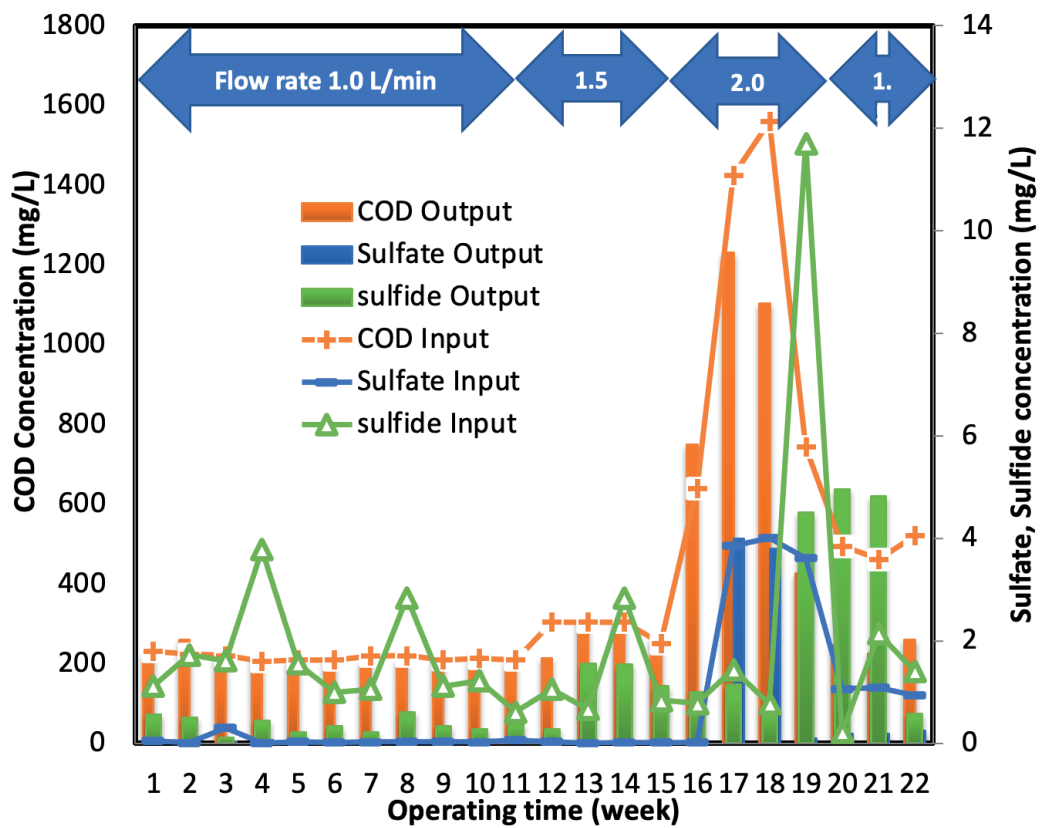
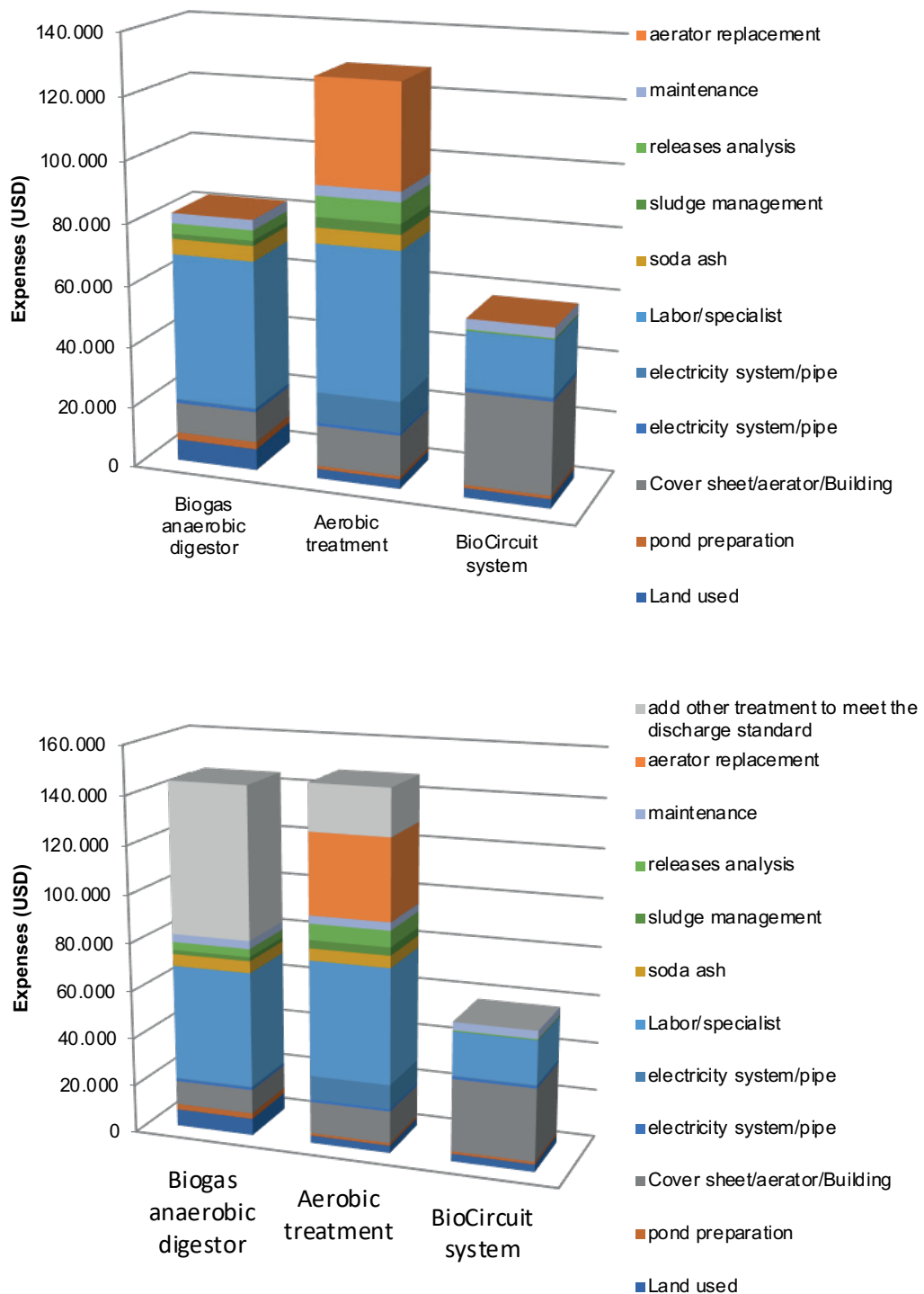


Figure 6. Wastewater treatment efficiency of the BioCircuit at various flow rates.



**Figure 7.** The investment cost and operation expenses (USD/5 y) of 5 m<sup>3</sup> BioCircuit wastewater treatment.

## Conclusions

The operational power consumption of the BioCircuit System (BCS) was calculated to be 0.257 kWh per cubic meter of treated wastewater. This represents a significant reduction of 88.90% in carbon footprint compared to traditional methods such as aerated lagoon treatment, translating to a

reduction of 50.94 kg CO<sub>2</sub> emissions per cubic meter of treated wastewater, or a substantial annual reduction of 183,384 kg CO<sub>2</sub> for a 10 m<sup>3</sup> plant.

Furthermore, the feasibility of implementing the BioCircuit System for wastewater treatment in practical applications was assessed in comparison to anaerobic and aerobic treatment methods. The analysis revealed a noteworthy cost-saving advantage, with approximately half of the expenses typically incurred over a 5-year operational period (amounting to 6,500 USD per cubic meter) being conserved (Figure 7).

These compelling economic benefits, coupled with the demonstrated efficiency and effectiveness of the BCS when integrated with group-forming shape bacteria communities, underscore its potential for widespread adoption across various industrial wastewater treatment applications.

## Acknowledgements

We are grateful to 1) Department of Food Science and Technology, Faculty of Agro and Bio Industry, Thaksin University for wastewater analysis laboratory support, 2) BioCircuit- Microbial fuel cell laboratory, Inno Green Tech Co., Ltd for BioCircuit built, set up, supply and services.

## Funding

This research was financially supported by the PMUC under Thailand government (project/grant no. C04F670053).

## Conflict of interest

The author declares no conflict of interest.

## Data availability statement

Data can be obtained from the corresponding author upon a reasonable request.

## Ethics committee approval

Ethics committee approval is not required for this study.

## Author's contribution statement

CS designed and conducted the group-forming shape bacterial screening and identification. CS conducted to analyze the electrical generation property and wastewater properties. CS designed and invented the BioCircuit. CS lead to built, set up the BioCircuit for wastewater treatment. All performed the experiment then CS wrote the manuscript.

## ORCIDs and emails of the authors

Chontisa Sukkasem | ORCID 0000-0001-8043-4981 | [chontisa.s@gmail.com](mailto:chontisa.s@gmail.com)

## References







- Alvarez, H. M., & Steinbüchel, A. (2002). Physiology, biochemistry, and molecular biology of mycobacteria. *Advances in biochemical engineering/biotechnology*, 74, 103–140. [https://doi.org/10.1007/3-540-45790-0\\_4](https://doi.org/10.1007/3-540-45790-0_4)
- Asensio, Y., Fernandez-Marchante, C. M., Lobato, J., Canizares, P., & Rodrigo, M. A. (2016). Influence of the fuel and dosage on the performance of double-compartment microbial fuel cells.

- Water research*, 99, 16–23. <https://doi.org/10.1016/j.watres.2016.04.028>
- Bridier, A., Briandet, R., Thomas, V., & Dubois-Brissonnet, F. (2011). Resistance of bacterial biofilms to disinfectants: a review. *Biofouling*, 27(9), 1017–1032. <https://doi.org/10.1080/08927014.2011.626899>
- Davey, M. E., & O'toole, G. A. (2000). Microbial biofilms: from ecology to molecular genetics. *Microbiology and molecular biology reviews*, 64(4), 847–867. <https://doi.org/10.1128/MMBR.64.4.847-867.2000>
- Fan, Y., Janicek, A., & Liu, H. (2024). Stable and high voltage and power output of CEA-MFCs internally connected in series (iCiS-MFC). *The European chemistry and biotechnology journal*, (1), 47–57. <https://doi.org/10.62063/ecb-17>
- Cummings, D., Caccavo Jr., F., Spring, S., & Rosenzweig, R.F. (1999). *Ferribacterium limneticum*, gen. nov., sp. nov., an Fe(III)-reducing microorganism isolated from mining-impacted freshwater lake sediments. *Archives of microbiology*, 171, 183–188. <https://doi.org/10.1007/s002030050697>
- Flemming, H. C., & Wingender, J. (2010). The biofilm matrix. *Nature reviews microbiology*, 8(9), 623–633. <https://doi.org/10.1038/nrmicro2415>
- Hall-Stoodley, L., Costerton, J. W., & Stoodley, P. (2004). Bacterial biofilms: from the natural environment to infectious diseases. *Nature reviews microbiology*, 2(2), 95–108. <https://doi.org/10.1038/nrmicro821>
- Huang, L., & Logan, B. E. (2008). Electricity generation and treatment of paper recycling wastewater using a microbial fuel cell. *Applied microbiology and biotechnology*, 80(2), 349–355. <https://doi.org/10.1007/s00253-008-1546-7>
- Kim, J. R., Jung, S. H., Regan, J. M., & Logan, B. E. (2007). Electricity generation and microbial community analysis of alcohol powered microbial fuel cells. *Bioresource technology*, 98(13), 2568–2577. <https://doi.org/10.1016/j.biortech.2006.09.036>
- Logan, B. E., Hamelers, B., Rozendal, R., Schröder, U., Keller, J., Freguia, S., Aelterman, P., Verstraete, W., & Rabaey, K. (2006). Microbial fuel cells: methodology and technology. *Environmental science and technology*, 40(17), 5181–5192. <https://doi.org/10.1021/es0605016>
- Logan, N. A., & De Vos, P. (2009). Genus I. *Bacillus* Cohn 1872. In P. De Vos et al. (Eds.), *Bergey's Manual of Systematic Bacteriology* (2nd ed., Vol. 3, pp. 21–127). Springer.
- Martin, H. M., & Huq, A. (2007). *Bacillus weihenstephanensis* Isolated from Fermented Fish Product, Hentak, in Bangladesh. *Journal of food protection*, 70(4), 1016–1020.
- Quan, X. C., Quan, Y. P., & Tao, K. (2012). Effect of anode aeration on the performance and microbial community of an air-cathode microbial fuel cell. *Chemical engineering journal*, 210, 150–156. <https://doi.org/10.1016/j.cej.2012.09.009>
- Rabaey, K., Boon, N., Höfte, M., & Verstraete, W. (2005). Microbial phenazine production enhances electron transfer in biofuel cells. *Environmental science and technology*, 39(9), 3401–3408. <https://doi.org/10.1021/es048563o>
- Sonmez, E., Avci, B., Mohamed, N., & Bermek, H. (2024). Investigation of performance losses in microbial fuel cells with low platinum loadings on air-cathodes. *The European chemistry and biotechnology journal*, (1), 11–26. <https://doi.org/10.62063/ecb-14>

- Stewart, P. S., & Franklin, M. J. (2008). Physiological heterogeneity in biofilms. *Nature reviews microbiology*, 6(3), 199-210. <https://doi.org/10.1038/nrmicro1838>
- Sukkasem, C., Xu, S., Park, S., Boonsawang, P., & Liu, H. (2008). Effect of nitrate on the performance of single chamber air cathode microbial fuel cells. *Water research*, 42(19), 4743-4750. <https://doi.org/10.1016/j.watres.2008.08.029>
- Sukkasem, C., Laehlah, S., Nhimman, A., O'thong, S., Boonsawang, P., Rarngnarong, A., Nisoa, M., & Kirdtongmee, P. (2011). Upflow bio-filter circuit (UBFC) biocatalyst microbial fuel cell (MFC) configuration and application to biodiesel wastewater treatment. *Bioresource technology*, 102, 10363-10370. <https://doi.org/10.1016/j.biortech.2011.09.007>
- Sukkasem, C., & Laehlah, S. (2013). Development of a UBFC biocatalyst fuel cell to generate power and treat industrial wastewaters. *Bioresource technology*, 146, 749-753. <https://doi.org/10.1016/j.biortech.2013.07.065>
- Sukkasem, C., & Laehlah, S. (2015). An economical upflow bio-filter circuit (UBFC): a biocatalyst microbial fuel cell for sulfate- sulfide rich wastewater treatment. *Water research*, 1(1), 8. <https://doi.org/10.1039/C4EW00028E>
- Wang, X., Cheng, S. A., Zhang, X. Y., Li, X. Y., & Logan, B. E. (2011). Impact of salinity on cathode catalyst performance in microbial fuel cells (MFCs). *International journal of hydrogen energy*, 36(21), 13900-13906. <https://doi.org/10.1016/j.ijhydene.2011.03.052>
- Zhuo, R., Ma, L., Fan, F. F., Gong, Y. M., Wan, X., Jiang, M. L., Zhang, X. Y., & Yang, Y. (2011). Decolorization of different dyes by a newly isolated white-rot fungi strain *Ganoderma* sp.En3 and cloning and functional analysis of its laccase gene. *Journal of hazardous materials*, 192(2), 855-873. <https://doi.org/10.1016/j.jhazmat.2011.05.106>

## RESEARCH ARTICLE

# Investigation of antiproliferative and antimicrobial activities of carbon nanofiber based aerogels loaded with rutin and krill oil

Berkan Aktas<sup>1</sup>  | Merve Gurboga<sup>2</sup>  | Sinem Angin<sup>2</sup>  | Pervin Rayaman<sup>3</sup>   
Elif Caliskan Salihi<sup>4</sup>  | Ozlem Bingol Ozakpinar<sup>1\*</sup> 

<sup>1</sup> Marmara University, Faculty of Pharmacy, Department of Biochemistry, Istanbul, Türkiye

<sup>2</sup> Marmara University, Institute of Health Sciences, Department of Biochemistry, Istanbul, Türkiye

<sup>3</sup> Marmara University, Faculty of Pharmacy, Department of Pharmaceutical Microbiology, Istanbul, Türkiye

<sup>4</sup> Marmara University, Faculty of Pharmacy, Department of Basic Pharmaceutical Sciences, Istanbul, Türkiye

\* Corresponding author: [ozlemozakpinar@gmail.com](mailto:ozlemozakpinar@gmail.com); Ph.: +90-533-633-5550.

**Citation:** Aktas, B., Gurboga, M., Angin, S., Rayaman, P., Salihi Caliskan, E., & Ozakpinar Bingol, Ö. (2024). Investigation of antiproliferative and antimicrobial activities of carbon nanofiber based aerogels loaded with rutin and krill oil. The European chemistry and biotechnology journal, 2, 53-66.  
<https://doi.org/10.62063/ecb-29>

**License:** This article is licensed under a Creative Commons Attribution-NonCommercial 4.0 International License (CC BY-NC 4.0).

**Peer review:** Externally peer reviewed.

**Received:** 27.06.2024

**Accepted:** 22.07.2024

**Published:** 25.07.2024



## Abstract

Cancer, the second-leading cause of death worldwide after cardiovascular diseases, is a deadly disease caused by numerous mutations that affect cell growth and differentiation. While there is no definitive cure for cancer yet, new target molecules are being identified with the help of developing technology, and appropriate treatment protocols are being developed. Since both normal and malignant cells are exposed to cytotoxic effects in traditional treatment methods, the development of less-side-effect and targeted treatment methods has become important. With the development of nanotechnology, the development of various nanodrug delivery systems (DDSs) has been targeted. In our study, we investigated the antiproliferative and antimicrobial activities of rutin-modified carbon nanofiber (ACNFr)-based aerogels loaded with krill oil (KO) (ACNFr-KO). Our results showed that ACNFr-KO aerogels were observed to have a significant anti-proliferative effect on the human breast cancer cell line MCF-7. In addition to this, ACNFr-KO aerogels were found to have antimicrobial activity against the gram-positive bacterium *E. faecalis* ATCC 29212. The results of our study suggest that rutin-modified CNF-based aerogels loaded with KO, which act as a DDS, have the potential to enhance targeted drug delivery and improve therapeutic outcomes in biomedical applications.

**Keywords:** Aerogel, antimicrobial effects, cancer, carbon nanofiber, krill oil



## Introduction

Cancer remains one of the most formidable health challenges in modern medicine, with a cure still eluding scientists despite extensive research efforts. Studies have shown that conventional treatments cause serious side effects and toxicity, and in some cases, resistance to chemotherapy and radiotherapy can develop (Dolatkah Laein et al., 2023). Therefore, it is important to develop new treatment strategies. In recent years, natural compounds have emerged as promising candidates for cancer treatment, leading to a surge in research focused on their therapeutic potential.

Flavonoids have been shown to have antioxidant and radical-scavenging properties on many diseases including cancer (Lin et al., 2012). Rutin, one of the flavonoids, is a glycoside containing rutinose attached to the OH-3 of quercetin (Agrawal et al., 2021). It has been shown that rutin has antioxidant, anti-inflammatory, anti-aging, and anticancer properties (Choi et al., 2021; Choi et al., 2016) and that it can be used as a protective drug since no toxicity was observed during long-term use (Youssef et al., 2022).

Krill oil (KO), extracted from *Euphausia superba*, is seen as an alternative to fish oil because it contains high levels of long-chain omega-3 polyunsaturated fatty acids (LC n-3 PUFA) (Tou et al., 2007; Winther et al., 2011). Various studies suggest that KO may have therapeutic effects in the treatment of many diseases, including various types of cancer. One study suggests that KO may suppress tumor growth in human colorectal cancer (CRC) (Jayathilake et al., 2022). In another study, it was reported that KO can regulate both tumor growth and tumor-associated angiogenesis via a novel mechanism (Hoon et al., 2022). It has also been found that the anti-proliferative property of KO is comparable with that of a chemotherapeutic drug, oxaliplatin (Jayathilake et al., 2019).

Despite the demonstrated efficacy of rutin and krill oil in cancer therapy both *in vitro* and *in vivo*, their clinical applications are limited due to several challenges such as poor water solubility, low absorption, and rapid metabolism (Manach et al., 2005; Nguyen et al., 2013; Sanchez et al., 2021). To overcome these limitations, nanotechnology has introduced innovative solutions, including the development of advanced DDSs. These nanocarrier systems are designed to enhance the solubility, stability, and targeted delivery of plant-based therapeutics, thereby improving their efficacy and applicability in cancer therapy. To overcome these challenges and achieve targeted cancer therapy, various drug delivery systems (DDSs) have been developed (Dobrzynska et al., 2020; Zhao et al., 2020; Naeem et al., 2023).

Carbon-based nanomaterials (CBNs) are among the carrier materials that attract attention. CBNs have high chemical resistance, efficient mechanical properties and biocompatibility properties (Demirhan et al., 2021; Zhang et al., 2016). Carbon nanofibers (CNFs) attract attention due to their different properties and applications (Magrez et al., 2006). The addition of CNFs to calcium alginate composite hydrogels can lead to an increase in mechanical properties and water diffusion (Llorens-Gamez and Serrona-Aroca, 2018). Alginates are of interest in drug delivery applications due to their biocompatibility and low toxicity properties (Putri et al., 2021).

In our study, we aim to develop rutin modified carbon nanofiber-based aerogels loaded with KO as a novel therapeutic approach. These aerogels are not only evaluated for their antiproliferative effects on various cancer cell lines, but also for their antimicrobial activities, providing a dual-functional platform for cancer treatment.

## Material and methods

### Reagents

The CNF was provided by Sigma Aldrich (>98% carbon basis), rutin ( $\geq 95\%$ ) was supplied by Aromel Chemistry (Konya, Türkiye), and KO was obtained from TAB Pharma (İstanbul, Türkiye). Dulbecco's Modified Eagle Medium/F12 (DMEM/F12) was purchased from PAN Biotech (Aidenbach, Germany). DMEM and fetal bovine serum (FBS) were obtained from Gibco (Rockville, MD, USA), MTT Cell Proliferation Assay Kit was provided by Thermo Fisher Scientific (Waltham, MA, USA). All other chemicals were obtained from Sigma-Aldrich (United Kingdom). All chemicals were of analytical grade purity.

### Activation of carbon nanofibers (CNFs)

CNFs were washed and purified from impurities by stirring with deionized water (DI) for 24 hours on a magnetic stirrer and then dried. Then, they were subjected to an acid treatment to convert them into active CNFs (ACNFs). Briefly, 3 g of CNF was soaked in 50 mL of 85%  $H_3PO_4$  for 24 hours at room temperature and left at 250°C to active CNF. The CNF was centrifuged with 50 mL of DI water at 5000 rpm for 30 minutes. This process was repeated until the pH became neutral. Once the pH was stabilized, it was dried at 85°C to obtain active carbon nanofibers (ACNFs) (Bingol Ozakpinar et al., 2023).

### Modification of ACNFs with rutin (ACNF<sub>r</sub>)

300 mg of rutin was dissolved in 2 mL of dimethyl sulfoxide (DMSO) until completely dissolved. 300 mg ACNF dispersion were dispersed DI water with ultrasonic water bath. The rutin solution was added to the ACNF dispersion in a total volume of 200 mL DI water and incubate at 37 °C in a shaking water bath for 24 hours. This mixture was centrifuged, washed with DI water, and then dried at 37 °C.

### Preparation of aerogels

To prepare aerogels, 4 mg of ACNF<sub>r</sub> was dispersed in 8 mL of DI water and added 1 mL of KO (dissolved in 1 mL of DMSO) to prepare a 0.4 mg/mL ACNF<sub>r</sub>-KO mixture. The mixture was added dropwise into 10 mL of sodium alginate solution (2 g/100 mL DI water). After stirring for 10 minutes with a magnetic stirrer, it was then added dropwise into 3 g of  $CaCl_2$ /100 mL DI water solution and allowed to stand at room temperature for 24 hours. For the ACNF<sub>r</sub> and ACNF dispersions, the identical procedure was used once more. The resultant aerogels were cleaned with distilled water, allowed to stand at room temperature for a full day, and then dried at 37 °C.

### Characterization of aerogels

The scanning electron microscope (SEM) was utilized to determine the surface structure and morphological features of the composite aerogels (Zeiss EVO MA 10). Prior to imaging, nanoparticles underwent a gold-palladium coating process using Quorum SC7620 Mini Sputter Coater for 180 seconds. An acceleration voltage of 10 kV was applied. The IRSpirit spectrometer (Shimadzu Corp, Kyoto, Japan) was used to record the FTIR (Fourier transform infrared) spectra of the samples. Measurements were taken in the range of 4000–450  $cm^{-1}$  with an average resolution of 4  $cm^{-1}$ .

### Cell culture studies

In this study, human colorectal cancer cell line (HT29- ATCC, HTB-38), human breast cancer cell line

(MCF-7-ATCC, HTB 22), human cervical cancer cell line (Hela-ATCC, CCL2), and human prostate cancer cell line (PC3-ATCC, CRL1435) were used. The cells were cultured in DMEM medium supplemented with 10% FBS and 1% penicillin-streptomycin at 37°C and 5% CO<sub>2</sub>.

### **Cell viability assessment**

The effects of ACNF, rutin, KO, and aerogels on HT29, MCF-7, Hela, and PC3 cells on cell viability were determined using the MTT (3-(4,5-dimethylthiazol-2-yl)-2,5-diphenyltetrazolium bromide) method (Beekman et al., 1996). Briefly, the cells were seeded in 96-well plates and cultured for 24 hours. The next day, ACNF (10, 50, 100 µg/mL), rutin (100, 200, 300 µg/mL), KO (10, 40, 80 µg/mL), rutin-modified ACNF (10, 50, 100 µg/mL) and aerogel (10, 50, 100 µg/mL) were applied to the cells. After incubation, After adding MTT solution to the wells, the cells were cultured for four hours in a CO<sub>2</sub> incubator. Using 630 nm as the reference wavelength, the optical density (OD) was measured at 570 nm in a multi-well plate reader (Biotech Instruments, Winooksi, VT, USA). All experiments were run twice, and each treatment was performed in triplicate. The following formula was used to determine cell viability:

$$[(\text{Average OD of treated cells}) / (\text{Average OD of control cells})] \times 100$$

### **Evaluation of antimicrobial activity of aerogels**

The antimicrobial properties of the rutin-modified composite aerogels and KO-loaded aerogels were investigated using the agar diffusion test after 30 minutes of UV application. Later, also the minimal bactericidal concentration (MBC)s and minimal fungicidal concentration (MFC)s of the aerogels were assessed.

**Agar well diffusion test:** As bacteria; *Enterococcus faecalis* ATCC 29212, *Staphylococcus aureus* ATCC 25923, *Pseudomonas aeruginosa* ATCC 27853, *Escherichia coli* ATCC 25922, *Staphylococcus epidermidis* ATCC 11228 and as yeast; *Candida albicans* ATCC 90028 strains were used. Bacteria were inoculated on Mueller Hinton Agar (MHA) 37 °C for 24 hours and *C. albicans* on Sabouraud Dextrose Agar (SDA), incubated at 35 °C for 48 hours. Colonies of microorganisms were cultivated in 0.85% NaCl physiological saline solution (PSS) to make up microorganism suspensions. Using the McFarland 0.5 standard turbidity as a guide, bacterial suspensions were adjusted to 10<sup>8</sup> CFU/mL and *C. albicans* suspensions to 10<sup>6</sup> CFU/mL. Using sterile swabs and aseptic circumstances, the microorganism suspensions were applied to the surface of the MHA for bacteria and the SDA for *C. albicans*. Next, 5 mm diameter wells were formed on the medium using a sterile punch. Next, 50 µL of the aerogels were added to the wells. Additionally, amphotericin B was utilized as a positive control for the yeast, meropenem was used for the bacteria, and PSS and solvent (DMSO) were used as the negative controls. Inoculated petri dishes were incubated for 18–24 hours at 37 °C for bacteria and 24–48 hours at 35 °C for yeast. The inhibition zones were measured in millimeters at the end of the incubation period. Three repetitions of the trials were conducted, and the average range of those replicates were determined (Peretz et al., 1990; Ritz et al., 1993; Balouiri et al., 2015).

**Detection of minimal inhibitor concentration (MIC) for bacteria:** The Clinical and Laboratory Standards Institute (CLSI) guidelines were followed while determining the minimum inhibitory concentration (MIC) of bacteria. The medium utilized was Cation Adjusted Mueller Hinton Broth (CAMHB). A bacteria suspension was prepared from the colonies in the 24-hour bacterial culture according to McFarland 0.5 turbidity, and the final inoculum concentration was diluted to 5x10<sup>5</sup> CFU/mL. The sterile U-based microdilution plates were placed 100 µL of the CAMHB. A quantity of 100 µL

aerogel samples were placed in the first wells and serial dilutions were made respectively. Then 5  $\mu$ L of bacterial suspension was added to the wells containing the aerogels and the plates incubated at 37 °C for 24 hours (CLSI 2020).

**Detection of MIC for yeasts:** The suspensions of yeasts, prepared from 18-24 hour agar cultures with physiological saline according to Mac Farland 1 standard, where the yeast suspensions were diluted to  $2 \times 10^3$  CFU/mL and used in the experiment (CLSI 2012, Berkow et al., 2020). Initially, 100  $\mu$ L of RPMI 1640 medium for yeasts were added to each well of the sterile 96-well microplates. Subsequently, 100  $\mu$ L of aerogel samples were introduced into the first wells of the plates, followed by 12 serial dilutions. Finally, the prepared *Candida albicans* suspension was added to all wells, and the microdilution plates were incubated at 35°C for 24 – 48 hours. (CLSI 2012, Berkow et al., 2020). At the end of this period, the lowest concentration of aerogels at which no growth of any microorganisms was observed was determined to be the minimum inhibitory concentration (MIC) value. Likewise, CAMHB, DMSO and RPMI were used as negative control. Meropenem and Amphotericin B were used as positive control (CLSI 2020; CLSI 2012; Berkow et al., 2020).

**Detection of minimal bactericidal and fungisidal concentrations:** Seeding was performed from each well of the microplate dilution containing the MIC value on Tryptic Soy Agar and Sabouraud Dextrose Agar in order to determine the minimal bactericidal concentration (MBC) and minimal fungicidal concentration (MFC) values of the aerogel samples. Then, the plates were left to incubation at 37 °C for 24 hours for bacteria and 48 hours for the yeast. Finally, after the incubation, the MBC and MFC values were determined according to the lowest values where no growing was seen observed (Misra and Sahoo, 2012).

## Results and discussion

### Characterization of aerogels

Characterization of the nanofibers and aerogel samples were done by using FTIR analysis and scanning electron microscopy (SEM). FTIR spectra of the ACNF and the aerogel samples were given in **Figure 1**. There is a stretching band at around 3300 which shows O-H bonds of the alginate matrix of the composite aerogel and does not exist in the spectra of ACNF. There is a sharp peak around 1600  $\text{cm}^{-1}$  belongs to C=O in the spectra of A(ACNF). The peaks between 1500  $\text{cm}^{-1}$  and 1000  $\text{cm}^{-1}$  correspond to C-C and C-O single bonds. There are some changes in the positions of the peaks between 1600 and 100  $\text{cm}^{-1}$  due to the modification of the structure with krill oil. There are also new peaks at around 2900  $\text{cm}^{-1}$  due to C-H stretching as a result of the krill oil modification (Bingol Ozakpınar et al., 2023; Calışkan Salihi et al., 2021; Wang et al., 2017; Demirhan et al., 2021).

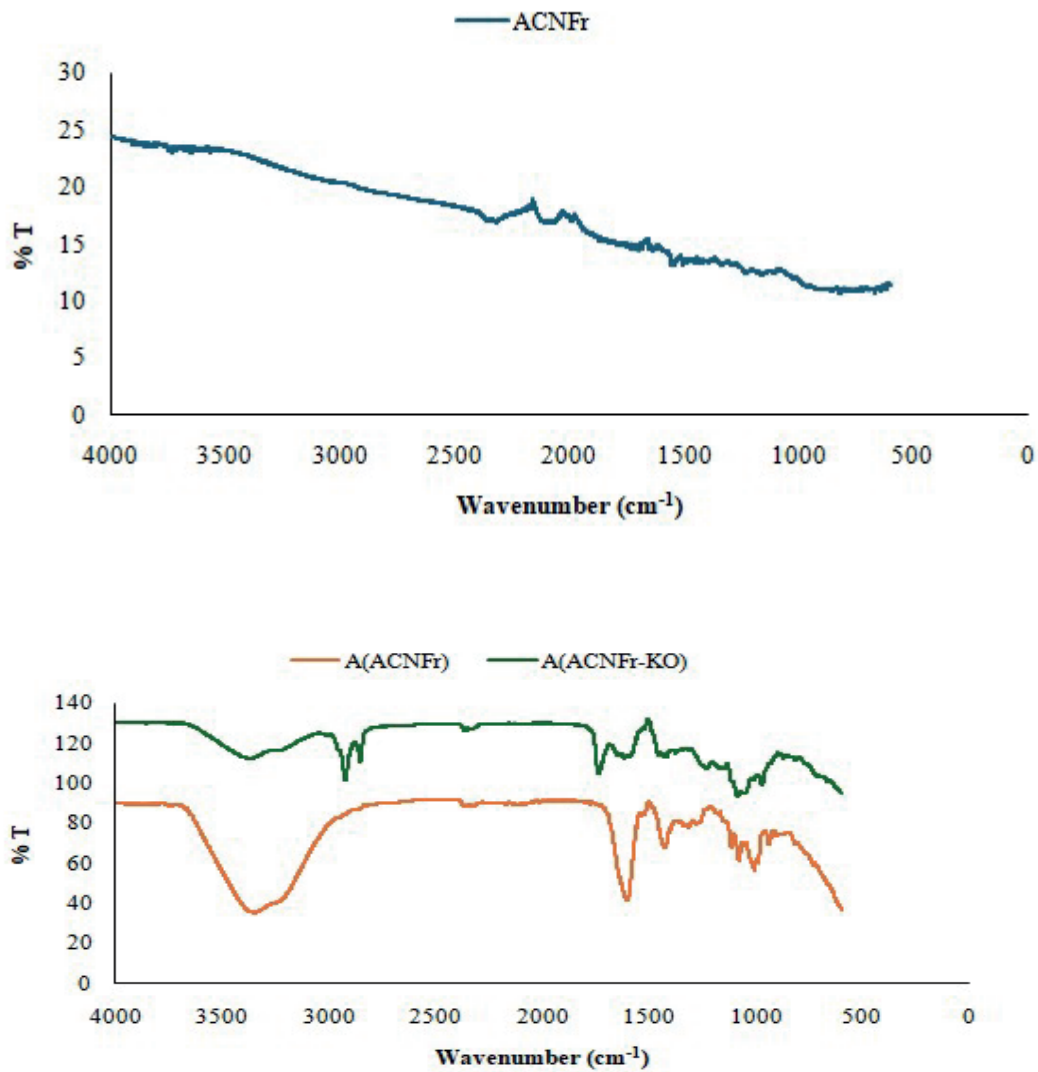


| **Figure 1.** FTIR spectra of the ACNFr and aerogels.

The physical structure and surface morphology of the aerogel samples were investigated by SEM. SEM photographs clearly show the porous and non-uniform physical structure of the aerogels (Figure 2).

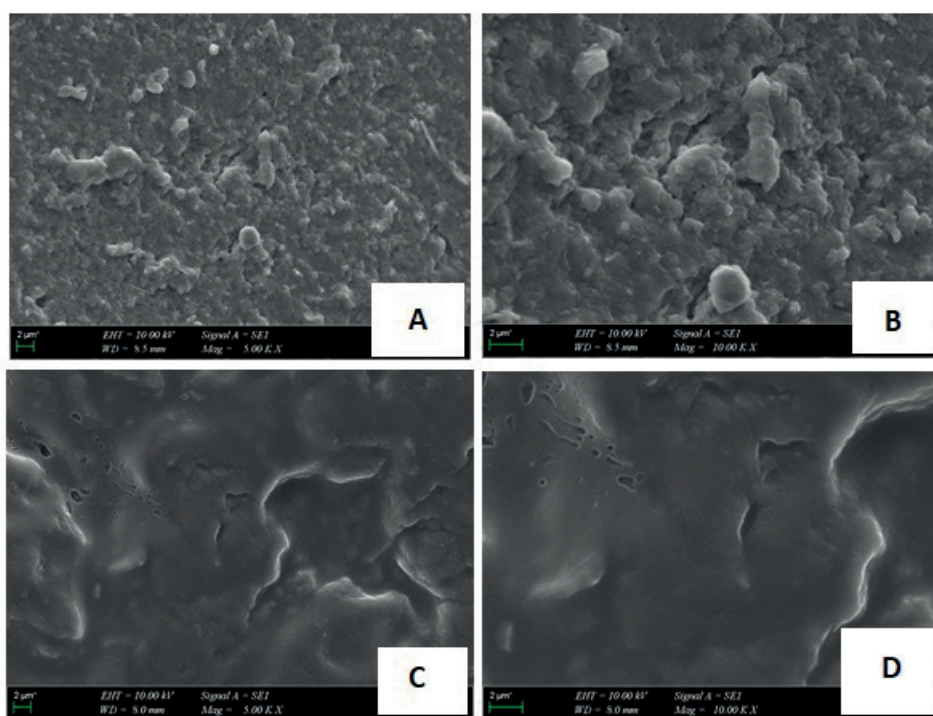


**Figure 2.** Representative SEM images of the aerogel samples. ACNFr (A, B) and ACNFr-KO (C, D).

### ***Antiproliferative effects of ACNF, rutin, KO and aerogel samples on the human cancer cell lines***

We investigated the antiproliferative effects of ACNF on cancer cell lines in our study. Treatment of HT29, MCF-7, HeLa, and PC3 cell lines with increasing concentrations of ACNF inhibited their proliferation in a dose-dependent manner in all cell lines (Figure 3). This inhibitory effect was observed to be particularly pronounced in HeLa cells. Ringel et al. (2014) demonstrated that carbon nanotubes (CNTs) and CNFs sensitized prostate and bladder cancer cells to the platinum-based chemotherapeutic carboplatin (CP) and cisplatin (CDDP). This sensitization resulted in an enhanced inhibition of both short- and long-term proliferation, as well as an increased induction of apoptosis. They also reported that the inhibitory effects of CNTs and CNFs alone on cellular viability were approximately 20%. In our study, this inhibitory effect was observed to be approximately 30% in PC-3 cells. This is likely due to the activation of CNFs. On the other hand, it was determined that the inhibitory effects on cancer cells did not change when ACNF was modified with rutin (ACNF<sub>r</sub>) or when it was in aerogel form (Aero (ACNF<sub>r</sub>)) (Figure 4).

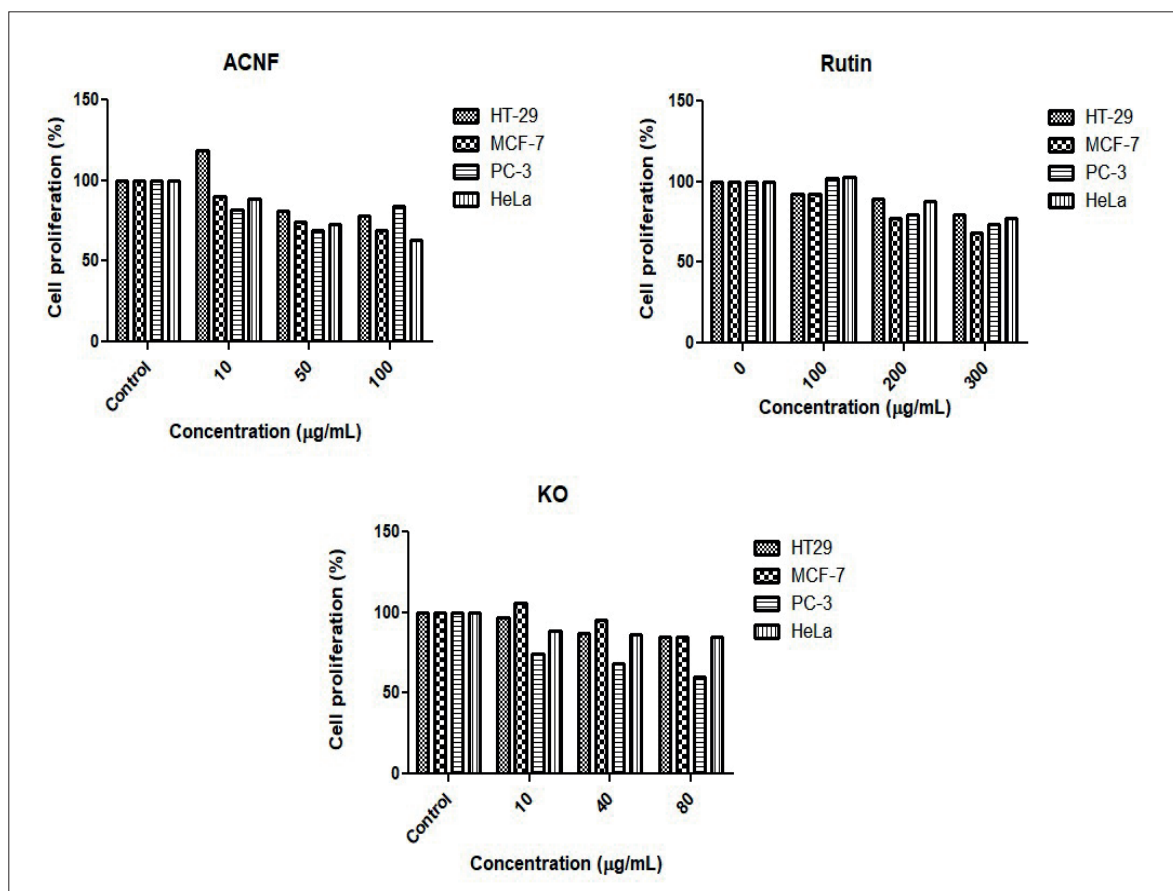


**Figure 3.** The antiproliferative effect of ACNF, rutin, and krill oil on HT-29, MCF-7, PC-3 and HeLa cell lines.

When rutin was applied at concentrations ranging from 0 to 300 µg/mL, it exhibited approximately a 23% antiproliferative effect in HeLa, HT-29, and PC-3 cells, while reducing cell viability by about 32% in MCF-7 cells (Figure 3). These findings support that rutin has antiproliferative effects in cancer cells. As it is well known, rutin is an anticancer flavonoid, and its efficacy has been demonstrated in numerous *in vivo* and *in vitro* studies (Iriti et al., 2017; Satari et al., 2021). Parallel to our study, Iriti et al. (2017) demonstrated the cytotoxic effects of rutin in MCF-7 cells in their research.

Krill oil (KO) is a natural compounds thought to play an effective role in cancer treatment and prevention (Jayathilake et al, 2022). Long-chain n-3 polyunsaturated fatty acids, particularly eicosapentaenoic and docosahexaenoic acids, and the powerful antioxidant astaxanthin are found in krill oil (Liu et al., 2024). In this study, we also evaluated the anti-carcinogenic effects of KO on the cancer cell lines (Figure 3). Each cell line was grown in media containing different concentrations (10, 40, and 80 µg/mL) of KO. The results revealed that the inhibition of cell viability increased with increasing dose and that KO had an antiproliferative effect. When evaluating the MTT results, we found that rutin applied alone exhibited a higher antiproliferative effect on HT-29, HeLa, and MCF-7 cells compared to KO applied alone. On the otherhand, KO's antiproliferative effect on PC-3 cells was significantly higher than that of rutin (40%). Interestingly, the rutin-modified aerogel loaded with KO composite, Aero (ACNF<sub>r</sub>-KO) exhibited a lower antiproliferative inhibition on cancer cells compared to the effect observed with KO alone.

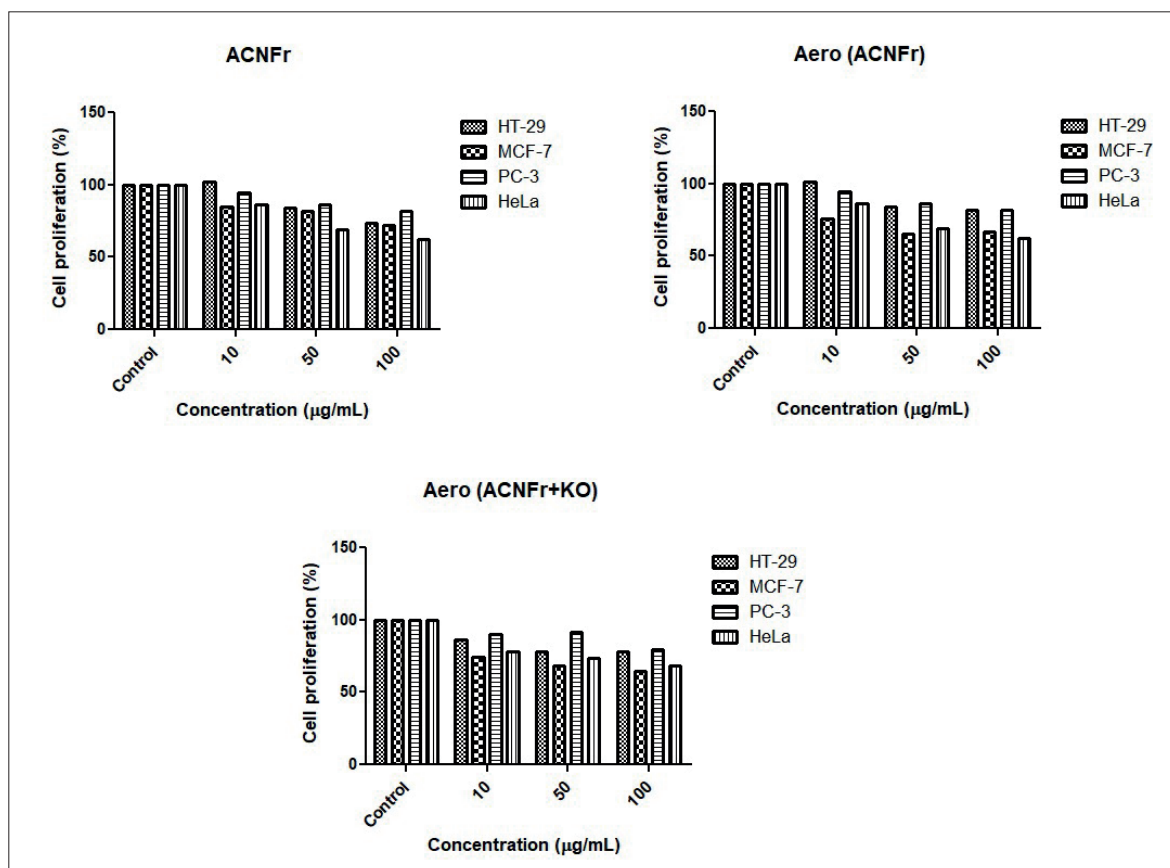


**Figure 4.** The antiproliferative effect of ACNFr, Aero(ACNFr), and Aero(ACNFr+KO) on HT-29, MCF-7, PC-3, and HeLa cell lines.

We found that the drug carrier Aero (ACNFr<sub>r</sub>-KO) composite we produced exhibited higher antiproliferative activity on cancer cells compared to Aero (ACNFr) composite across all cell lines. This inhibitory effect was particularly pronounced at the highest concentration of Aero (ACNFr<sub>r</sub>-KO) composite, especially in MCF-7 (64%) and HeLa (68%) cells. The different effects of aerogels on different cell lines may be due to the different biological properties of the cells and the way aerogels interact with the cells.

#### **Determination of antimicrobial activities of aerogels**

As can be seen in Table 1, Aero (ACNFr<sub>r</sub>-KO) showed antibacterial activity against *E. faecalis* ATCC 29212, which is one of the Gram-positive microorganisms, and formed an inhibition zone of 11.21 mm. However, it was found to be ineffective against other microorganisms. *Enterococcus faecalis* (*E. faecalis*), which is found in the normal flora of the oral cavity, is a Gram-positive microorganism that plays a primary role in the pathogenesis of recurrent infections (Tariq et al, 2023). This bacterium, which contains virulence factors against host cells, causes approximately 80 to 90% of hospital-acquired infections attributed to enterococci. As an opportunistic pathogen, *E. faecalis* has the opportunity to cause serious diseases, sometimes with fatal consequences, especially when the host's immune system is weakened. It is also responsible for the development of chronic infections such as surgical wound infections, bacteremia, endodontic infections, infective endocarditis, abdominal infections, and urinary tract infections (Ardila et al., 2023).



**Table 1.** Inhibition zones of aerogel composite systems determined by agar well diffusion method (mm).

	<i>Enterococcus faecalis</i> ATCC 29212	<i>Staphylococcus aureus</i> ATCC 25923	<i>Staphylococcus epidermidis</i> ATCC 11228	<i>Pseudomonas aeruginosa</i> ATCC 27853	<i>Escherichia coli</i> ATCC 25922	<i>Candida albicans</i> ATCC 90028
ACNF	0.00	0.00	0.00	0.00	0.00	0.00
ACNFr	0.00	0.00	0.00	0.00	0.00	0.00
A(ACNFr)	0.00	0.00	0.00	0.00	0.00	0.00
A(ACNFr+KO)	<b>11.21</b>	0.00	0.00	0.00	0.00	0.00
QRILL OIL	0.00	0.00	0.00	0.00	0.00	0.00
RUTIN	0.00	0.00	0.00	0.00	0.00	0.00
Meropenem (10µg/mL)	18.32	32.80	42.73	29.10	30.12	0.00
Amphotericin B (100µg/mL)	0.00	0.00	0.00	0.00	0.00	22.73

As seen in Table 2, the MIC of Aero (ACNFr-KO) was determined to be 50 mg/mL against *E. faecalis* ATCC 29212. The MBC of Aero (ACNFr-KO) was also found to be 100 mg/mL against *E. faecalis* ATCC 29212. However, this aerogel did not have any effect on the other microorganisms in our study. We have not found any study related with the antimicrobial effect of Aero (ACNFr+KO). Accordingly, our findings might be useful in the area related with aerogel composite systems, which were mentioned above.

**Table 2.** Detection of antimicrobial activity of aerogels by microdilution (µg/mL).

	<i>Enterococcus faecalis</i> ATCC 29212		<i>Staphylococcus aureus</i> ATCC 25923		<i>Staphylococcus epidermidis</i> ATCC 11228		<i>Pseudomonas aeruginosa</i> ATCC 27853		<i>Escherichia coli</i> ATCC 25922		<i>Candida albicans</i> ATCC 90028	
	MIC	MBC	MIC	MBC	MIC	MBC	MIC	MBC	MIC	MBC	MIC	MBC
ACNF	0.00	0.00	0.00	0.00	0.00	0.00	0.00	0.00	0.00	0.00	0.00	0.00
ACNFr	0.00	0.00	0.00	0.00	0.00	0.00	0.00	0.00	0.00	0.00	0.00	0.00
A(ACNFr)	0.00	0.00	0.00	0.00	0.00	0.00	0.00	0.00	0.00	0.00	0.00	0.00
A(ACNFr+KO)	<b>50</b>	<b>100</b>	0.00	0.00	0.00	0.00	0.00	0.00	0.00	0.00	0.00	0.00
KRILL OIL	0.00	0.00	0.00	0.00	0.00	0.00	0.00	0.00	0.00	0.00	0.00	0.00
RUTIN	0.00	0.00	0.00	0.00	0.00	0.00	0.00	0.00	0.00	0.00	0.00	0.00
Meropenem (10µg/mL)	8	16	2	4	0.25	0.50	0.5	2	0.06	0.12	0.00	0.00
Amphotericin B (100µg/mL)	0.00	0.00	0.00	0.00	0.00	0.00	0.00	0.00	0.00	0.00	1	4

## Conclusion

Drug delivery systems (DDS) play an important role in cancer treatment by providing effective delivery of drugs to the target site and reducing side effects. This study investigates antiproliferative and antimicrobial effects of rutin and KO using alginate aerogel nanoparticles. Our study suggests that by using natural products such as rutin and KO, it is possible to develop more effective treatment strategies by delivering drugs to cancer cells. Further studies are needed on different types of cancer. Additionally, the antimicrobial activity of ACNFr-KO aerogels suggests their potential for drug development. Targeted delivery of rutin using ACNFr aerogels has the potential to offer a new treatment strategy for cancer and infection therapy.

## Acknowledgements

### Funding

The research reported in this paper was funded in part by TUBITAK under grant number 2209-A University Students Research Projects Support Program: 1919B012210670.

### Conflicts of interest

There are no conflicts of interest among the authors.

### Data availability statement

Data can be obtained from the corresponding author upon a reasonable request.

### Ethics committee approval

Ethics committee approval is not required for this study.

### Authors' contribution statement

Study conception and design: O.B.O, Data collection: B.A, M.G., S.A., E.C.S., P.R., O.B.O, Manuscript draft preparation: B.A., O.B.O., M.G., S.A., All authors reviewed the results and approved the final version of the manuscript.

### ORCIDs and emails of the authors

Berkan Aktas | ORCID 0009-0001-0449-5907| [aktasberkan44@gmail.com](mailto:aktasberkan44@gmail.com)

Merve Gurboga | ORCID 0000-0003-4614-7094| [mervegurboga@gmail.com](mailto:mervegurboga@gmail.com)

Sinem Angin | ORCID 0009-0006-1996-1444| [sinemangn@gmail.com](mailto:sinemangn@gmail.com)

Pervin Rayaman | ORCID 0000-0002-0487- 8692| [pgocer@marmara.edu.tr](mailto:pgocer@marmara.edu.tr)

Elif Caliskan Salihi | ORCID 0000-0001-7852-3782| [caliskanelif@gmail.com](mailto:caliskanelif@gmail.com)

Ozlem Bingol Ozakpinar | ORCID 0000-0003-0287-5639| [ozlemozakpinar@gmail.com](mailto:ozlemozakpinar@gmail.com)

## References

Agrawal, PK., Agrawal, C., & Blunden, G. (2021). Rutin: a potential antiviral for repurposing as a SARS-CoV-2 main protease (mpro) inhibitor. *Natural product communications*, 16(4), 1–12. <https://doi.org/10.1177/1934578X21991723>

- Ardila, C.M., Jiménez-Arbeláez, G.A., & Vivares-Builes, A.M. (2023). The Potential Clinical Applications of a Microfluidic Lab-on-a-Chip for the Identification and Antibiotic Susceptibility Testing of *Enterococcus faecalis*-Associated Endodontic Infections: A Systematic Review. *Dentistry journal*, 12(1), 5, 12(1). <https://doi.org/https://doi.org/10.3390/dj12010005>
- Balouiri, M., Sadiki, M., & Ibsouda, S.K. (2016). Methods for in Vitro Evaluating Antimicrobial Activity: A Review. *Journal of pharmaceutical analysis*, 6, 71–79. <https://doi.org/10.1016/j.jpha.2015.11.005>
- Beekman, A.C., Barentsen, A.R., Woerdenbag, H.J., Van Uden, W., Pras, N., Konings, A.W., eFery, F. S., Galal, A.M., & Wikström, H. V. (1997). Stereochemistry-dependent cytotoxicity of some artemisinin derivatives. *Journal of natural products*, 60(4), 325–330. <https://doi.org/10.1021/np9605495>
- Berkow, E. L., Lockhart, S. R., & Ostrosky-Zeichner, L. (2020). Antifungal Susceptibility Testing: Current Approaches. *Clinical microbiology reviews*, 33(3), e00069-19. <https://doi.org/10.1128/CMR.00069-19>
- Bingol Ozakpinar, O., Havva, D., Gurboga, M., Sayin, F.S., Ozsavci, D., & Caliskan Salihi, E. (2023). Carbon Nanofiber—Sodium Alginate Composite Aerogels Loaded with Vitamin D: The Cytotoxic and Apoptotic Effects on Colon Cancer Cells. *Gels*, 9(7), 561. <https://doi.org/10.3390/gels9070561>
- Calışkan Salihi, E., Wang, J., Kabacaoğlu, G., Kirkulak, S., & Šiller, L. (2021). Graphene oxide as a new generation adsorbent for the removal of antibiotics from waters. *Separation science and technology*, 56(3), 453–461. <https://doi.org/10.1080/01496395.2020.1717533>
- Choi, S.J., Lee, S.N., Kim, K., Joo, daH., Shin, S., Lee, J., Lee, H.K., Kim, J., Kwon, S.B., Kim, M.J., Ahn, K.J., An, I.S., An, S., & Cha, H.J. (2016). Biological effects of rutin on skin aging. *International journal of molecular medicine*, 38(1), 357–363. <https://doi.org/10.3892/ijmm.2016.2604>
- Choi, S.-S., Park, H.-R., & Lee, K.-A. (2021). A Comparative Study of Rutin and Rutin Glycoside: Antioxidant Activity, Anti-Inflammatory Effect, Effect on Platelet Aggregation and Blood Coagulation. *Antioxidants*, 10(11), 1696. <https://doi.org/10.3390/antiox10111696>
- Clinical and Laboratory Standards Institute (CLSI). (2012). Reference Method for Broth Dilution Antifungal Susceptibility Testing of Yeasts; 4th Informational Supplement, M27-S4. *CLSI, Wayne PA, USA*.
- Clinical and Laboratory Standards Institute (CLSI). (2020). Performance Standards for Antimicrobial Susceptibility Testing. 30th Ed, January *CLSI supplement M100 Wayne, PA: Clinical and Laboratory Standards Institute*.
- Demirhan, K., Bingol Ozakpinar, O., & Salihi, E.C. (2021). Green and one step modification of graphene oxide using natural substances. *Fullerenes, nanotubes and carbon nanostructures*, 29(9), 716–723. <https://doi.org/10.1080/1536383X.2021.1884074>
- Dobrzynska, M., Napierala, M., & Florek, E. (2020). Flavonoid Nanoparticles: A Promising Approach for Cancer Therapy. *Biomolecules*, 10(9), 1268. <https://doi.org/10.3390/biom10091268>
- Dolatkhah Laein, G., Safarian, S., Delasaeimarvi, S., Ahmadi, G.S., Dadfar, S., Bakhshi, E., & Rashidzade, A.R. (2023). The Use of Curcumin in the Treatment of Colorectal, Breast, Lung, and Prostate Cancers: An in vivo Study Update. *Journal of lab animal research*, 2(6), 72–85. <https://doi.org/10.3390/lab2060072>

[doi.org/10.58803/jlar.v2i6.33](https://doi.org/10.58803/jlar.v2i6.33)

- Hoon, K., Youngjin, R., Sang Yong, P., Chungil Lee, Sujin, L., Seongbin, C., Hyang-Yeol, L., Soon Auck, H., Tae Jin, L., Soon Chul, M., Seok-Joong, Y., Yung Hyun, C., Wun-Jae, K., & Sung-Kwon, M. (2022). In vitro and in vivo anti-tumor efficacy of krill oil against bladder cancer: Involvement of tumor-associated angiogenic vasculature. *Food research international*, 156, 111144. <https://doi.org/10.1016/j.foodres.2022.111144>
- Iriti, M., Kubina, R., Cochis, A., Sorrentino, R., Varoni, E.M., Kabala-Dzik, A., Azzimonti, B., Dziedzic, A., Rimondini, L., & Wojtyczka, R.D. (2017). Rutin, a Quercetin Glycoside, Restores Chemosensitivity in Human Breast Cancer Cells. *Phytotherapy research*, 31(10), 1529–1538. <https://doi.org/10.1002/ptr.5878>
- Jayathilake, A.G., Kadife, E., Kuol, N., Luwor, R.B., Nurgali, K., & Su, X.Q. (2022). Krill oil supplementation reduces the growth of CT-26 orthotopic tumours in Balb/c mice. *BMC complementary medicine and therapies*, 22(1), 34. <https://doi.org/10.1186/s12906-022-03521-4>
- Jayathilake, A.G., Kadife, E., Luwor, R.B., Nurgali, K., & Su, X.Q. (2019). Krill oil extract suppresses the proliferation of colorectal cancer cells through activation of caspase 3/9. *Nutrition & metabolism*, 16, 53. <https://doi.org/10.1186/s12986-019-0382-3>
- Lin, J. P., Yang, J.S., Lin, J.J., Lai, K.C., Lu, H.F., Ma, C.Y., Sai-Chuen Wu, R., Wu, K.C., Chueh, F.S., Gibson Wood, W., & Chung, J.G. (2012). Rutin inhibits human leukemia tumor growth in a murine xenograft model in vivo. *Environmental toxicology*, 27(8), 480–484. <https://doi.org/10.1002/tox.20662>
- Liu, Y., Robinson, A.M., Su, X.Q., & Nurgali, K. (2024). Krill Oil and Its Bioactive Components as a Potential Therapy for Inflammatory Bowel Disease: Insights from In Vivo and In Vitro Studies. *Biomolecules*, 14(4), 447. <https://doi.org/10.3390/biom14040447>
- Llorens-Gámez, M., & Serrona.-Aroca, Á. (2018). Low-Cost Advanced Hydrogels of Calcium Alginate/Carbon Nanofibers with Enhanced Water Diffusion and Compression Properties. *Polymers*, 10(4), 405. <https://doi.org/10.3390/polym10040405>
- Magrez, A., Kasas, S., Salicio, V., Pasquier, N., Seo, J.W., Celio, M., Catsicas, S., Schwaller, B., & Forró, L. (2006). Cellular toxicity of carbon-based nanomaterials. *Nano letters*, 6(6), 1121–1125. <https://doi.org/10.1021/nl060162e>
- Manach, C., Williamson, G., Morand, C., Scalbert, A., & Rémésy, C. (2005). Bioavailability and bioefficacy of polyphenols in humans. I. Review of 97 bioavailability studies. *The american journal of clinical nutrition*, 81(1), 230S–242S. <https://doi.org/10.1093/ajcn/81.1.230S>
- Misra R., & Sahoo S.K. (2012). Antibacterial Activity of Doxycycline-Loaded Nanoparticles, Düzgüneş N. *Methods in Enzymology*. (Ed), Academic Press, 509, pp. 61–85. <https://doi.org/10.1016/B978-0-12-391858-1.00004-6>
- Naeem, A., Yu, C., Zang, Z., Zhu, W., Deng, X., & Guan, Y. (2023). Synthesis and Evaluation of Rutin-Hydroxypropyl  $\beta$ -Cyclodextrin Inclusion Complexes Embedded in Xanthan Gum-Based (HPMC-g-AMPS) Hydrogels for Oral Controlled Drug Delivery. *Antioxidants*, 12(3), 552. <https://doi.org/10.3390/antiox12030552>
- Nguyen T.A., Liu B., Zhao J., Thomas D.S., & Hook J.M. (2013). An investigation into the supramolecular

- structure, solubility, stability and antioxidant activity of rutin/cyclodextrin inclusion complex. *Food chemistry*, 136, 186–192. <https://doi.org/10.1016/j.foodchem.2012.07.104>
- Nishida K. (2021). Recent Advances in Lipid-Based Drug Delivery. *Pharmaceutics*, 13(7), 926. <https://doi.org/10.3390/pharmaceutics13070926>
- Perez, C., P.M., & Bazerque, P. (1990). An Antibiotic Assay by the Agar-Well Diffusion Method. *Acta Biologicae et Medicine Experimentails*, 15, 113–115.
- Putri, A.P., Picchioni, F., Harjanto, S., & Chalid, M. (2021). Alginate Modification and Lectin-Conjugation Approach to Synthesize the Mucoadhesive Matrix. *Applied sciences*, 11(24), 11818. <https://doi.org/10.3390/app112411818>
- Ringel, J., Erdmann, K., Hampel, S., Kraemer, K., Maier, D., Arlt, M., Kunze, D., Wirth, M. P., & Fuessel, S. (2014). Carbon nanofibers and carbon nanotubes sensitize prostate and bladder cancer cells to platinum-based chemotherapeutics. *Journal of biomedical nanotechnology*, 10(3), 463–477. <https://doi.org/10.1166/jbn.2014.1758>
- Sánchez C.A.O., Zavaleta E.B., García G.R.U., Solano G.L., & Díaz M.P.R. (2021). Krill oil microencapsulation: Antioxidant activity, astaxanthin retention, encapsulation efficiency, fatty acids profile, in vitro bioaccessibility and storage stability. *LWT*, 147, 111476. <https://doi.org/10.1016/j.lwt.2021.111476>
- Satari, A., Ghasemi, S., Habtemariam, S., Asgharian, S., & Lorigooini, Z. (2021). Rutin: A Flavonoid as an Effective Sensitizer for Anticancer Therapy; Insights into Multifaceted Mechanisms and Applicability for Combination Therapy. *Evidence-based complementary and alternative medicine*, 9913179. <https://doi.org/10.1155/2021/9913179>
- Tariq, R., Khurshid, Z., Ahmed Farooqui, W., & Adanir, N. (2023). Anti-bacterial efficacy of Aloe vera against *E. Faecalis* in comparison to other intracanal medicaments: A systematic review and meta-analysis. *The Saudi dental journal*, 35(5), 451–467. <https://doi.org/10.1016/j.sdentj.2023.05.007>
- Tou, J.C., Jaczynski, J., & Chen, Y.C. (2007). Krill for human consumption: nutritional value and potential health benefits. *Nutrition reviews*, 65(2), 63–77. <https://doi.org/10.1111/j.1753-4887.2007.tb00283.x>
- Wang, J., Salihi, E.C., & Šiller, L. (2017). Green reduction of graphene oxide using alanine. *Materials Science and Engineering: C*, 72, 1–6. <https://doi.org/10.1016/j.msec.2016.11.017>
- Winther, B., Hoem, N., Berge, K., & Reubsæet, L. (2011). Elucidation of phosphatidylcholine composition in krill oil extracted from *Euphausia superba*. *Lipids*, 46(1), 25–36. <https://doi.org/10.1007/s11745-010-3472-6>
- Youssef, S.S.M., Ibrahim, N.K., El-Sonbaty, S.M., & El-Din Ezz, M.K. (2022). Rutin Suppresses DMBA Carcinogenesis in the Breast Through Modulating IL-6/NF-κB, SRC1/HSP90 and ER-α. *Natural product communications*, 17(9), 1934578-. <https://doi.org/10.1177/1934578X221118213>
- Zhang, B., Wang, Y., & Zhai, G. (2016). Biomedical applications of the graphene-based materials. *Materials science and engineering: C*, 61, 953–64. <https://doi.org/10.1016/j.msec.2015.12.073>
- Zhao, J., Jiang, K., Chen, Y., Chen, J., Zheng, Y., Yu, H., & Zhu, J. (2020). Preparation and Characterization of Microemulsions Based on Antarctic Krill Oil. *Marine drugs*, 18(10), 492. <https://doi.org/10.3390/md18100492>